Investigations into the Mechanisms of Cell Death: The Common Link between Anticancer Nanotherapeutics and Nanotoxicology

Shalini Minocha

A dissertation submitted to the faculty of the University of North Carolina at Chapel Hill in partial fulfillment of the requirements for the degree of Doctor of Philosophy in the Division of Molecular Pharmaceutics in the UNC Eshelman School of Pharmacy.

Chapel Hill
2012

Approved By:

Russell J. Mumper, Ph.D.

Michael Jay, Ph.D.

Moo J. Cho, Ph.D.

Alexander Tropsha, Ph.D.

Andrew J. Ghio, M.D.

ABSTRACT

SHALINI MINOCHA: Investigations into the Mechanisms of Cell Death: The Common Link between Anticancer Nanotherapeutics and Nanotoxicology
(Under the direction of Russell J. Mumper, Ph.D.)

Nanotoxicology and anticancer nanotherapeutics are essentially two sides of the same coin. The nanotoxicology discipline deals with the nanoparticle (NP)-induced toxicity and mechanisms of cell death in healthy cells, whereas anticancer agents delivered via nano-based approaches aim to induce cell death in abnormally proliferating cancer cells. The objectives of the studies presented herein were two-fold; to (a) systematically study the physico-chemical properties and cell death mechanisms of model NPs and (b) utilize the knowledge gained from cell death-nanotoxicity studies in developing a potentially novel anticancer nanotherapeutic agent. For the first objective, the effect of a distinguishing characteristic, *i.e.*, surface carbon coating on the matched pairs of carbon-coated and non-coated copper and nickel NPs (Cu, C-Cu, Ni and C-Ni) on the physico-chemical properties and toxicity in A549 alveolar epithelial cells were evaluated. The effect of carbon coating on particle size, zeta potential, oxidation state, cellular uptake, release of soluble metal and concentration dependent toxicity of Cu and Ni NPs was systematically evaluated. A significant effect of carbon coating was observed on the physico-chemical properties, interaction with cellular membranes, and overall toxicity of the NPs. C-Cu NPs, compared to Cu NPs, showed four-fold lower release of soluble copper, ten-fold higher cellular uptake and protection against surface oxidation. In toxicity assays, C-Cu NPs induced higher

mitochondrial damage than Cu NPs whereas Cu NPs were associated with a significant damage to plasma membrane integrity. Nickel and carbon coated nickel NPs were less toxic compared to Cu and C-Cu NPs. Thus, by studying the effect of carbon coating, correlations between physico-chemical properties and toxicity of NPs were established.

The second objective was focused on utilizing nano-based approaches for the intracellular delivery of an anticancer agent, Cytochrome c (Cyt c), to breast cancer cells for inducing apoptosis. Cytochrome c is an endogenous mitochondrial protein and upon its release to cytosol, leads to apoptotic cell death. Although the mechanism by which Cyt c induces apoptosis theoretically makes it an attractive anti-cancer therapeutic agent, the lack of physicochemical characteristics required for successful cell permeation requires the use of delivery systems such as nanocarriers to facilitate its intracellular delivery. Cytochrome c, being a protein, is susceptible to changes in structural integrity and aggregation which might occur upon exposure to organic solvents and high shear/stress conditions, often used during nanoparticle preparation. Furthermore, successful delivery to cell cytosol requires endosomal release. Therefore, to deliver Cyt c intracellularly, while maintaining conditions for its stability, entrapment was performed using a film hydration method with 1,2-dioleoyl-3-trimethylammonium-propane and cholesterol (DOTAP-Chol) liposomes. It was shown that modulation of hydration buffer pH from 7 to 8.5 increased entrapment of Cyt c in DOTAP-Chol liposomes from 2% to 30%. The optimized formulation showed apoptotic activity in MDA-MB-231 cells. It was also shown that no aggregation, secondary and heme crevice structure change and deamidation was observed for Cyt c released from optimized formulation and that released Cyt c retained apoptotic activity after storage of formulation for twenty eight days at 4 ^{o}C.

To my parents Pradeep Minocha and Sunita Minocha, and my husband, Sumit Rawal.

ACKNOWLEDGEMENTS

These past five years in UNC as a graduate student have been great. I have grown both personally and professionally and this would not have been possible without the support and encouragement of a lot of people. Dr. Mumper has been a great teacher and mentor. I would like to express my sincere thanks to him for his constant support and motivation. I have learnt a lot from him in all these years. I am deeply grateful to him for giving me the freedom to pursue my research interests, allowing me to learn from my mistakes and always encouraging me to present my research findings. I am also very grateful to my doctoral dissertation committee members, Drs. Michael Jay, Moo J. Cho, Alexander Tropsha and Andrew J. Ghio for their help and advice. I would like to thank the Seminconductor Research Corporation for funding the project on nanotoxicology.

My sincere thanks go to all the staff, administrative members and facility supervisors at UNC for helping me throughout my PhD. I would also like to thank all the past and present members of Dr. Mumper's lab for making the time in the lab enjoyable and fun.

I would especially like to thank my family, who has given me unconditional strength, love and support to face the challenging times. I would like to thank my parents and my brother, Mukul, for their sacrifices, support and blessings. Words cannot express how thankful I am to my husband, Sumit, who has been there with me through the thick and thins. This would not have been possible without your constant love and support. I am blessed to have you in my life.

TABLE OF CONTENTS

LIST OF TABLES

LIST OF FIGURES

LIST OF ABBREVIATIONS AND SYMBOLS

ABTS	2,2’-azino-bis(3-ethylbenzthiazoline-6-sulfonic acid
ANOVA	analysis of variances
APAF1	apoptotic protease activating factor 1
APAF1	apoptotic protease activating factor 1
Asn	asparagines
Asp	aspartic acid
Bak	BCL-2 homologous antagonist/killer
Bax	BCL-2 associated X protein
Bcl2	B-cell lymphoma 2
BCL-xl	basal cell lymphoma-extra large
B-Gal	beta-galactosidase
BID	BCL-2 interacting domain
BSA	bovine serum albumin
C-Cu	carbon coated copper
Cd	cadmium
CD	circular dichroism
CdTe	cadmuium telluride
Chol	cholesterol
CL	cardiolipin
C-Ni	carbon coated nickel
CS	circumsporozoite

CVD	chemical vapor deposition
Cys	cysteine
Cyt c	cytochrome c
DI	de-ionized
DLS	dynamic light scattering
DMEM	dulbecco's modified eagle medium
DMF	dimethylformamide
DOPE	dioleoyl-sn-glycero-phosphoethanolamine
DOPS	1,2-dioleoyl-sn-glycero-phospho-serine
DOTAP	1,2-dioleoyl-3-trimethylammonium-propane
E. coli	escherichia coli
EE	entrapment efficiency
EGFP	enhanced green fluorescent protein
FBS	fetal bovine rerum
FTE	freeze thaw + extrusion
GFP	green fluorescent protein
Gln	glutamine
Glu	glutamic acid
Gly	glycine
HCMEC	human cardiac microvascular endothelial cells
HFL-1	human fetal lung fibroblasts cells
HII	inverted hexagonal structures
His	histidine

HPLC	high performance liquid chromatography
HRP	horse radish peroxidase
HSA	human serum albumin
ICP-MS	inductively coupled plasma mass spectroscopy
IEF	iso electric focusing
LBL	layer-by-layer
LDH	lactate dehydrogenase
Leu	leucine
MCL1	myeloid cell leukemia sequence 1
Met	methionine
MTT	(3-(4,5-Dimethyl-2-thiazolyl)-2,5-diphenyl-2H-tetrazolium bromide)
N-MPG	N-(mercaptopropionyl)-glycine
NPs	nanoparticles
NRK cells	normal rat kidney cells
NSP	nanoporous silicon particles
PBS	phosphate buffered saline
PEI	polyethyleneimine
PI	isoelectric point
PI	propidium iodide
PIC	polyionic complex
PLGA	poly lactic-co-glycolic acid
PM	particulate matter
PPAAc	poly(propylacrylic acid) complex

PTD	protein transduction domain
QD	quantum dots
RES	reticuloendothelial system
RNAse	ribonuclease
ROS	reactive oxygen species
r-SLPI	recombinant secretory leukocyte protease inhibitor
RT	room temperature
Sco2	synthase of cytochrome c oxidase
SDS PAGE	sodium dodecyl sulfate polyacrylamide gel electrophoresis
SE	sonication + extrusion
SOD	superoxide dismutase
SOD	superoxide dismutase
STS	staurosporine
TAT	trans-activating transcriptional activator
TEM	transmission electron microscopy
Trp	tryptophan
Tyr	tyrosine
w/o	water-in-oil
w/o/w	water-in-oil-in-water
XPS	x-ray photoelectron spectroscopy

Chapter I

Metal-Based Nanoparticles and their Toxicity

1.1 Summary

Nanoparticles, due to their small size and unique properties, offer tremendous opportunities and applications in many fields. The risk of exposure of nanoparticles to humans is yet to be fully known, since only limited data is available on exposure that can occur during occupational settings. Metal NPs have gained most popularity in terms of applications and according to a recent analysis report by project on emerging nanotechnologies, five out of six materials currently referenced in nanotechnology consumer products are metal based. The rapid growth in the number and use of NPs requires rapid and reliable methods to test their toxicity potential. *In-vitro* cell culture based methods can provide information on the mechanism of toxicity and differences in toxicity between various NPs. However, the dynamic nature of NPs in cell culture media can lead to changes in NP composition, agglomeration and release of toxic ions and can complicate the interpretation of results from nanotoxicity studies if careful and detailed investigations into the physico-chemical properties are not undertaken. This chapter provides an introduction to the nanotoxicity field and emphasizes the need to rigorously evaluate the physico-chemical properties of NPs along with their toxicity. The sections in this chapter will focus on (1) introduction to the emergence of the nanotoxicity field, (2) issues in evaluating NP toxicity

and regulatory status for monitoring NP toxicity (3) increasing applications of metal NPs, (4) literature review of studies on metal NP toxicity evaluation in-vitro, and (5) the need to systematically evaluate the physico-chemical properties of NPs and rationale for choosing carbon coated and non-coated copper and nickel NPs for toxicity evaluation studies.

1.2 Emergence of Nanotoxicity Field and Relevance

Nanoparticles are defined by the National Nanotechnology Initiative and the Food and Drug Administration as particles with at least one dimension less than 100 nm. Here after, engineered or manufactured nanoparticles will be referred to as NPs. Nanoparticles due to their small size offer exciting opportunities for application in various fields as diverse as medicine, semiconductor, agriculture and information technology. The unique characteristic of NPs is their small size that creates larger surface areas compared to large particles with same mass per unit volume (Nel et al., 2006). Unique properties of NPs have opened many avenues for a variety of new applications. There are already 1317 nanotechnology based products in nanotechnology consumer products inventory (nanotechproject.org, 2012). Along with the increase in manufacturing capability and applications of NPs over the past decade, there has also been considerable increase in research efforts dedicated to understand the adverse effects of NPs.

Historically, particle based toxicity has been attributed to air-borne particulate matter and inorganic materials. Exposure to particulate matter from pollution has been correlated to mortalities caused by cardiovascular and respiratory diseases (Pope et al., 2004). Furthermore, research has shown that particular size fractions PM_{10} (particulate matter with an average aerodynamic diameter of 10 micron or less) present in the environment correlate to health risks. Particle fraction composed of particulate matter with an average diameter of

2.5 micron or less ($PM_{2.5}$) and ultrafine particles (less than 100 nm) have also been investigated as potential concerns to human health (Donaldson et al., 2001). Asbestos related toxicity is well documented and has been linked with mesothelioma (Boffetta, 1998). NPs, however, are different from ultrafine particles in many ways. Ultrafine particles are highly heterogeneous and polydisperse whereas NPs usually are of well defined chemical compositions and their size and surface properties can be modified depending on surface coatings (Oberdorster et al., 2005). Given the unique properties of NPs, their increasing applications and differences from airborne ultrafine particles, the discipline of nanotoxicology emerged. Oberdoster et al., referred to nanotoxicology as an emerging discipline evolving from studies of ultrafine particles and defined it as "science of engineered nanodevices and nanostructures that deals with their effects on living organisms" (Oberdorster et al., 2005). Toxicity of NPs has been shown to be more than large particles of similar compositions and a clear size dependent increase in toxicity has been demonstrated. The higher toxicity of NPs over larger particles has been attributed to increased proportion of atoms on the NP surface as the size decreases. Moreover, especially below 100 nm, there is an exponential increase in the percent surface atoms on the NP surface (**Figure 1.1**). It was also suggested that not only the extent of toxicity but type of interaction with cellular and sub cellular structures can be different for NPs, given their higher reactivity and change in surface properties at such small size (Donaldson et al., 2004; Oberdorster et al., 2005). Additionally, it has been shown that ultrafine particles and NPs due to their small size could evade the defense mechanisms such as macrophages in lungs and can translocate from alveolar epithelium to systemic circulation (Simko and Mattsson, 2010). Thus, it is very important to systematically evaluate the potential adverse effects of NP exposure and more

importantly to determine the physico-chemical characteristics of NPs that may give rise to NP toxicity so that the best of nanotechnology could be harnessed while maintaining human and environmental safety.

1.3 Issues in Evaluating NP Toxicity and Regulatory Status for Monitoring NP Toxicity

Some reports pertaining to *in-vitro* toxicity evaluations are rather perplexing since the testing results of the same or very similar material in different labs has given different results. The variation in toxicity data of NPs can be attributed to source, method of dispersion, interference with absorbance or fluorescence data and most importantly lack of detailed physical and chemical characterization. For example, Worl-Knirsch et al. reported that false positive results were obtained when carbon nanotube toxicity was tested with the MTT ((3-(4,5-Dimethylthiazol-2-yl)-2,5-diphenyltetrazolium bromide) assay because the nanotubes interfered with the measured absorbance (Worle-Knirsch et al., 2006). Similar results were observed while testing carbon NP toxicity with neutral red dye (Monteiro-Riviere and Inman, 2006). As carbon NPs have large surface area and adsorptive properties, neutral red was adsorbed on the NP surface and showed false negative results. Special precautions, proper controls and use of multiple cytotoxicity assays has been suggested to overcome possibly conflicting results (Stone et al., 2009). Nanoparticles are usually dispersed in relevant biological media before testing their toxicity. Change in particle size, agglomeration, composition and release of toxic metal ions are some of the issues that have been reported, thus it is very important to measure the physico-chemical characteristics and toxicity of NPs in relevant biological media (Maiorano et al., 2010; Murdock et al., 2008; Warheit, 2008). The dynamic nature of NPs has given rise to difficulties in assessing the contribution of the

nanoparticulate state towards observed toxicity. Therefore, the need to correlate the physico-chemical properties of NPs with toxicity end points has been much emphasized (Powers et al., 2006; Warheit, 2008). Another aspect of NP toxicity evaluation is to understand the mechanisms underlying these toxic manifestations. A hierarchical oxidative stress paradigm has been suggested by Nel et al. (Nel et al., 2006). They emphasize a tiered approach towards evaluation of NP toxicity, starting with antioxidant defense responses followed by inflammatory pathway and finally effects on mitochondria.

Seaton et al. described in their review that "Hazard of a material translates into risk by exposure of humans and /or their environment to the agent in question, and risk is reduced by control of exposure usually guided by regulation based on understanding of the mechanism of action" (Seaton et al., 2009). The widespread application of NPs in various products poses a risk of exposure to humans and the environment at various stages of the NP lifecycle. Starting from small scale synthesis on the bench to large scale commercial production to transfer operations requiring manipulation of NPs into products to consumer end use to final disposal, all stages are portals where NP exposure can occur (Oberdorster et al., 2005; Seaton et al., 2010). Thus, it is important to regulate the potential levels of exposure and be aware of risks associated with exposure. However, establishing the limits for NP exposure has been complicated for various reasons. Limited data on real life exposure scenarios (such as increase in the levels of NP concentration while transfer and handling operations of NPs) is available and shows higher particulate concentration compared to background (Hirano, 2009; Seaton et al., 2009). Furthermore, due to varied applications of NPs, the regulatory authority which would pass regulations also differs. Thus far, no specific regulatory requirements exist for NPs compared to their bulk counterparts. Recently, FDA guidance on the use of

nanotechnology by the food and cosmetic industries has been released for public comment (FDAfactsheet, 2012).

1.4 Increasing Applications of Metal NPs

According to a recent analysis report by project on emerging nanotechnologies, five out of six NP materials currently referenced in nanotechnology consumer products are metal based (nanotechproject.org, 2012). Metal based NPs have a myriad of applications ranging from their use in semiconductors, in imaging and as antimicrobial agents, to name just a few. Furthermore, the possibility of modifying their surfaces by coating with various functional groups can further enhance their application potential. **Table 1.1** provides a compilation of applications of various metal based NPs. Considering the tremendous increase in the use and production of metal based NPs, toxicity testing requires development of rapid and reliable methods. Since, *in-vivo* testing is time consuming, expensive and requires animal use, *in-vitro* testing of NP toxicity has been vastly employed. Although, *in-vitro* tests are relatively rapid and inexpensive as compared to *in-vivo* tests, many issues relating to changing NP physico-chemical characteristics in biological media complicates interpretation of *in-vitro* toxicity results. Thus, there exists a need to systematically evaluate the toxicity of NPs such that one characteristic can be studied at a time and some level of correlation can be made between the physico-chemical characteristics and observed toxicity end points. Tremendous efforts have been dedicated towards assessing toxicity of metal NPs using *in-vitro* methods. Therefore, the next section will present the chronological review of literature for the past ten years in metal based *in-vitro* toxicity analysis. The review pertains to the type of metal NP, cell line, mechanism of toxicity and special attention was paid to whether any correlation between physico-chemical properties and toxicity was evaluated

1.5 Literature Review

Jaeger et al. studied the *in-vitro* toxicity of TiO_2 NPs (20 nm) in HaCaT keratinocytes by evaluating increases in ROS (reactive oxygen species), damage to mitochondrial DNA, and micronucleus formation (Jaeger et al., 2012). The authors observed a 2.2-fold and a 1.8-fold increase in micronucleus formation after treatment with 5 µg/mL (48 h) and 10 µg/mL (24 h) doses of TiO_2, respectively. They reported damage to mitochondria as a result of increased ROS, however, the effect of particle size and distribution on toxicity was not examined.

Murray et al. studied the *in-vitro* toxicity of dextran coated superparamagnetic iron oxide NPs of varied particle sizes (15 nm, 20 nm, and 50 nm) acquired from different sources (Murray et al., 2012). The toxicity was evaluated in HEK human epidermal keratinocytes and murine epidermal cells. The authors reported differences in internalization of NPs depending upon the source. A decrease in HEK cell viability was observed from 20 nm NPs, while 15 nm and 50 nm NPs did not result in decrease in viability. However, the authors did not investigate the underlying reasons for differences in toxicity and internalization from the NPs of different sizes and sources.

Mbeh et al. assessed the toxicity of magnetite (Fe_3O_4) NPs with different surface coatings (Mbeh et al., 2012). Three types of coatings were evaluated: (a) a shell of amine containing silane (i.e., Fe_3O_4-NH_2), (b) a shell of silica (i.e., Fe_3O_4-SiO_2), and (c) a shell of amine containing silane over a shell of silica (i.e., Fe_3O_4-SiO_2-NH_2). The toxicity of these NPs was systematically evaluated in A549 cells. Higher cytotoxicity was reported with amine coated NPs (i.e., Fe_3O_4-NH_2) compared to other coatings. Interestingly, the authors also monitored the effect of time for which the NPs were suspended in cell culture medium

prior to their exposure to cells. Higher toxicity was observed for NPs which were suspended for 24 h compared to the NPs which were suspended for 2 h. The difference in cytotoxicity was attributed to the change in composition of NPs during their suspension in cell culture medium.

The toxicity of 24 nm Ag NPs was studied in THP-1 macrophage cell line by Martinez-Gutierrez et al. (Martinez-Gutierrez et al., 2012). Ag NPs have been proposed as anti-bacterial agents and therefore this study also evaluated the anti-bacterial activity of Ag NPs in a panel of bacteria isolated from medical devices used in hospital intensive care units. Although Ag NPs were highly effective in inhibiting bacterial growth even for resistant strains, significant increase in toxicity was associated with 12.5 µg/mL dose in THP-1 cells. Therefore, the authors concluded that the beneficial and harmful effects of use of Ag NPs on biomedical devices needed to be carefully weighed.

Saquib et al. evaluated the toxicity of TiO_2 NPs (30.6 nm, rutile) in human amnion epithelial cells (WISH) (Saquib et al., 2012). A dose range of 0.62-10 µg/mL was evaluated and a significant increase in ROS and reduction in glutathione levels were observed at 10 µg/mL. The dose dependent cytotoxicity observed in WISH cells was attributed to increase in ROS.

Silver NP toxicity was evaluated by Mukherjee et al. in HaCaT keratinocytes and HeLa cervix epithelial adenocarcinoma cell lines (Mukherjee et al., 2012). A dose and time dependent increase in toxicity and a decrease in glutathione levels was observed in both cell lines. A significant difference in the sensitivity of two cell lines towards Ag NPs was observed, where HeLa cells were more sensitive and this was attributed to naturally occurring low antioxidant level in HeLa cells compared to HaCaT cells.

Choi et al. studied the toxicity of gold NPs (30 nm) in A549 human lung alveolar epithelial cells and reported an IC_{50} of 49 µg/mL using the MTT assay after 24 h exposure (Choi et al., 2012). The authors demonstrated coating of the negatively-charged gold NPs with components of serum in cell culture medium and uptake of the protein coated NPs in A549 cells. Intrinsic (increased mRNA expression of pro-apoptotic proteins bax and bak) and extrinsic (increased caspase-8 activity) apoptotic pathways were shown to be involved in gold NP induced cell damage.

Hematite (α-Fe_2O_3) NP and microparticle toxicity was evaluated in lung cancer cell lines (BEAS-2B and IMR-90) (Bhattacharya et al., 2012). In this study, the genotoxic effects of both microparticles and NPs at 50 µg/mL concentrations were observed. The authors reported only slightly higher toxicity from NP exposure as compared to microparticles and this was attributed to higher agglomeration of NPs in comparison to microparticles. In conclusion, the authors highlighted the importance of characterizing physico-chemical properties of NPs and correlating them to the observed cytotoxic effect.

The cytotoxicity of cadmium (Cd)-based quantum dots (QD), specifically CdTe (cadmuium telluride) was studied by Chen et al. using the MTT assay (Chen et al., 2012). The cytotoxicity of CdTe QDs was reported to be higher than $CdCl_2$ at equivalent intracellular Cd^{2+} ions concentrations. The abnormally high local concentration of Cd^{2+} ions in the peri-nuclear region after treatment with CdTe QDs was linked to the additional toxicity due to nanoscale effects of CdTe QDs.

The toxicity of TiO_2 NPs with UVA co-exposure was evaluated in retinal pigment epithelial cells (ARPE-19) (Sanders et al., 2012). Nanoparticles of different sizes (22-214 nm) and compositions (anatase, rutile, and anatase/rutile) were evaluated. It was found that

UVA co-exposure increased the toxicity of TiO_2 NPs. The 25 nm anatase and 31 nm anatase/rutile were reported as highly phototoxic with an IC_{50} of < 5 µg/mL, and 142 nm anatase and 214 nm rutile were reported as least phototoxic. The authors reported the increased cytotoxicity of TiO_2 NPs with UVA co-exposure due to increased reactivity of TiO_2 NPs. A systematic correlation was drawn between higher reactivity of TiO_2 NPs (quantified by an acellular thiobarbituric acid reactive substances assay) and IC_{50} values measured in cell-based cytotoxicity assays.

Sun et al. evaluated a panel of metal oxide NPs (CuO, silica, TiO_2 and Fe_2O_3) for their toxicity *in-vitro* in A549 cells (Sun et al., 2012). They reported that CuO NPs were highly toxic and resulted in 30% viability after 24 h treatment with 30 µg/mL dose, whereas other NPs except silica (slightly toxic) were not found to be toxic at the same dose. A significant increase in LC3-II protein (microtubule associated protein1 light chain 3) and accumulation of autophagosomes in A549 cells after treatment with CuO NPs was observed. Therefore, autophagy was reported as a possible mechanism by which CuO NPs induced cell-death. However, no information was presented on particle size assessment or aggregation potential of the panel of NPs that were tested.

Park et al. studied the effect of particle size on cytotoxicity, inflammation, and genotoxicity of Ag NPs *in-vitro* in L929 fibroblasts and RAW 264.7 macrophages (Park et al., 2011). Three different particle sizes: 20 nm, 80 nm, and 113 nm were evaluated. It was found that 20 nm particles displayed higher toxicity than 80 nm and 113 nm particles. The authors investigated the role of acellular ROS production as a possible reason for higher cytotoxicity observed with 20 nm particles, however, this poorly correlated with ROS generation potential of different sized NPs in cell-based assays. The authors also reported

higher sensitivity of L929 fibroblasts towards NP induced cytotoxicity compared to RAW 264.7 cells. The possibility of higher release of Ag ions in lysosomes of cells was suggested as a possible reason for higher toxicity with 20 nm particles. However, no direct correlation or underlying reasons were reported for higher toxicity observed with 20 nm particle compared to larger sized 80 nm and 113 nm NPs.

Zhang et al. compared the toxicities of TiO_2, ZnO, SiO_2 and Al_2O_3 NPs (primary size 20 nm) in human fetal lung fibroblasts cells (HFL-1) (Zhang et al., 2011). They reported that ZnO showed most cytotoxicity in HFL-1 cells compared to other NP types. A dose range of 250-1500 µg/mL was tested for all NPs and a dose dependent increase in cytotoxicity was reported. The dose range used by the authors was particularly higher compared to other studies. Furthermore, no correlations were drawn between the higher toxicity of ZnO and its physico-chemical properties compared to other NPs. A similar report by Sun et al. also compared the toxicities of six different metal oxide NPs (Sun et al., 2011). Toxicity of ZnO, CuO, Fe_2O_3, Fe_3O_4, MgO and Al_2O_3 NPs in human cardiac microvascular endothelial cells (HCMEC) was evaluated at two time points (12 h and 24 h) and six dose levels with a maximum dose of 100 µg/mL. The authors reported ZnO and CuO as most toxic NPs followed by MgO, and reported no toxic effects of Fe_2O_3, Fe_3O_4 and Al_2O_3 NPs in HCMEC's. However, similar to previous studies, this study also did not correlate the physico-chemical characteristics of the NPs displaying toxicity versus the "non-toxic" NPs in order to understand the origin of toxicity and concluded that compositional differences exist in toxicity of NPs. Although, the particles size and zeta potential analysis indicated higher agglomeration and close to zero zeta potential of Fe_2O_3 and Fe_3O_4 NPs compared to other NP types, this observation was not discussed.

Afeseh Ngwa et al. evaluated the neurotoxicity potential of Mn NPs in N27 dopaminergic neuronal cells (Afeseh Ngwa et al., 2011). They characterized particle size of Mn NPs upon suspension in cell culture media and reported agglomeration of NPs ranging from 100 nm to 900 nm in size. The neurotoxic effects of Mn NPs in dopaminergic N27 cells were characterized by an elevation of ROS and induction of apoptosis (caspase 3 activation). However, the authors reported that ROS was not the only mechanism leading to cell death as co-incubation of antioxidants did not rescue cells. Autophagic cell death (overexpression of LC 3 protein) was reported to be another pathway induced by Mn NPs as cause of neurotoxicity.

A systematic study of Ag NP and Ag microparticles to induce hemolysis was studied by Choi et al. (Choi et al., 2011).The authors studied the effect of surface citrate coating and size on hemolysis. They tested citrate coated Ag NPs (< 100 nm), non coated Ag NPs (35 nm), citrate coated Ag microparticles and heat treated Ag microparticles (to remove surface citrate coating). They evaluated the effect of varying suspension conditions (DI water, PBS and PBS/Plasma mixtures) on agglomeration of NPs in order to compare the physico-chemical properties of particles in media conditions relevant to hemolysis analysis. The authors reported that agglomeration varied with changing the media conditions and higher agglomeration was observed in PBS and PBS/plasma mixtures compared to DI water. Furthermore, higher hemolytic activity due to NPs compared to microparticles was observed. The higher hemolytic activity due to NPs compared to microparticles was correlated to higher Ag ion release and higher surface area of NPs compared to microparticles.

Horev-Azaria et al. described a modeling approach to understand and rank the parameters that were critical to toxicity of Co NPs and Co ions *in-vitro* (Horev-Azaria et al.,

2011). The effects of Co NPs and Co ions were evaluated in six cell lines using different concentrations (0.05-1 mM), two time points (48 h and 72 h) and various cytotoxicity assays (such as MTT, neutral red membrane integrity and alamar blue assays). As per their modeling analysis, the critical parameters influencing toxicity were ranked as follows: concentration > compound type (Co NP versus Co ions) > cell model > duration. They also correlated the toxicity effects of Co NPs to the release of Co ions from aggregated Co NPs.

Teodoro et al. reported on the mechanism of mitochondrial toxicity of Ag NPs in rat liver mitochondria (Teodoro et al., 2011). The authors reported that Ag NPs affected the mitochondrial membrane potential and altered the permeability of mitochondrial membranes. They further reported that mitochondrial injury due to Ag NPs affected oxidative phophorylation and respiratory functions.

Hackenberg et al. evaluated the toxicity of ZnO NPs (< 100 nm primary size) in primary human nasal mucosa cells *in-vitro* in the air-liquid interface (Hackenberg et al., 2011). The effect of ZnO was evaluated on mitochondrial damage, plasma membrane integrity, DNA fragmentation and pro-inflammatory potential. A significant genotoxicity (DNA fragmentation) at 10µg/mL and cytotoxicity at 50 µg/mL was reported. Additionally potent pro-inflammatory potential was observed at 5 µg/mL ZnO NP dose. The authors also tested the toxicity of ZnO powder for comparison but did not observe any genotoxicity or cytotoxicity at equivalent doses. The authors suggested role of both Zn^{2+} ions and NPs themselves in mediating the genotoxic and cytotoxic effects.

Naqvi et al evaluated the dose- and time-dependent toxicity of tween 80-coated superparamagnetic iron oxide NPs of mean diameter 30 nm on murine macrophage (J774) cells (Naqvi et al., 2010). The study also aimed at investigating the role of oxidative stress in

this toxicity. Higher concentrations (300-500 µg/mL) of NP and prolonged exposure of ~ 6 h resulted in reduced viability of 55-65%, while lower concentrations (25-200 µg/mL) and a 3 h exposure resulted in 95% viability. The cell membrane injury induced by NPs showed both concentration and time dependent killing as well as enhanced production of ROS at higher concentrations. The authors concluded that the NP concentration was critical to avoid oxidative stress-induced cell injury and death.

Horie et al. studied the toxicity of TiO_2 NP (< 100 nm) in HaCaT keratinocytes (Horie et al., 2010). The authors observed and reported formation of secondary TiO_2 particles (aggregates) upon dispersion in DMEM media supplemented with FBS. No significant toxicity was observed except a weak apoptotic response (6-7% apoptotic cells after 24 h exposure) which was attributed to increase in ROS.

Li et al. reported toxicity of Au NPs (35 nm) in human lung fibroblast cells (MRC-5) (Li et al., 2010).They showed increased oxidative stress, lipid hydroperoxides generation and autophagy as a mechanism of cell death and toxicity. A comprehensive analysis of mechanism of toxicity was carried out by the authors. However, little information was presented on physico-chemical properties of Au NPs and their possible correlation to toxicity mechanisms.

Samberg et al. studied the toxicity of Ag NPs (unwashed, washed and carbon coated) on HEK human keratinocyte cells using a variety of cell viability assays and measurement of pro-inflammatory cytokines (Samberg et al., 2010). They reported that Ag NPs (unwashed which contained formaldehyde and methanol as by product contaminants of the synthesis process) were highly toxic and pro-inflammatory whereas the washed NPs (serial washing by PBS) and carbon coated Ag NPs did not display significant toxicity. Thus, the authors

concluded that the residual contaminants in the unwashed NPs were responsible for inducing cytotoxic effects.

Liu et al. reported on the toxicity of TiO_2 NPs in PC12 neuronal cell line as result of increased ROS that lead to apoptosis (Liu et al., 2010). Increased ROS was concluded as a mechanism of apoptosis as pretreatment with N-(mercaptopropionyl)-glycine (N-MPG), an ROS scavenger inhibited apoptosis.

Choi et al. compared the toxicity of PEG modified MnO and Fe_3O_4 NPs with commercially available medical contrast agent Feridex in breast cancer, lung adenocarcinoma and glioblastoma cells (Choi et al., 2009). They reported that no toxicity was observed after 18 h incubation with PEG modified MnO, Fe_3O_4 NPs or Feridex at a concentration of 500 µg/mL. It was found that only after 2 days and 4 days, did PEG coated MnO NPs display toxicity.

Kim et al. studied the toxicity of Ag NPs in comparison to $AgNO_3$ in human hepatoma cells to assess the role of Ag^+ ions in toxicity of Ag NPs (Kim et al., 2009). The Ag NPs were de-ionized using an ion exchange resin before exposing the NP suspension to cell culture. They report equivalent toxicity and ROS induction by $AgNO_3$ and Ag NPs; however the expression of metallothionein 1b (a protein presumably reported to be increased by Ag^+ ions) was elevated only in $AgNO_3$ treated cells. The authors concluded that the toxicity of Ag NPs was due to NPs themselves rather than Ag^+ ions, however they discussed the possibility of release of Ag^+ ions from Ag NPs in cell culture media during their incubation with cells.

Ponti et al. studied the toxicity of Co NPs and Co^{2+} ions in BALB/3T3 mouse fibroblast cells (Ponti et al., 2009). They found that Co NPs were more toxic than Co^{2+} ions at shorter incubation times (2 h and 24 h). However, 72 h after incubation, the toxicity

profiles was similar for Co^{2+} ions and Co NPs when only 35% of Co^{2+} ions were released from Co NPs after 72 h under cell culture conditions. Thus, they attributed the toxicity of CO NPs due to both Co^{2+} ions and the NPs themselves.

Ghio et al., studied the effect of secondary organic aerosols and inorganic acids (constituents of particulate matter in ambient air) on the toxicity of Fe_3O_4 NPs in BEAS 2B human bronchial epithelial cells (Ghio et al., 2009). The authors showed that cell associated Fe concentrations were significantly higher than controls only after co-exposure of Fe_3O_4 NPs with secondary organic aerosols and inorganic acids. Concomitantly, an increase in oxidative stress and IL-8 levels were also observed in cells exposed to Fe_3O_4 NPs with secondary organic aerosols and inorganic acids. Therefore, the authors concluded that secondary organic aerosols and inorganic acids interacted with Fe_3O_4 NPs to change their cellular uptake and consequently their toxicity.

Horie et al. studied the effect of protein adsorption by various metal NPs (ZnO, CeO_2, TiO_2, SiO_2 and Fe_2O_3) on cell viability in A549 and HaCaT cells (Horie et al., 2009). They hypothesized and showed that after incubating cells with supernatants (obtained after centrifuging the NP and media mixture), significant decrease in cell viability was observed. They also showed that the decrease in cell viability was specifically induced by loss of protein from media because the decrease in cell viability was not observed from incubation with supernatants (when NPs were pre-incubated with FBS (fetal bovine serum)). The loss in cell viability due to protein adsorption by NPs was specifically relevant for inherently low toxicity NPs such as TiO_2 compared to ZnO NPs where release of Zn^{2+} ions can also induce toxicity.

Monteiller et al. evaluated in their studies with TiO_2 NPs and fine particles, the comparative correlation of descriptors (surface area versus mass) of concentration with toxicity (Monteiller et al., 2007). They dosed equal masses of TiO_2 NPs and fine particles to A549 cells and found that at equivalent mass, TiO_2 NPs produced much stronger pro-inflammatory and oxidative stress response than fine particles. They concluded that surface area descriptor better correlated with toxicity and plays an important role in reactivity and inflammatory potential as particle size decreases.

Limbach et al. have shown that NPs containing active and reactive metals can act as "trojan horses" for carrying the reactive metal in cells (Limbach et al., 2007). The authors systematically tested a series of similarly shaped and sized SiO_2 NPs containing Fe, Co, Mn and Titania and respective metal salts for their potential to induce oxidative stress *in-vitro*. They reported that the oxidative stress induced upon treatment with metal containing SiO2 NPs was much higher than salt solutions. They concluded that NPs carrying catalytically active metal sites can induce oxidative stress by a "trojan horse" type mechanism.

1.6 Need for Systematic Studies Correlating Metal NP Toxicity/Mechanisms with Metal NP Physico-chemical Characteristics

Metal NPs have seen tremendous growth in both production and applications in recent years. The increasing use and exposure of metal-based NPs warrants rigorous and systematic toxicity evaluations to maximize the benefit/risk ratio of the immense advancements, the metal NPs have to offer. Although the field of nanotoxicology is still in its infancy, many research efforts have been dedicated to understanding the mechanisms underlying toxicity of metal-based NPs *in-vitro* in cell lines of different origins. The challenges associated with determining toxicity of metal NPs are multifold and include factors such as size, zeta

potential, surface area, composition, hydrophobicity, impurities and importantly release of toxic metal ions that might contribute to the toxicity (**Figure 1.2**). Many studies outlined in literature review above investigated the detailed mechanisms of toxicity of a single metal NP or a group of metal NPs, however only a few studies have shown the correlation of NP physico-chemical characteristics with the observed toxicity. Thus, systematic studies that can deconvolute the reasons underlying toxicity of metal NPs are required to aid in understanding "which physico-chemical properties result in toxicity" so that manufacturing of safe and applicable NPs could be directed.

Copper and nickel NPs are being used in a variety of applications. Various applications of Cu and Ni NPs are summarized in **Table 1.1**. Oxidation of Cu and Ni NPs can alter the surface properties and hence carbon coating on the surface of metal NPs can help protect them against oxidation (Luechinger et al., 2008). Although surface carbon coating preserves the functionality, it can result in a change in physico-chemical properties and toxicity of Cu and Ni NPs and it is important that the effect of surface coating on the physico-chemical properties and toxicity of metal NPs is investigated. Therefore, it was decided to investigate the physico-chemical characteristics and toxicity of matched pairs of non-coated Cu and Ni NPs and carbon-coated Cu and Ni NPs. The hypothesis was that carbon coated NPs will have different physico-chemical properties including their interactions with the surrounding media and cells than non-coated NPs, which will influence the resultant toxicity in cell-based assays.

Table 1.1 Metal NPs and their Diverse Applications

NP Type	Applications	Reference
Al, Al_2O_3	Wear resistant coatings, fuel and drug delivery systems	(Tyner et al., 2004; Wagner et al., 2007)
Ag, C-Ag	Antimicrobial agent in medical devices, wound dressing, clothing and water purification systems	(Chaloupka et al., 2010; Choi et al., 2011)
Au	Imaging, radiotherapy enhancement	(Boisselier and Astruc, 2009; Cai et al., 2008)
Cd	Quantum dots, bioimaging, diagnosis	(Chen et al., 2012; Su et al., 2011)
Cu, C-Cu	Bacteriostatic and antifungal agents, conducting inks, batteries, fuel cells, catalysts and antifouling agents	(Barrabes et al, 2006; Nicola et al., 2005; Tarasov et al., 2002; Yoon et al., 2007; Zhang et al., 2007)
Co	Information storage, magnetic fluid, catalyst	(Puntes et al., 2001)
Fe_2O_3, Fe_3O_4	Drug delivery, imaging and diagnosis	(Kumar et al., 2007; Lanone et al., 2009; Na et al., 2009)
MgO	Antimicrobial agents	(Jin and Yiping, 2012)
Mn, MnO	Catalyst, fuel additive, colorant	(Han et al., 2005)
Ni, C-Ni	Catalyst and magnetic properties	(Park et al., 2005; Wang etal., 2008)
TiO_2	Sunscreen, photovoltaic devices, degradation of organic environmental contaminants	(Klaine et al., 2008; Kwon et al., 2008; Muneer et al., 2002)
ZnO	Cosmetics, catalysts, composite materials	(Veranth et al., 2007)

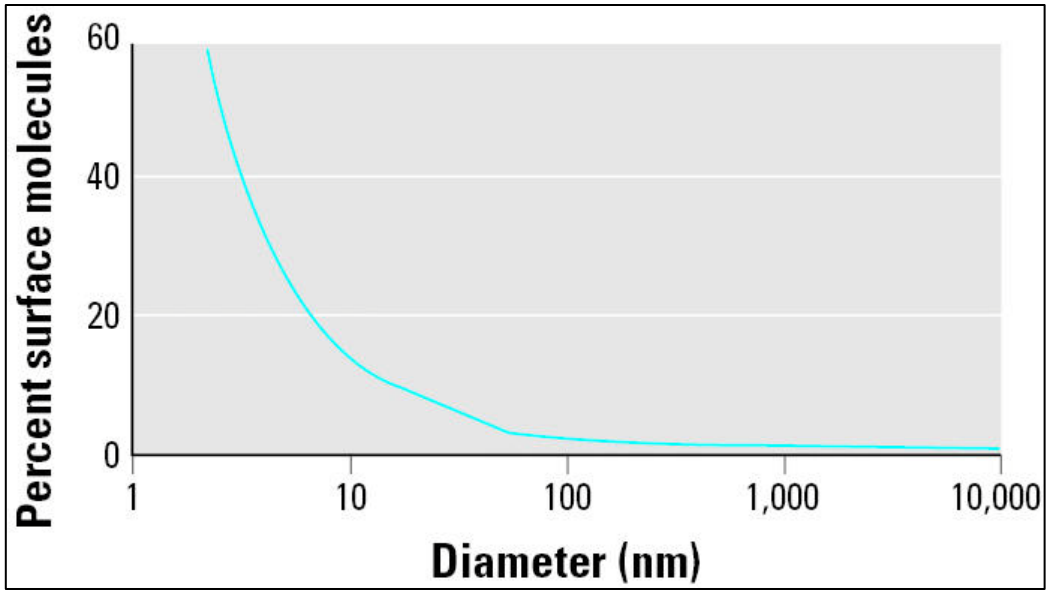

Figure 1.1 Percent surface molecules versus size relationships for NPs. The percentage of surface molecules in NPs increases exponentially as their size decreases below 100 nm. This can have profound implications on the reactivity of NPs and their resultant toxicity. Figure from Oberdorster et al. (Oberdorster et al., 2005)

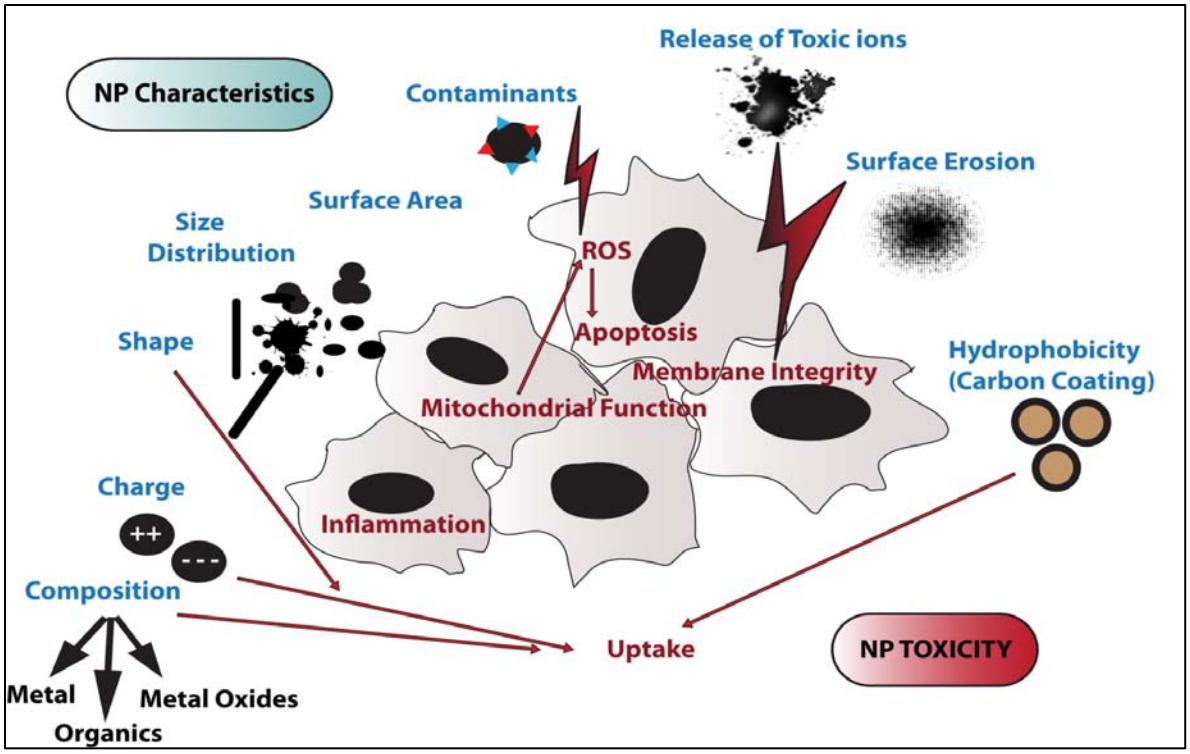

Figure 1.2 Nanoparticle physico-chemical properties and toxicity mechanisms. Various NP physico-chemical properties such as size, surface charge, release of toxic metal ions and surface coating can influence their interaction with surrounding media and cells during *in-vitro* toxicity testing and lead to differences in toxicity end-points. Therefore, it is imperative to carefully study the physico-chemical characteristics of NPs before and during toxicity analysis.

1.7 References

Afeseh Ngwa, H., Kanthasamy, A., Gu, Y., Fang, N., Anantharam, V., Kanthasamy, A.G., 2011. Manganese nanoparticle activates mitochondrial dependent apoptotic signaling and autophagy in dopaminergic neuronal cells. Toxicol Appl Pharmacol 256, 227-240.

Barrabes N, J.J., Dafinov A, Medina F, Fierro JLG, Sueiras JE, Salagre P, Cesteros Y., 2006. Catalytic reduction of nitrate on Pt-Cu and Pd-Cu on active carbon using continuous reactor: The effect of copper nanoparticles. Appl Catal B-Environ 62, 77-85.

Bhattacharya, K., Hoffmann, E., Schins, R.F., Boertz, J., Prantl, E.M., Alink, G.M., Byrne, H.J., Kuhlbusch, T.A., Rahman, Q., Wiggers, H., Schulz, C., Dopp, E., 2012. Comparison of micro- and nanoscale Fe(+)(3)-containing (Hematite) particles for their toxicological properties in human lung cells in vitro. Toxicol Sci 126, 173-182.

Boffetta, P., 1998. Health effects of asbestos exposure in humans: a quantitative assessment. Med Lav 89, 471-480.

Boisselier, E., Astruc, D., 2009. Gold nanoparticles in nanomedicine: preparations, imaging, diagnostics, therapies and toxicity. Chem Soc Rev 38, 1759-1782.

Cai, W., Gao, T., Hong, H., Sun, J., 2008. Applications of gold nanoparticles in cancer nanotechnology Nanotechnology, Science and Applications 2008, 17-32.

Chaloupka, K., Malam, Y., Seifalian, A.M., 2010. Nanosilver as a new generation of nanoproduct in biomedical applications. Trends Biotechnol 28, 580-588.

Chen, N., He, Y., Su, Y., Li, X., Huang, Q., Wang, H., Zhang, X., Tai, R., Fan, C., 2012. The cytotoxicity of cadmium-based quantum dots. Biomaterials 33, 1238-1244.

Choi, J., Reipa, V., Hitchins, V.M., Goering, P.L., Malinauskas, R.A., 2011. Physicochemical characterization and in vitro hemolysis evaluation of silver nanoparticles. Toxicol Sci 123, 133-143.

Choi, S.J., Oh, J.M., Choy, J.H., 2009. Toxicological effects of inorganic nanoparticles on human lung cancer A549 cells. J Inorg Biochem 103, 463-471.

Choi, S.Y., Jeong, S., Jang, S.H., Park, J., Park, J.H., Ock, K.S., Lee, S.Y., Joo, S.W., 2012. In vitro toxicity of serum protein-adsorbed citrate-reduced gold nanoparticles in human lung adenocarcinoma cells. Toxicol In Vitro 26, 229-237.

Donaldson, K., Stone, V., Clouter, A., Renwick, L., MacNee, W., 2001. Ultrafine particles. Occup Environ Med 58, 211-216, 199.

Donaldson, K., Stone, V., Tran, C.L., Kreyling, W., Borm, P.J., 2004. Nanotoxicology. Occup Environ Med 61, 727-728.

FDAfactsheet, 2012. http://www.fda.gov/Food/GuidanceComplianceRegulatoryInformation/GuidanceDocuments/ucm300914.htm?source=govdelivery.

Ghio, A.J., Dailey, L.A., Richards, J.H., Jang, M., 2009. Acid and organic aerosol coatings on magnetic nanoparticles increase iron concentrations in human airway epithelial cells. Inhal Toxicol 21, 659-667.

Hackenberg, S., Scherzed, A., Technau, A., Kessler, M., Froelich, K., Ginzkey, C., Koehler, C., Burghartz, M., Hagen, R., Kleinsasser, N., 2011. Cytotoxic, genotoxic and pro-inflammatory effects of zinc oxide nanoparticles in human nasal mucosa cells in vitro. Toxicol In Vitro 25, 657-663.

Han, M.J., Ozaki, T., Yu, J., 2005. Electronic structure and magnetic properties of small manganese oxide clusters. J Chem Phys 123, 34306.

Hirano, S., 2009. A current overview of health effect research on nanoparticles. Environ Health Prev Med 14, 223-225.

Horev-Azaria, L., Kirkpatrick, C.J., Korenstein, R., Marche, P.N., Maimon, O., Ponti, J., Romano, R., Rossi, F., Golla-Schindler, U., Sommer, D., Uboldi, C., Unger, R.E., Villiers, C., 2011. Predictive toxicology of cobalt nanoparticles and ions: comparative in vitro study of different cellular models using methods of knowledge discovery from data. Toxicol Sci 122, 489-501.

Horie, M., Nishio, K., Fujita, K., Endoh, S., Miyauchi, A., Saito, Y., Iwahashi, H., Yamamoto, K., Murayama, H., Nakano, H., Nanashima, N., Niki, E., Yoshida, Y., 2009. Protein adsorption of ultrafine metal oxide and its influence on cytotoxicity toward cultured cells. Chem Res Toxicol 22, 543-553.

Horie, M., Nishio, K., Fujita, K., Kato, H., Endoh, S., Suzuki, M., Nakamura, A., Miyauchi, A., Kinugasa, S., Yamamoto, K., Iwahashi, H., Murayama, H., Niki, E., Yoshida, Y., 2010. Cellular responses by stable and uniform ultrafine titanium dioxide particles in culture-medium dispersions when secondary particle size was 100 nm or less. Toxicol In Vitro 24, 1629-1638.

Jaeger, A., Weiss, D.G., Jonas, L., Kriehuber, R., 2012. Oxidative stress-induced cytotoxic and genotoxic effects of nano-sized titanium dioxide particles in human HaCaT keratinocytes. Toxicology 296, 27-36.

Jin, Z., Yiping, H., 2012. Antibacterial activities of magnesium oxide (MgO) nanoparticles against foodborne pathogens Journal of Nanoparticle Research 13, 6877-6885.

Kim, S., Choi, J.E., Choi, J., Chung, K.H., Park, K., Yi, J., Ryu, D.Y., 2009. Oxidative stress-dependent toxicity of silver nanoparticles in human hepatoma cells. Toxicol In Vitro 23, 1076-1084.

Klaine, S.J., Alvarez, P.J., Batley, G.E., Fernandes, T.F., Handy, R.D., Lyon, D.Y., Mahendra, S., McLaughlin, M.J., Lead, J.R., 2008. Nanomaterials in the environment: behavior, fate, bioavailability, and effects. Environ Toxicol Chem 27, 1825-1851.

Kumar, A., Sahoo, B., Montpetit, A., Behera, S., Lockey, R.F., Mohapatra, S.S., 2007. Development of hyaluronic acid-Fe2O3 hybrid magnetic nanoparticles for targeted delivery of peptides. Nanomedicine 3, 132-137.

Kwon, S., Fan, M., Cooper, A.T., Yang, H., 2008. Photocatalytic Applications of Micro- and Nano-TiO2 in Environmental Engineering. Crit. Rev. Environ. Sci. Technol. 38, 197–226.

Lanone, S., Rogerieux, F., Geys, J., Dupont, A., Maillot-Marechal, E., Boczkowski, J., Lacroix, G., Hoet, P., 2009. Comparative toxicity of 24 manufactured nanoparticles in human alveolar epithelial and macrophage cell lines. Part Fibre Toxicol 6, 14.

Li, J.J., Hartono, D., Ong, C.N., Bay, B.H., Yung, L.Y., 2010. Autophagy and oxidative stress associated with gold nanoparticles. Biomaterials 31, 5996-6003.

Limbach, L.K., Wick, P., Manser, P., Grass, R.N., Bruinink, A., Stark, W.J., 2007. Exposure of engineered nanoparticles to human lung epithelial cells: influence of chemical composition and catalytic activity on oxidative stress. Environ Sci Technol 41, 4158-4163.

Liu, S., Xu, L., Zhang, T., Ren, G., Yang, Z., 2010. Oxidative stress and apoptosis induced by nanosized titanium dioxide in PC12 cells. Toxicology 267, 172-177.

Luechinger, N.A., Athanassiou, E.K., Stark, W.J., 2008. Graphene-stabilized copper nanoparticles as an air-stable substitute for silver and gold in low-cost ink-jet printable electronics. Nanotechnology 19, 445201.

Maiorano, G., Sabella, S., Sorce, B., Brunetti, V., Malvindi, M.A., Cingolani, R., Pompa, P.P., 2010. Effects of cell culture media on the dynamic formation of protein-nanoparticle complexes and influence on the cellular response. ACS Nano 4, 7481-7491.

Martinez-Gutierrez, F., Thi, E.P., Silverman, J.M., de Oliveira, C.C., Svensson, S.L., Vanden Hoek, A., Sanchez, E.M., Reiner, N.E., Gaynor, E.C., Pryzdial, E.L., Conway, E.M., Orrantia, E., Ruiz, F., Av-Gay, Y., Bach, H., 2012. Antibacterial activity, inflammatory response, coagulation and cytotoxicity effects of silver nanoparticles. Nanomedicine 8, 328-336.

Mbeh, D.A., Franca, R., Merhi, Y., Zhang, X.F., Veres, T., Sacher, E., Yahia, L., 2012. In vitro biocompatibility assessment of functionalized magnetite nanoparticles: biological and cytotoxicological effects. J Biomed Mater Res A 100, 1637-1646.

Monteiller, C., Tran, L., MacNee, W., Faux, S., Jones, A., Miller, B., Donaldson, K., 2007. The pro-inflammatory effects of low-toxicity low-solubility particles, nanoparticles and fine

particles, on epithelial cells in vitro: the role of surface area. Occup Environ Med 64, 609-615.

Monteiro-Riviere, N., Inman, A., 2006. Challenges for assessing carbon nanomaterial toxicity to the skin. Carbon 44, 1070-1078.

Mukherjee, S.G., O'Claonadh, N., Casey, A., Chambers, G., 2012. Comparative in vitro cytotoxicity study of silver nanoparticle on two mammalian cell lines. Toxicol In Vitro 26, 238-251.

Muneer, M., Singh, H.K., Bahnemann, D., 2002. Semiconductor-mediated photocatalysed degradation of two selected priority organic pollutants, benzidine and 1,2-diphenylhydrazine, in aqueous suspension. Chemosphere 49, 193-203.

Murdock, R.C., Braydich-Stolle, L., Schrand, A.M., Schlager, J.J., Hussain, S.M., 2008. Characterization of nanomaterial dispersion in solution prior to in vitro exposure using dynamic light scattering technique. Toxicol Sci 101, 239-253.

Murray, A.R., Kisin, E., Inman, A., Young, S.H., Muhammed, M., Burks, T., Uheida, A., Tkach, A., Waltz, M., Castranova, V., Fadeel, B., Kagan, V.E., Riviere, J.E., Monteiro-Riviere, N., Shvedova, A.A., 2012. Oxidative Stress and Dermal Toxicity of Iron Oxide Nanoparticles In Vitro. Cell Biochem Biophys Epub ahead of reprint.

Na, H.B., Song, I.C., Hyeon, T., 2009. Inorganic nanoparticles for MRI contrast agents Advanced Materials 21, 2133-2148.

nanotechproject.org, 2012. http://www.nanotechproject.org/inventories/consumer/analysis_draft/

Naqvi, S., Samim, M., Abdin, M., Ahmed, F.J., Maitra, A., Prashant, C., Dinda, A.K., 2010. Concentration-dependent toxicity of iron oxide nanoparticles mediated by increased oxidative stress. Int J Nanomedicine 5, 983-989.

Nel, A., Xia, T., Madler, L., Li, N., 2006. Toxic potential of materials at the nanolevel. Science 311, 622-627.

Nicola Cioffi, L.T., Nicoletta Ditaranto, Giuseppina Tantillo, Lina Ghibelli, Luigia Sabbatini, Teresa Bleve-Zacheo, Maria D'Alessio, P. Giorgio Zambonin, and Enrico Traversa, 2005. Copper Nanoparticle/Polymer Composites with Antifungal and Bacteriostatic Properties. Chemistry of Materials 17, 5255-5262.

Oberdorster, G., Oberdorster, E., Oberdorster, J., 2005. Nanotoxicology: an emerging discipline evolving from studies of ultrafine particles. Environ Health Perspect 113, 823-839.

Park J, K.E., Son SU, Park MH, Lee KM, Kim J, Kim KW, Noh H-J, Park J-H, Bae CJ, Park J-G, Hyeon T, 2005. Monodisperse nanoparticles of Ni and Nio:synthesis, characterization,

self-assembled superlattices and catalytic applications in the suzuki coupling reactions. Adv. Mater 17, 429-434.

Park, M.V., Neigh, A.M., Vermeulen, J.P., de la Fonteyne, L.J., Verharen, H.W., Briede, J.J., van Loveren, H., de Jong, W.H., 2011. The effect of particle size on the cytotoxicity, inflammation, developmental toxicity and genotoxicity of silver nanoparticles. Biomaterials 32, 9810-9817.

Ponti, J., Sabbioni, E., Munaro, B., Broggi, F., Marmorato, P., Franchini, F., Colognato, R., Rossi, F., 2009. Genotoxicity and morphological transformation induced by cobalt nanoparticles and cobalt chloride: an in vitro study in Balb/3T3 mouse fibroblasts. Mutagenesis 24, 439-445.

Pope, C.A., 3rd, Burnett, R.T., Thurston, G.D., Thun, M.J., Calle, E.E., Krewski, D., Godleski, J.J., 2004. Cardiovascular mortality and long-term exposure to particulate air pollution: epidemiological evidence of general pathophysiological pathways of disease. Circulation 109, 71-77.

Powers, K.W., Brown, S.C., Krishna, V.B., Wasdo, S.C., Moudgil, B.M., Roberts, S.M., 2006. Research strategies for safety evaluation of nanomaterials. Part VI. Characterization of nanoscale particles for toxicological evaluation. Toxicol Sci 90, 296-303.

Puntes, V.F., Krishnan, K.M., Alivisatos, A.P., 2001. Colloidal nanocrystal shape and size control: the case of cobalt. Science 291, 2115-2117.

Samberg, M.E., Oldenburg, S.J., Monteiro-Riviere, N.A., 2010. Evaluation of silver nanoparticle toxicity in skin in vivo and keratinocytes in vitro. Environ Health Perspect 118, 407-413.

Sanders, K., Degn, L.L., Mundy, W.R., Zucker, R.M., Dreher, K., Zhao, B., Roberts, J.E., Boyes, W.K., 2012. In vitro phototoxicity and hazard identification of nano-scale titanium dioxide. Toxicol Appl Pharmacol 258, 226-236.

Saquib, Q., Al-Khedhairy, A.A., Siddiqui, M.A., Abou-Tarboush, F.M., Azam, A., Musarrat, J., 2012. Titanium dioxide nanoparticles induced cytotoxicity, oxidative stress and DNA damage in human amnion epithelial (WISH) cells. Toxicol In Vitro 26, 351-361.

Seaton, A., Tran, L., Aitken, R., Donaldson, K., 2009. Nanoparticles, human health hazard and regulation. J R Soc Interface 7 Suppl 1, S119-129.

Seaton, A., Tran, L., Aitken, R., Donaldson, K., 2010. Nanoparticles, human health hazard and regulation. J R Soc Interface 7 Suppl 1, S119-129.

Simko, M., Mattsson, M.O., 2010. Risks from accidental exposures to engineered nanoparticles and neurological health effects: a critical review. Part Fibre Toxicol 7, 42.

Stone, V., Johnston, H., Schins, R.P., 2009. Development of in vitro systems for nanotoxicology: methodological considerations. Crit Rev Toxicol 39, 613-626.

Su, Y., Peng, F., Jiang, Z., Zhong, Y., Lu, Y., Jiang, X., Huang, Q., Fan, C., Lee, S.T., He, Y., 2011. In vivo distribution, pharmacokinetics, and toxicity of aqueous synthesized cadmium-containing quantum dots. Biomaterials 32, 5855-5862.

Sun, J., Wang, S., Zhao, D., Hun, F.H., Weng, L., Liu, H., 2011. Cytotoxicity, permeability, and inflammation of metal oxide nanoparticles in human cardiac microvascular endothelial cells: cytotoxicity, permeability, and inflammation of metal oxide nanoparticles. Cell Biol Toxicol 27, 333-342.

Sun, T., Yan, Y., Zhao, Y., Guo, F., Jiang, C., 2012. Copper oxide nanoparticles induce autophagic cell death in a549 cells. PLoS One 7, e43442.

Tarasov S, K.A., Belyaev S, Lerner M, Tepper F, 2002. Study of friction reduction by nanocopper additives to motor oil. Wear 252, 63-69.

Teodoro, J.S., Simoes, A.M., Duarte, F.V., Rolo, A.P., Murdoch, R.C., Hussain, S.M., Palmeira, C.M., 2011. Assessment of the toxicity of silver nanoparticles in vitro: a mitochondrial perspective. Toxicol In Vitro 25, 664-670.

Tyner, K.M., Schiffman, S.R., Giannelis, E.P., 2004. Nanobiohybrids as delivery vehicles for camptothecin. J Control Release 95, 501-514.

Veranth, J.M., Kaser, E.G., Veranth, M.M., Koch, M., Yost, G.S., 2007. Cytokine responses of human lung cells (BEAS-2B) treated with micron-sized and nanoparticles of metal oxides compared to soil dusts. Part Fibre Toxicol 4, 2.

Wagner, A.J., Bleckmann, C.A., Murdock, R.C., Schrand, A.M., Schlager, J.J., Hussain, S.M., 2007. Cellular interaction of different forms of aluminum nanoparticles in rat alveolar macrophages. J Phys Chem B 111, 7353-7359.

Wang H, K.X., Zhang J, Li J, 2008. Large scale synthesis and characterization of Ni nanoparticles by solution reduction method. Bull Mater Sci 31, 97-100.

Warheit, D.B., 2008. How meaningful are the results of nanotoxicity studies in the absence of adequate material characterization? Toxicol Sci 101, 183-185.

Worle-Knirsch, J.M., Pulskamp, K., Krug, H.F., 2006. Oops they did it again! Carbon nanotubes hoax scientists in viability assays. Nano Lett 6, 1261-1268.

Yoon, K.Y., Hoon Byeon, J., Park, J.H., Hwang, J., 2007. Susceptibility constants of Escherichia coli and Bacillus subtilis to silver and copper nanoparticles. Sci Total Environ 373, 572-575.

Zhang XF, D.X., Huang H, Wang DK, Lv B, Lei JP, 2007. High permittivity from defective carbon coated Cu nanocapsules. Nanotechnology 18.

Zhang, X.Q., Yin, L.H., Tang, M., Pu, Y.P., 2011. ZnO, TiO(2), SiO(2,) and Al(2)O(3) nanoparticles-induced toxic effects on human fetal lung fibroblasts. Biomed Environ Sci 24, 661-669.

Chapter II

Studies on Nanotoxicity Motivate and Lead to Studies on Anticancer Nanotherapeutics

Chapter I describes the emergence of the nanotoxicology field and the importance of correlating the physico-chemical properties to mechanisms of cell death. For this purpose, Cu, C-Cu, Ni and C-Ni were chosen as model NPs and Chapter IV will describe the studies on these NPs in detail. In nanotoxicology studies, the mechanisms that induce cell death are studied and cell death is an undesirable effect. In contrast, anticancer agents aim to induce cell death in cancer cells because they have a tendency to proliferate abnormally. Induction of apoptosis (a form of cell death) is one of the mechanisms by which anticancer agents act. Therefore, the knowledge gained from understanding mechanisms of cell death such as apoptosis can be applied to devise anticancer nanotherapeutics. Cytochrome c (Cyt c) is an endogenous protein involved in inducing apoptosis, thus nanocarrier-based approach will be used for delivering Cyt c (an anticancer agent) intracellularly for inducing cell death in breast cancer cells. Although, it at first may seem that studies on nanotoxicity and intracellular delivery of Cyt c are unrelated, essentially they are the two sides of the same coin (**Figure 2.1**). Chapter III will describe various aspects of intracellular protein delivery and Chapter V will focus on specific studies to demonstrate stability and intracellular delivery of Cyt c.

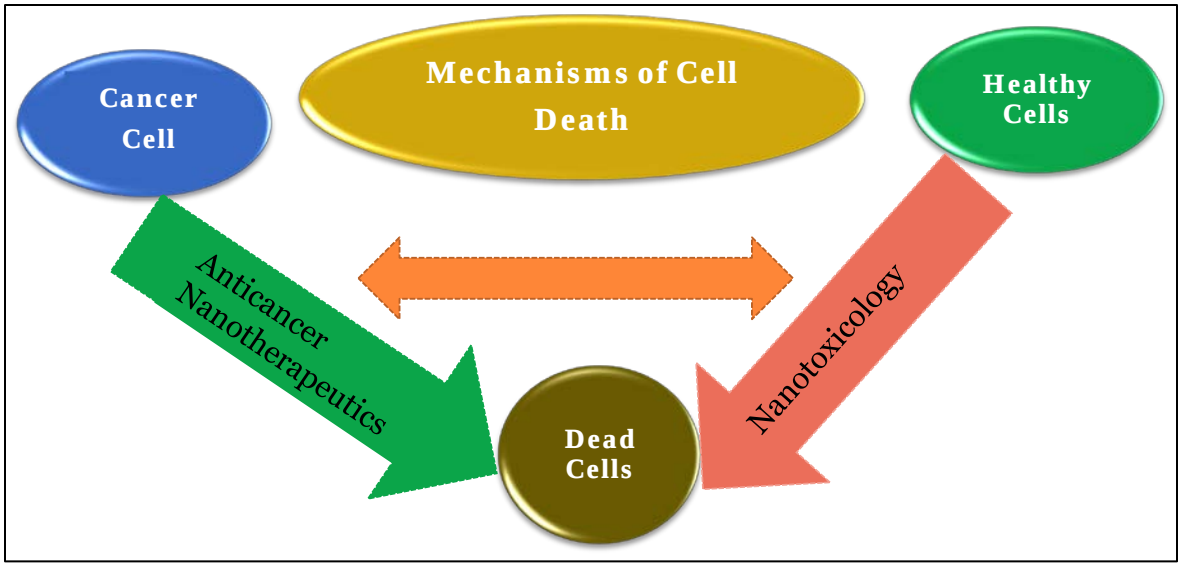

Figure 2.1 Mechanisms of cell death: The common link between nanotoxicology and anticancer nanotherapeutics. In nanotoxicology, cell death is an undesirable effect whereas in anticancer therapeutics, mechanisms to induce cell death are sought. Apoptosis is one of the mechanisms by which cell death occurs. Cytochrome c is an endogenous protein involved in inducing apoptosis. Therefore, intracellular delivery of Cyt c will be studied to induce apoptosis in breast cancer cells.

Chapter III

Nanocarrier-based Intracellular Protein Delivery: Challenges and Opportunities

3.1 Background

Though only accounting for 8% of currently marketed therapeutic products, biologics represent more than 42% of the global pharmaceutical pipeline and are positioned to surpass small molecules as the top grossing drugs by 2014 (Evaluatepharma, 2012). Proteins, the cellular workhorses of cells and largest class of marketed and pipeline biologics, play a role in almost every biochemical process, including digestion, respiration, cellular signaling and homeostasis. With exquisite specificity and biological activity, proteins find broad applications as leading therapies for cancer, infectious disease, and many autoimmune diseases. As of 2011, the Pharmaceutical Research and Manufacturers of America's report on "Biotechnology Medicines in Development" listed 901 new biotechnology medicines currently in development, of which monoclonal antibodies and therapeutic proteins account for almost 400 – up by 40% in just 3 years (PHRMA, 2012).

The field of drug discovery has progressed remarkably over the last two decades, yet challenges remain in intracellular protein delivery. Technological advances in high throughput screening and studies on cellular, metabolic, and signaling pathways have rapidly and reliably identified vast libraries of new drug targets; however, these targets localize in

the cellular or sub-cellular environment, making access a new and noteworthy challenge. Intracellular targets remain elusive for all classes of drugs, but especially for proteins, which are often too large and too polar to permeate the cell membrane alone (Torchilin and Lukyanov, 2003).

Research groups have utilized a variety of strategies to deliver therapeutic proteins intracellularly. More than two decades ago, Robert Langer suggested that therapeutic proteins would necessitate novel delivery systems, in part because they are inherently more complex than their conventional small molecule counterparts (Langer, 1990). Differences in size and physico-chemical properties between small molecules and proteins naturally demand a completely new set of strategies to formulate and deliver proteins. In fact, proteins with remarkable homogeneity display markedly different physico-chemical properties. Slight changes in amino acids on an antibody can display huge differences in solubility, viscosity, and thermodynamic stability (Yadav et al., 2012).

In theory, protein drugs need only be delivered in low doses due to their relatively specific mode of action; however, therapeutic potential and clinical application of protein drugs are frequently hampered by various obstacles to successful delivery (Frokjaer and Otzen, 2005; Wang, 1999), and these obstacles compound when delivering to intracellular targets. Rapid elimination of proteins from the systemic circulation due to renal clearance, enzymatic degradation, uptake by the reticuloendothelial system (RES), and accumulation in non-target tissues have been described as the primary hurdles for protein delivery (Torchilin and Lukyanov, 2003). Additionally, serious concerns for protein immunogenicity (due to protein unfolding and aggregation) and low efficacy (often due to inefficient cell entry) limit the landscape of protein therapeutics (Torchilin and Lukyanov, 2003). Thus, two major

challenges in intracellular delivery of therapeutic proteins are (a) limited cellular permeation and endosomal release into cytosol and (b) their susceptibility to undergo physical and chemical degradation which may lead to loss of activity and pose a risk of immunogenicity. Utilizing nanocarrier-based carriers to deliver therapeutic proteins to the cytoplasm and subcellular compartments of the cell represents a promising strategy to expand the landscape of therapeutic products for some of the most debilitating diseases (Gu et al., 2011). Many factors determine the success of a nanocarrier based system including entrapment of therapeutic cargo in the nanocarrier as well its efficient cellular uptake. Several review papers have emphasized the factors important in nanocarrier based drug delivery (Li et al., 2012; Torchilin, 2006). However, most of the research efforts in intracellular protein delivery have been dedicated towards developing strategies to enhance cell permeation and endosomal release and less attention has been paid to formulation and process related stress conditions that may lead to instability of protein therapeutics. Therefore, the following sections will focus on: (1) review of literature pertaining to approaches used for intracellular delivery of proteins for the last twenty years, paying special attention to whether or not protein stability was assessed, (2) common pathways for physical and chemical instability of proteins, (3) need for evaluating protein stability as part of protein delivery approach, (4) importance of endosomal release in intracellular protein delivery and (5) finally, this chapter will end with the introduction of Cyt c which serves to highlight the opportunity to deliver a potentially therapeutic protein intracellularly as an anti-cancer therapeutic.

3.2 Literature Review

Many research efforts have been dedicated in recent years towards intracellular delivery of therapeutic proteins. The following section provides a review of intracellular

protein delivery literature for the last twenty years. During review, the focus was to cover the approaches used for intracellular delivery of proteins and to assess whether or not protein structural stability and activity was evaluated as part of that approach. The review follows a chronological order starting with most recent reports.

Bacterial inclusion bodies have been suggested as protein delivery systems recently (Villaverde et al., 2012). Bacterial inclusion bodies are aggregates of recombinant proteins formed in (*Escherichia coli*) *E. coli* during their recombinant protein production. Leukemia inhibitory factor and catalase are some of the proteins that have been reported to be delivered *in-vitro* in cytosol using this approach to rescue cells from serum starvation and oxidative stress (Vazquez et al., 2012). The authors (Villaverde et al., 2012) reported that inclusion bodies holds promise in intracellular protein delivery due to their mechanically robust nature and biocompatibility, but questions remain regarding use of inclusion bodies as protein delivery systems due to the inherent nature of inclusion bodies, which contains both partially unfolded aggregated proteins and native folded proteins. Aggregation of therapeutic proteins is a huge challenge to the successful application of therapeutic proteins and inclusion bodies are protein aggregates by their nature (Ventura and Villaverde, 2006; Wang, 2005). Another class of delivery agents reported recently was peptides stapled with hydrophobic moieties. The approach used in the development of this class of agents was to increase the permeation and stability of small peptides by chemically introducing a hydrophobic moiety (stapling) to inherently hydrophilic peptides to form conformationally stable mini-proteins which had potent biological activity and permeation characteristics. Many stapled peptides for disruption of protein-protein interactions have been applied for both *in-vitro* and *in-vivo* applications (Bernal et al., 2010; Moellering et al., 2009). A detailed review by Verdine et

al., provides information on recent developments in stapled peptides (Verdine and Hilinski, 2012). Nanoporous silicon particles (NSP) with agarose coating were reported for intracellular delivery of model protein bovine serum albumin (BSA) (De Rosa et al., 2011). It was reported that BSA from agarose coated NSP's was more stable against trypsin digestion challenge compared to BSA from bare NSP's as tested via sodium dodecyl sulfate polyacrylamide gel electrophoresis (SDS PAGE) and high performance liquid chromatography (HPLC). It was also reported that agarose coating enhanced intracellular delivery of BSA. Intracellular delivery of proteins via layer-by-layer (LBL) polyelectrolyte nanocarriers was investigated by Shu et al. (Shu et al., 2010). They studied the encapsulation of a model protein BSA by the LBL method. The particles consisted of various layers of poly-electrolytes on a core. A silica nanoparticle with β-cyclodextrin shell was the core. BSA was adsorbed onto the β-cyclodextrin shell. Layers of positively charged cysteamine conjugated chitosan and negatively-charged dextran sulfate were deposited on BSA coated silicon core and crosslinking between various layers of chitosan was achieved by inducing disulfide linkage of cysteines. The authors showed that BSA retained its structural integrity after release from this nanocarrier system as the α-helix content of native and released BSA was similar. They also showed that maintenance of structural integrity was dependent on number of layers of chitosan because structural changes in BSA were observed when chitosan layer was present in close proximity to BSA. Foltopoulou et al. reported the delivery of recombinant Sco2 (synthase of Cytochrome c oxidase) protein *in-vitro* in various cell lines and also primary fibroblast cells using a recombinant fusion protein of TAT with Sco2 expressed in *E.Coli* (Foltopoulou et al., 2010). The authors reported partial recovery of functions associated with Sco2 protein in cells deficient of Cytochrome c oxidase. It was

also reported that the TAT Sco2 fusion protein was highly aggregated in inclusion bodies and had to be dissolved in 1 M arginine after which, it was relatively stable for 2 months at room temperature as determined by western blotting. Kundu et al. reported the use of silk fibroin protein from mulberry silkworms *bombyx mori* as carriers for VEGF (Kundu et al., 2009). Silk fibroin protein is a biomacromolecule composed of 5507 repeated sequence of Gly-Ala-Gly-Ala-Gly-Ser amino acids. They loaded VEGF protein (which is positively charged) onto preformed negatively-charged silk NPs (which were formed using a DMSO dehydration method), and reported sustained release of VEGF over three weeks. However, no stability or activity assays were used to characterize released VEGF. Single protein nanocapsules with a protein core and a shell of polymeric film have been proposed as intracellular protein delivery systems (Yan et al., 2010). Enhanced Green Fluorescent Protein (EGFP), caspase, BSA and Horse Radish Peroxidase (HRP) were surface modified with acrylamide groups and cross polymerized with degradable or non-degradable functional moieties and delivered to Hela cells. During the process of acrylamide attachment on protein surface and crosslinking, exposure to DMSO and alkaline conditions were used. The authors reported that fluorescence spectra of EGFP resembled native EGFP, however, no other assay for studying protein stability was used.

Recombinant secretory leukocyte protease inhibitor (r-SLPI) delivery *in-vitro* in lung derived cells for potential treatment of inflammatory lung diseases was investigated by Gibbons et al. (Gibbons et al., 2009). The authors reported high (74%) encapsulation of r-SLPI (11.7 KDa) in 1,2-dioleoyl-sn-glycero-phospho-serine and cholesterol liposomes (DOPS-Chol). The stability of liposomal r-SLPI was confirmed using western blotting and protection from cathepsin mediated r-SLPI degradation was also tested. Subsequently,

delivery and pharmacokinetics of aerosolized liposomal r-SLPI was also investigated in asthma guinea pig models and it was reported that liposomal r-SLPI had lower clearance and higher intracellular residence times than free r-SLPI (Gibbons et al., 2011).

Son et al. studied the optimization of an anti DNA antibody 3D8scFv for potential intracellular delivery using poly lactic-co-glycolic acid (PLGA) NPs prepared by a water-in-oil-in- water (w/o/w) encapsulation process (Son et al., 2009). A systematic study was undertaken to understand the effect of exposure of antibody to organic solvents and shear stress conditions. The antibody was recovered from the primary emulsion and assessed for structural integrity using circular dichroism (CD) and fluorescence techniques and functionality was assessed using ELISA and agarose gel electrophoresis. The authors also studied the effect of various stabilizers like PEG, trehalose, mannitol and heparin on structural integrity and functionality and concluded that mannitol provided most protection of antibody against various stress conditions. Lee et al. proposed use of polyionic complex (PIC) micelles composed of copolymers of PEG as the neutral block and poly[N-(N'-(2-aminoethyl)-2-aminoethyl)aspartamide] as the anionic block (Lee et al., 2009). They modified Cyt c with citraconic acid and cis-aconitic acid as Cyt c citraconamide and Cyt c cis-aconitic amide and encapsulated the modified Cyt c in PIC micelles. The modification of Cyt c lysines with citraconic acid and cis-aconitic acids was reported to change the PI of Cyt c from 9.6 to 3.7 and 3.4 and facilitate encapsulation. The authors also reported that *in-vitro* at pH 5.5 (endosomal pH), 50-80% of Cyt c reverted back to unmodified Cyt c and that the activity of released Cyt c was similar to native Cyt c as measured by 2,2'-azino-bis(3-ethylbenzthiazoline-6-sulfonic acid) (ABTS) assay. The authors also studied the uptake of modified Cyt c micelles in HuH cells, but no assay to assess the apoptotic activity of PIC

encapsulating modified Cyt c was performed. It is interesting that lysine groups of Cyt c were modified since it is well known that lysine groups of Cyt c play an important role in mediating its apoptotic activity. Furthermore, only 50 to 80 % modified Cyt c reverted to the unmodified form. Therefore there is a high likelihood that only part of delivered Cyt c would be available for activity. Also, the ABTS assay used to test activity of Cyt c is a non-specific assay which only tests the ability of Cyt c to oxidize/reduce the ABTS reagent and may not be the ideal assay to measure the apoptotic ability of Cyt c. Reddy et al. reported the intracellular delivery of superoxide dismutase (SOD) using PLGA NPs for intracellular delivery of SOD *in-vitro* in human brain neurons against H_2O_2 induced oxidative stress (Reddy et al., 2008). A double emulsion method was used to prepare NPs. SOD and rat serum albumin aqueous solution was exposed to PLGA solution in chloroform and also probe sonicated. Authors included rat serum albumin with SOD based on previous reports which concluded that inclusion of human serum albumin (HSA) protected ribonuclease (RNAse) protein against aggregation and conformational changes by competing for interfaces in the emulsification process (Sah, 1999). The authors reported that SOD-PLGA NPs offered higher protection in human brain neurons against H_2O_2 induced oxidative stress compared to SOD solution but no structural stability investigations were conducted. Dalkara et al. suggested for intracellular delivery of proteins use of dimerizable amphiphile-cholesterol conjugated to spermine with a cysteine group which could dimerize to form $(\text{cholesterol-spermine})_2$ (Dalkara et al., 2006). They reported formation of a complex of $(\text{cholesterol-spermine})_2$ with DOPE and also used phycoerytherin as a model protein to demonstrate *in-vitro* intracellular delivery potential of this complex. Soane et al. reported on the intracellular delivery of B-cell lymphoma 2 (Bcl2) proteins in neuronal cells using TAT

peptide to enhance cell survival (Soane and Fiskum, 2005). They expressed the fusion protein TAT-Bcl-2Δloop (with loop deletion in Bcl) in *E.Coli* and the purified fusion protein integrity was verified using SDS-PAGE. Intracellular delivery of the fusion protein was shown to protect the neuronal cells against staurosporine induced apoptosis in neuronal cells.

Abbing and coworkers utilized a virus-like particle approach to intracellularly deliver green fluorescent protein (GFP) by conjugating the inner core polyoma virus protein VP2 with GFP to create an inward-facing fusion protein within the VP1 pentamer cavity. This capsoid was internalized into cells and showed regular structure and stability for several months (Abbing et al., 2004). CA Lackey and colleagues studied the delivery of streptavidin to the cytosol of Jurkat T-cell lymphoma cells utilizing an antibody-targeted polymer-protein conjugate (Lackey et al., 2002). The anti-CD3 antibody bound to the CD3 receptor, which rapidly internalized the streptavidin-biotinylated poly(propylacrylic acid) complex (PPAAc). The PPAAc was reported as a pH-sensitive polymer capable of disrupting membranes at the lowered pH within endosomes. This process released streptavidin into cytosol of the cell while trafficked the monoclonal anti-CD3 antibody to the lysosome for degradation. The uptake was shown to be dose dependent and endosomal release was also demonstrated. The ternary complex showed 73% of the delivered streptavidin was released into the cytoplasm, whereas the binary complex (without PPAAC) showed only 29% release into the cytoplasm. A western blot to quantify streptavidin activity in the cytoplasm of the cells was also carried out. The authors also reported no degradation of the delivered streptavidin as demonstrated by an identical cytoplasmic band from the crude cell homogenate.

Lin-Lee et al. demonstrated the intracellular delivery of a bacterial cytosine deaminase, a 45 kDa enzyme which upon co-administration of 5-fluorocytosine is capable of

synthesizing the potent cell killer 5-fluorouracil (Lin-Lee et al., 2002). The simple recombinant fusion strategy proved successful at retaining the function and stability of the protein for several days, likely due to cytoplasmic compartmentalization from degradative enzymes. Given the mechanism of entry provided by the malaria circumsporozoite (CS) protein, a membrane ligand that mediates liver-specific invasion, this prodrug strategy showed promise as a strategy for the treatment of liver diseases, like hepatocellular carcinoma and mild-to-moderate chronic cholestatic liver disease. Two different cell lines were utilized to verify that entry was facilitated by receptor-mediated endocytosis: HepG2, which contains receptors for CS protein, and HL60, which does not. Additionally, cell-killing experiments were performed with various treatments. Although cell death was observed through the study range, neither specific activity nor biophysical characterization of the internalized protein was performed.

In the last decade, protein transduction domains stand out as a popular method to deliver therapeutic proteins to the cytoplasm and nucleus of cells. Morris et al. successfully delivered 30 kDa green fluorescent protein (GFP), 119 kDa beta-galactosidase (B-Gal) proteins, and two full-length specific antibodies intracellularly in a fully biologically active form utilizing a novel protein transduction domain (PTD) – peptide sequences that efficiently crossed biological membranes independent of transporters or receptor-mediated endocytosis – coined Pep-1 (Morris et al., 2001). Importantly, the proteins required no chemical coupling or denaturation steps. To mediate intracellular delivery, Pep-1 condenses on and around the protein through noncovalent hydrophobic interactions to form stable complexes. Interaction between the Pep-1 carrier and each protein was measured by size exclusion chromatography, which eluted primarily as 65-70 kDa protein with a small fraction eluting as large aggregates

greater than 160 kDa. An optimum ratio of Pep-1:protein was reported for maximal transfection efficiency, where too few Pep-1 molecules resulted in no delivery and too many resulted in precipitation or aggregation of the protein. Greater than 80% transfection efficiency was observed for GFP and B-Gal. Pep-1 also delivered both FITC-conjugated anti-Lamp-1 and monoclonal anti-beta-actin antibodies into cells, while preserving their ability to recognize their respective antigen observed via characteristic labeling of actin and lysosomes of the cells. Quantitative activity assessments and biophysical evaluation of structural integrity of the delivered protein were not performed.

Briscoe and colleagues delivered superoxide dismutase (SOD) to pulmonary epithelium using a pH-sensitive liposome (Briscoe et al., 1995). Enzymes such as SOD may help control the production of oxygen radicals, which develop as a result of respiratory insufficiency or exposure to pulmonary toxins. The group was able to entrap between 5 and 15% of initially added SOD in DOPE and DOSG (1-oleoyl-2-oleoyl-sn-glycero-3-succinate) liposomes, which released their contents between pH 4.5 and 5.5. SOD activity (assayed by enzymatic measurement), increased by 5-fold when fetal rat lung distal epithelial cells were incubated with untargeted DOPE-DOSG liposomes and by 6-fold with surfactant protein. A targeted DOPE-DOSG liposomes. Expectedly, the addition of a targeting modality increased delivery of the enzyme to the lung cells, but did not necessarily improve the delivery of active enzyme.

Mumtaz and Bachhawat described an effective *in-vivo* method to intracellularly deliver dextranase, an enzyme that degrades dextran (Mumtaz and Bachhawat, 1994). The group prepared liposomes to encapsulate dextranase and PEG-dextranase conjugates. It was shown that free dextranase, liposomal dextransase or free PEG-dextranase were not able to degrade

the FITC-dextan injected after the administration of the enzyme. In contrast, only liposomally delivered PEG-dextranase was catalytically active inside the cell after administration, yet only 10% was active after 24 hours. Importantly, PEG provided a stabilizing influence on the enzyme against intracellular degradation.

Various issues in physical and chemical stability of proteins that can arise during formulation and processing of protein drugs in nanocarriers are discussed below.

3.3 Common Physical and Chemical Instability Issues in Proteins

3.3.1 Physical Instability

Stabilizing and destabilizing forces in protein folding

Folded proteins have marginal stability as the free energy change between the unfolded and folded state is very small, typically in the range of 5-20 Kcal /mol (Dill, 1990; Pace et al., 1996). This explains the sensitivity of proteins to changes in their environment and also highlights the need to understand the effect of various process and formulation conditions on conformational stability of protein drugs. Many theories have been proposed to explain the forces involved in folding of proteins. Electrostatic, van der Waal's attractive forces, hydrogen bonding and hydrophobic forces have been proposed to explain protein folding. Although there are discrepancies in the literature as to which forces play a dominant role in protein folding, hydrophobic forces have been proposed to predominantly contribute to protein folding (Kauzmann, 1959). It was suggested that burial of non polar amino acids in the protein core away from water on the surface leads to folding. Further evidences in support of this theory have been site directed mutagenesis studies where replacement of an amino acid leads to change in protein stability proportional to oil-water partitioning behavior of the changed amino acid (Matsumura et al., 1988). The major factor that opposes protein

folding is entropy. Positive entropy refers to increase in randomness and disorder. Since protein folding involves collapse into restricted conformations in small volumes of space, this leads to restricted rotation in side chains and backbone. However, in the unfolded state there is no restriction and freedom of rotation (Dill, 1990).

Aggregation

One of the most common and initial stages of physical protein instability is protein aggregation. Aggregation refers to the formation of higher order protein structures such as oligomers or multimers which eventually lead to precipitation and loss of activity. Aggregates can form from either native or non-native proteins (Chi et al., 2003b; Philo and Arakawa, 2009). In native aggregation, proteins associate with each other to form oligomers or multimers due to their tendency to stick to each other in complementary regions. Insulin is one protein that undergo native type aggregation (Pekar and Frank, 1972). Non-native aggregates are formed from partially or completely unfolded proteins (Chi et al., 2003b). Non-native type of aggregation is more likely to occur during formulation and processing of protein during encapsulation in delivery systems.

In protein delivery, polymeric carriers such as PLGA has been the most commonly used system (Jiskoot et al., 2011). During preparation of PLGA NPs, water-in-oil emulsion (w/o) or w/o/w type emulsions are commonly used. Organic solvents such as dichloromethane, acetone, methanol, ethanol or a mixture of these are used to dissolve the polymer. Along with exposure to organic solvents, additional stresses experienced by proteins during the preparation process are high temperatures, sonication and stirring /shearing stresses. Therefore, it is highly likely that during the encapsulation process, either partial or complete unfolding occurs which can lead to aggregation and loss of activity of

protein and may also lead to lower encapsulation of proteins since a part of protein mass would be present as aggregates. Various mechanisms through which aggregation can occur are summarized in a review by Philo et al. (Philo and Arakawa, 2009) and **Figure 3.1** illustrates these mechanisms. Precipitation of aggregates and physical adsorption of the partially or completely unfolded proteins may also occur as a result of protein unfolding.

3.3.2 Chemical Instability

Chemical instability refers to either breakage or formation of a new bond in the protein structure. Most common types of chemical instability encountered with proteins are summarized below.

Deamidation

Deamidation is the breakage of the side chain amide bond in side chains of glutamine (Gln) and asparagine (Asn) residues. Deamidation reaction involves the formation of five membered cyclic imide and subsequent hydrolysis of the amide functional group. (Manning et al., 1989; Wang, 1999). Since the hydrolysis of the amide bond involves succeeding amino acid, deamidation is dependent on the steric hindrance of the neighboring amino acid residues. Studies in peptides where the neighboring amino acid to Asn was changed from Glycine (Gly) to Leucine (Leu), the rate of deamidation slowed down by 50-fold due to increased steric hindrance of Leu compared to Gly (Geiger and Clarke, 1987). Deamidation of Asn is more common in alkaline pH solutions (Haley et al., 1966). The effects of deamidation on biological activity of proteins have been highly variable. Deamidation may lead to decrease or loss of biological activity (Charache et al., 1977; Friedman et al., 1991; Moss et al., 2005), no change in biological activity (Brange et al., 1992) or may even lead to increase in biological activity (Furaya et al., 2006). In some cases, extensive aggregation

resulting from initial deamidation has also been observed (Nilsson et al., 2002). Thus, any potential for deamidation of protein should be confirmed if formulation conditions if alkaline pH is employed during formulation of proteins in nanocarriers.

Oxidation

Methionine (Met), Cysteine (Cys), Histidine(His), Tyrosine (Tyr) and Tryptophan (Trp) are the most common sites of oxidation in proteins. Oxidation may occur due to atmospheric oxygen, dissolved oxygen radicals in solution, metal ions and light (photooxidation). Met and Cys are more susceptible to oxidation due to the presence of thiol groups. Met oxidation results in formation of methionone sulfoxide and methionine sufone and Cys oxidation leads to the formation of sulfenic acid and cysteic acid (Manning et al., 1989; Wang, 1999). Depending on the location of oxidation susceptible amino acids, formation of intermolecular and intramolecular disulfide bonds are possible. Intramolecular disulfide linkage may lead to changes in conformation of proteins which results in aggregation and intermolecular crosslinks and then possibly to the formation of higher order aggregates (Astafieva et al., 1996; Li et al., 1995). Bityrosine intermolecular linkages have also been reported (Cromwell et al., 2006). The position of the amino acid susceptible to oxidation also influences extent of oxidation. For example, Met^{170} in human growth hormone is not susceptible to hydrogen peroxide exposure whereas Met^{14} oxidation has been observed in biosynthetic human growth hormone (Becker et al., 1988; Teh et al., 1987). Methionine oxidation has also been reported to lead to loss of biological activity in parathyroid hormone(Nabuchi et al., 1995), human stem cell factor (Hsu et al., 1996), calcitonin (Riniker et al., 1968) and corticotropin releasing factor (Vale et al., 1981) . Thus, it is important to monitor for oxidation of proteins if the protein under consideration is susceptible to oxidation

or conditions employed during formulation (as alkaline pH, metal catalysts and oxidants) promote oxidation.

Hydrolysis/Proteolysis

Hydrolysis, or proteolysis, refers to the breakage of peptide bond in the amino acid backbone of protein. Although, peptide linkage is very stable, X-Asp-Y type bonds are most susceptible to hydrolysis (Manning et al., 1989; Wang, 1999). It has been reported that the susceptibility of hydrolysis of Asp residues are 100-fold greater than other residues in dilute acids (Schulz, 1967). Aspartic acid-Proline and Asp-Gly peptide bonds are known to be particularly susceptible (Powell, 1994). Proteolysis at Asp residues has been reported in lysozyme (Ahern and Klibanov, 1985) and ribozyme (Zale and Klibanov, 1986) in acidic conditions. In insulin, deamidation reactions at Asn (A-21 or B3) leads to formation of Asp or iso-Asp which then leads to hydrolysis (Brange et al., 1992).

A summary of the most common conditions that can lead to physical and chemical instability in proteins are presented below. Understanding the factors that lead to protein unfolding can help minimize the exposure of proteins to these conditions during nanocarrier formulation.

Organic Solvents

The major force behind maintaining protein stability is hydrophobic interactions in the protein core. Thus, it has been proposed that exposure of proteins to organic solvents leads to denaturation because organic solvents decrease the free energy of unfolding of the non-polar residues in proteins and therefore decreases the free energy difference between folded and unfolded states (Kauzmann, 1959). Rees et al. showed with 23 proteins and 37 different non-aqueous solvents that protein structures are unfolded and elongated in non-aqueous solvents

compared to aqueous solvents (Rees and Singer, 1956). Interestingly, Griebenow et al. showed with lysozyme and subtilisin that mixtures of organic solvents and water induce more unfolding of proteins compared to organic solvents alone (Griebenow and Klibanov, 1996). They used acetonitrile, propanol and tetrahydrofuran as organic solvents and showed that with 60% (v/v) mixtures of organic solvents in water that the α-helix content of proteins was much lower than in pure organic solvents. They attributed this effect to much restricted motion of protein chains in anhydrous environment compared to organic solvent-water mixtures. This observation is also pertinent to presence of organic-water mixtures during preparation of polymeric NPs in w/o or w/o/w emulsions (Sah, 1999).

Temperature

The tendency of proteins to unfold with temperature shows a parabolic relationship. It has been shown that both low and high temperatures tend to induce protein unfolding (Graziano et al., 1997; Privalov, 1990; Privalov and Gill, 1988). Unfolding associated with increase in temperature results from increase in enthalpy and entropy of the system. The increase in unfolding and aggregation upon heating has been observed for many therapeutically relevant proteins like streptokinase (Azuaga et al., 2002) and recombinant human interferon-γ (Mulkerrin and Wetzel, 1989). Higher temperatures (~ 60 ^{o}C for 1 h) have also used in introducing pegylated lipids into preformed liposomes (Iden and Allen, 2001). Thus, the effect of exposure to high temperatures on encapsulated proteins should be evaluated. At low temperatures, interaction of non polar residues with water has been suggested to drive the unfolding of proteins. It has been proposed that the penalty of unfavorable interaction between non polar residues in proteins and water decrease with decrease in temperature and results in unfolding. This low temperature induced unfolding

phenomenon has been termed as cold denaturation (Graziano et al., 1997; Privalov, 1990; Privalov and Gill, 1988). An assessment of effect of freeze thaw cycles on protein stability during lyophilization cycle development of therapeutic proteins is very common (Carpenter et al., 1997; Tang and Pikal, 2004). Cold denaturation is also very pertinent to encapsulation of proteins in liposomes as use of freeze thaw cycles has been suggested as a method to increase entrapment of protein in liposomes (Mayer et al., 1986; Mayer et al., 1985; Pick, 1981). As proteins are sensitive to both high and low temperatures, the effect of freeze thaw on protein stability should also be considered.

Solution conditions (pH, ionic strength and salts)

Proteins are composed of both positively-charged (eg. lysine, arginine) and negatively-charged (eg. glutamic acid, aspartic acid) amino acids. The pH at which a protein carries equal negative and positive charge is known as isoelectric point (PI). The overall charge of the protein depends on solution pH. If the pH of solution is below the PI of the protein, protein carries a net positive charge and if the solution pH is above the PI of the protein, the net charge on protein is negative. pH and charge density plays an important role in protein unfolding (Chi et al., 2003b). At extremes of pH, protein unfolding is observed because the charge density on the folded protein is higher than in unfolded form (Dill, 1990). At a pH near the PI of the protein, aggregation can be observed because the overall charge of protein is very low near its PI and can be insufficient for maintaining colloidal stability. Colloidal stability between two protein particles can be explained on the basis of DLVO theory (Derjaguin and Landau, 1941; Verwey and Overbeek, 1948). According to this theory, the overall potential energy on a particle is a sum of opposing electrostatic repulsive and van der Waals attractive forces. Particles can be colloidally stable if they are sufficiently charged to

maintain repulsive forces and maintain a separation distance. However, if the repulsive forces of the particles are not sufficient to keep them apart then they can collide and aggregate. Apart from pH, ionic strength can also play an important role in protein stability and aggregation as it has been reported that under high salt concentrations, ions can shield the inherent charge of the protein and decrease the repulsive forces leading to aggregation (Chi et al., 2003a). The effect of salt type on protein stability has been explained on the basis of hoffmeister series in which ions are arranged according to their potential to stabilize or destabilize proteins. Altering the structure of water bound to proteins and direct binding of ions to macromolecules have been suggested to be the causes of the ranking of ions in the series (Zhang and Cremer, 2006). Additionally, as mentioned above, the pH can also influence chemical stability of proteins. Therefore, the evaluation of pH, ionic strength and salt conditions on physical and chemical stability of proteins is important.

3.4 Need for Evaluating Protein Stability as Part of Protein Delivery Approach

Proteins are polymers of amino acids which fold into specific compact three dimensional structures in their native state. Proteins are very susceptible to change in their environment and can participate in many different interactions, from non-specific hydrophobic interactions to van der Waals attraction to electrostatic repulsion. These interactions can lead to proteins degradation, typically classified as physical or chemical degradation, through a variety of mechanisms: unfolding, aggregation, or change in chemical integrity. Each of these paths is deleterious and ultimately leads to decreased activity of the therapeutic. As listed above, many delivery strategies ranging from classic PLGA NPs, liposomes to newer approaches like fusion proteins and stapled peptides have been proposed for enhancing intracellular delivery of proteins, however these strategies impose a variety of

stresses on the protein during formulation and regardless of method, primarily the focus of studies is on the delivery of the biologic to the site of action; rarely conformational stability and chemical integrity of the delivered biologic was addressed. Three dimensional protein structure (or conformation) and chemical integrity plays an important role in execution of their biological function. Thus, factors that may lead to physical and chemical instability in proteins should be addressed in conjuction with approaches being investigated to enhance intracellular protein delivery.

3.5 Importance of Inducing Endosomal Release in Intracellular Protein Delivery

Internalization of therapeutic cargo in cells often involves endocytosis, a pathway where various therapeutic cargo is taken up by cells into intracellular vesicles called endosomes. One of the major challenges in intracellular protein delivery is inducing release of therapeutic cargo from endosomes to cytosol. Early endosomes have an acidic environment (pH 5) and mature to late endosomes which can fuse with lysosomes (cellular organelles rich in proteolytic enzymes (Bareford and Swaan, 2007). A schematic of endocytic pathway is shown in **Figure 3.2**. To overcome the challenge of therapeutic cargo entrapped in endosomes, researchers have focused on understanding mechanisms of endosomal release and on agents that can induce endosomal release. Much inspiration in this area comes from viruses, which are naturally engineered with components capable of inducing endosomal release. Fusion of viral components with endosomal lipid membranes and pore formation in the endosomal membrane have been suggested as mechanisms used by viruses to induce release of viral proteins in cytosol of cells (Greber et al., 1993; Hogle, 2002). Various natural and chemical agents have been researched and used for inducing endosomal escape for intracellular delivery of proteins. The mechanisms by which these

natural and chemical agents induce endosomal release are pore formation in endosomal membrane, fusion with endosomal membrane, and disrupting endosomal membrane by proton sponge effect or photochemical sensitizers (Cho et al., 2003; Liang and Lam, 2012; Varkouhi et al., 2011). Some examples of agents which have been used for intracellular protein delivery include cationic lipids such as DOTAP where tertiary amine groups interact with anionic endosomal lipids to form inverted hexagonal structures (HII) and induce endosomal release of cargo. Inclusion of cholesterol and dioleoyl-sn-glycero-phosphoethanolamine (DOPE) with DOTAP has been suggested to enhance HII phase formation and enhance endosomal release (Cho et al., 2003; Hafez et al., 2001). Trans-activating transcriptional activator (TAT) peptide has been used for both internalization of hydrophilic protein cargo through plasma membrane and induction of endosomal release. TAT peptide contains arginine and lysine amino acid residues which help in membrane penetration and destabilization (Trabulo et al., 2010). Polymers like polyethyleneimine (PEI) have titratable amine residues which upon protonation can induce influx of ions and water from cytosol to endosome and induce endosomal rupture. PEI polymers have been used for protein delivery but suffer from disadvantages of high toxicity (Didenko et al., 2005). Various small molecules like chloroquine and methylamine can also induce endosome rupture but also have high toxicity (Mellman et al., 1986). These mechanisms and various agents for inducing endosomal release have recently been reviewed and should be referred for further details (Bareford and Swaan, 2007; Liang and Lam, 2012; Varkouhi et al., 2011).

The above discussion emphasizes the importance of pursuing a holistic approach to intracellular delivery of proteins where intracellular protein delivery approach should focus on developing strategies that overcome challenge of protein entrapment and stability in

delivery system, its cellular uptake and inducing endosomal release. Therefore, the evaluation of structural and chemical integrity of the protein cargo should be an integral part of assessment of the success of the delivery system. The following sections will focus on the protein Cyt c as its intracellular delivery to induce apoptosis in breast cancer cells *in-vitro* was studied.

3.6 Cytochrome C Structure and Properties

Cytochrome c is a 12 KDa heme protein, composed of 104 amino acids. It is a basic protein with 8 positive charges at physiological pH. It is an almost globular protein with a channel running from outer surface up to the heme atom known as the "heme crevice" (Dickerson, 1971). Heme in Cyt c is bound covalently to two cysteines (Cys ^{14} and Cys ^{17}) and also bound co-ordinatively to Met ^{80} and His^{18} (Mirkin et al., 2007). Cytochrome c amino acid sequences have been extremely conserved across various species. Additionally, the charge distribution of lysines on the sides of the molecule lining the hydrophobic core and negative character on one side of molecule is also conserved (Dickerson, 1971) (**Figure 3.3**). Cyt c plays a very important role in respiration as an electron carrier between complex III and complex IV in mitochondria and recently, Cytochrome c has also been implicated to play a very important role in apoptosis (Ow et al., 2008).

3.7 Role of Cyt c in Apoptosis

Apoptosis is a tightly regulated form of cell death, triggered when a cell senses that it is in its best interest to quietly die rather than passing the harmful metabolites or signals to neighboring cells. The concept of apoptosis or programmed cell death has evolved over the years and it is understood now that apoptosis (**Figure 3.4**) occurs via an intrinsic pathway or extrinsic pathway (Kasibhatla and Tseng, 2003). Intrinsic apoptosis pathway is initiated via

growth factors, cytokines, DNA damage and proceeds through mitochondria. The intrinsic apoptotic signals such as increased reactive oxygen species (ROS) levels in cells triggers release of Cyt c, a mitochondrial protein into cytoplasm where Cyt c participates and facilitates apoptotic protease activating factor 1 (APAF1) and caspase 9 recruitment into a complex known as apoptosome. This then leads to activation of caspase 9 and further activation of effector caspases. Members of the BCL2 gene family are important players in execution of intrinsic apoptosis. They are classified into the pro-apoptotic members Bax (BCL-2 associated X protein), Bak (BCL-2 homologous antagonist/killer) and BID (BCL-2 Interacting Domain) and anti-apoptotic members BCL2, BCL-xl (Basal cell lymphoma-extra large), MCL1 (Myeloid cell leukemia sequence 1).

The antiapoptotic members complex with the pro-apoptotic proteins and prevent them from initiating the caspase cascade. Once activated, t-BID helps Bax and Bak oligomerization and these oligomerized proapoptotic proteins form pores in the mitochondrial membrane through which proteins such as Cyt c move into cytoplasm and initiate apoptosome formation and caspase activation (Hickman, 1992; Kasibhatla and Tseng, 2003; Lowe and Lin, 2000). Extrinsic apoptosis pathway includes death receptors such as Fas/CD95, TNFR1, DR3, DR4 and DR5. Activation of these pathways leads ultimately to caspase 8 activation which activates the effector caspases such as caspase 3 ultimately responsible for cellular protein digestion and cell shrinkage. Caspases are a group of enzymes in the cells abbreviated for cysteine aspartate proteases. Apoptosis also involves translocation of phosphatidyl serine from inner to outer leaflet of the plasma membrane.

3.8 Altered Apoptosis Pathways in Breast Cancer

As mentioned above BCL2, BCL-xl, MCL1 belong to antiapoptotic family proteins and Bax, Bak and BID belong to proapoptotic protein family members. There are several studies indicating an imbalance between antiapoptotic and proapoptotic proteins in breast cancer. Reduction in expression of Bax, an important protein required in mitochondrial pore formation and Cyt c release has been observed in primary breast cancer tissues which also correlated well with overall survival (Krajewski et al., 1995). The expression of Bax in 119 women with metastatic breast cancer was studied via immunohistochemical analysis. Results from the studies of Bargou et al. in human breast tumors grown *in-vivo* in SCID mice also showed decreased Bax expression and that the expression was revived by gene transfer (Bargou et al., 1996). As far as BCL-2 protein is concerned, over expression of BCL-2 and BCL-xl in breast cancer has been observed in number of studies (Callagy et al., 2008; Krajewski et al., 1999; Nadler et al., 2008; Reed, 1996; Teixeira et al., 1995; Thomadaki and Scorilas, 2008). In a study by Krajewski et al. BCL-2 protein over expression was found in 80% of tumors tested which included both node positive and negative primary tumors.

3.9 Potential of Delivering Cyt C as an Anticancer Nanotherapeutic in Breast Cancer cells

Cytochrome c microinjected in various cancer cells has shown to activate apoptotic cell death.(Li et al., 1997; Schafer et al., 2006; Zhivotovsky et al., 1998) Zhivotovsky et al.(Zhivotovsky et al., 1998) showed induction of apoptosis after microinjection of 20 uM Cyt c in normal rat kidney cells (NRK cells). Li et al. (Li et al., 1997) also observed apoptosis after microinjection of Cyt c in human embryonic kidney 293 cells. They also tested other heme containing proteins such as myoglobin, hemoglobin in order to check for

specificity of Cyt c in inducing apoptotic cell death and only Cyt c was shown to induce apoptosis. Interestingly, breast cancer cells show unique sensitivity to apoptosis to exogenously administered Cyt c. It has been shown that when cytosolic extracts from various cell lines were supplemented with exogenous Cyt c and monitored for caspase activity, higher caspase activity was observed in a series of malignant mammary epithelial cell lines compared to cancer cells from other origin such as lung, prostate, colon and ovary(Schafer et al., 2006). Thus, Cyt c is a direct and specific apoptogen and a viable anticancer agent especially for the treatment of breast cancer.

However, due to its hydrophilic, positively charged nature and propensity for degradation by plasma proteases, Cyt c lacks the physicochemical characteristics required for successful permeation and delivery to cancer cells. Thus, it requires a carrier to mediate its intracellular delivery.

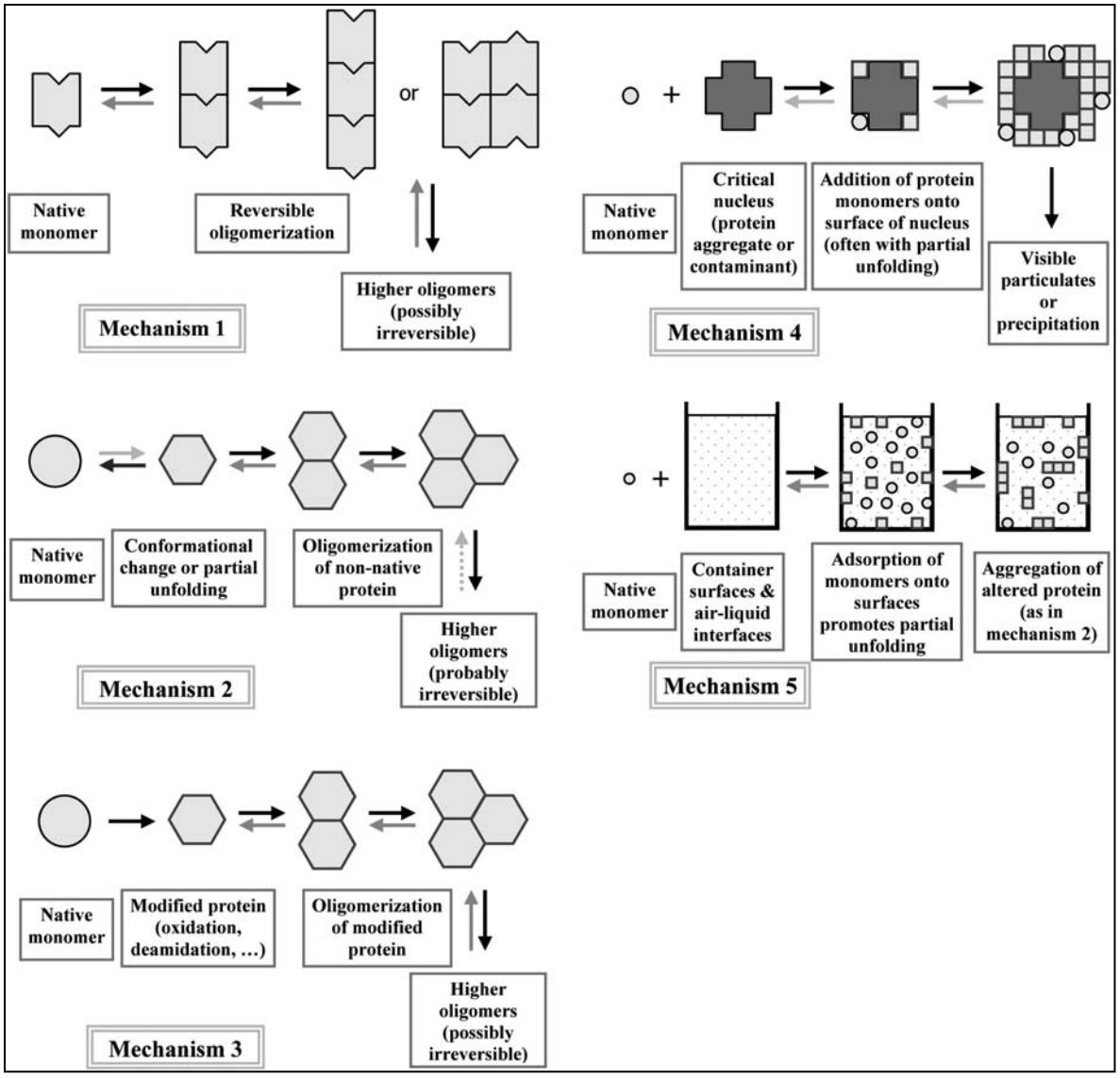

Figure 3.1 Schematic illustrating common protein aggregation mechanisms (1) native protein aggregation, (2) aggregation of conformationally altered protein, (3) aggregation of chemically altered protein, (4) nucleus assisted protein aggregation and (5) aggregation due to inceased air water interface and adsorption on container walls. Figure from Philo et al. (Philo and Arakawa, 2009).

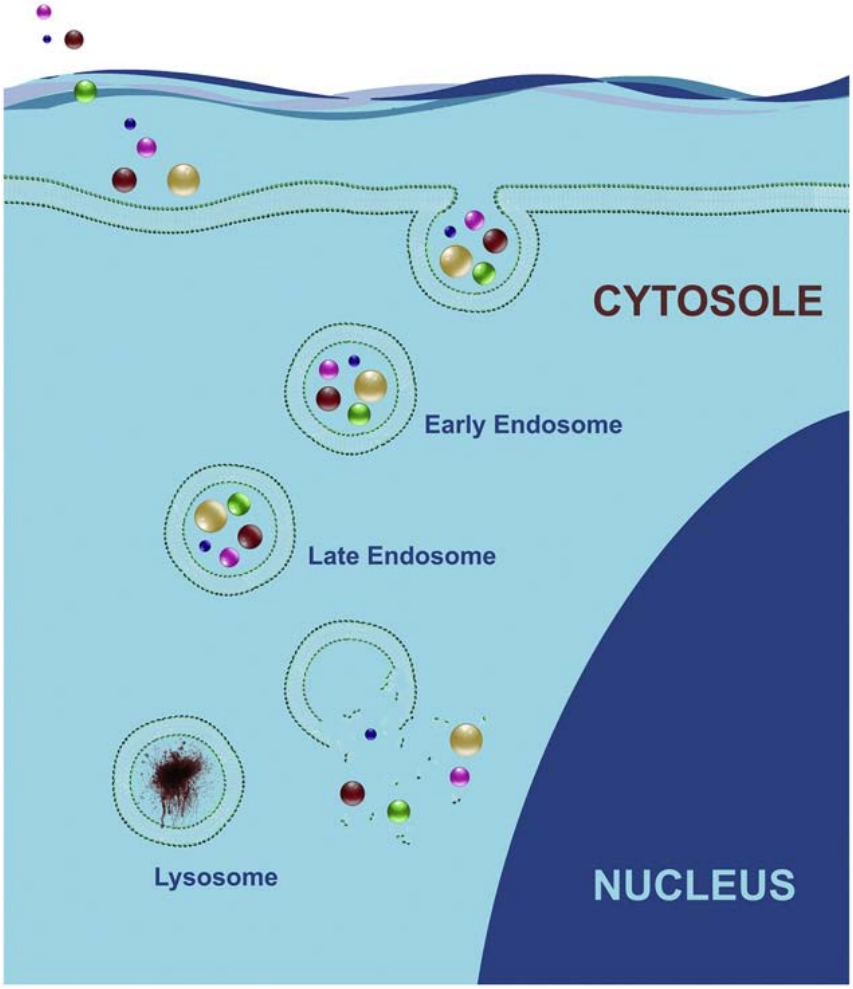

Figure 3.2 Schematic illustrating endosomal release as major challenge in intracellular protein delivery. Therapeutic protein cargo (different colored spheres) can be taken by endocytic pathway into early endosomes which later mature into late endosomes and fuse with lysosomes. Lysosomes are cellular organalles rich in proteolytic enzymes and can denature protein. Therefore, efficient endosomal release is central to efficacy of protein delivery systems. Figure from Varkouhi et al. (Varkouhi et al., 2011)

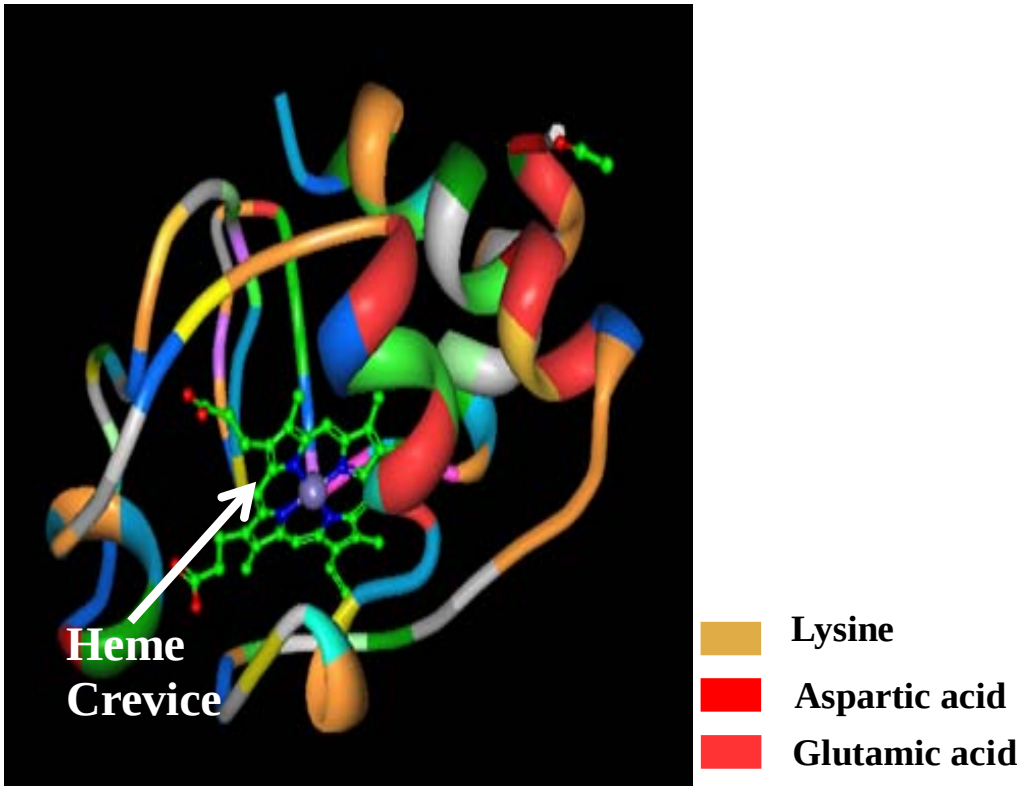

Figure 3.3 Cytochrome c (Cyt c) - three dimensional structure. Cytochrome c is a globular protein with a heme moiety in the centre. Cytochrome c is lined with positively-charged lysines on either side of heme crevice and negatively-charged amino acids on one end. Figure from protein data bank (Bushnell et al., 1990; www.rcsb.org)

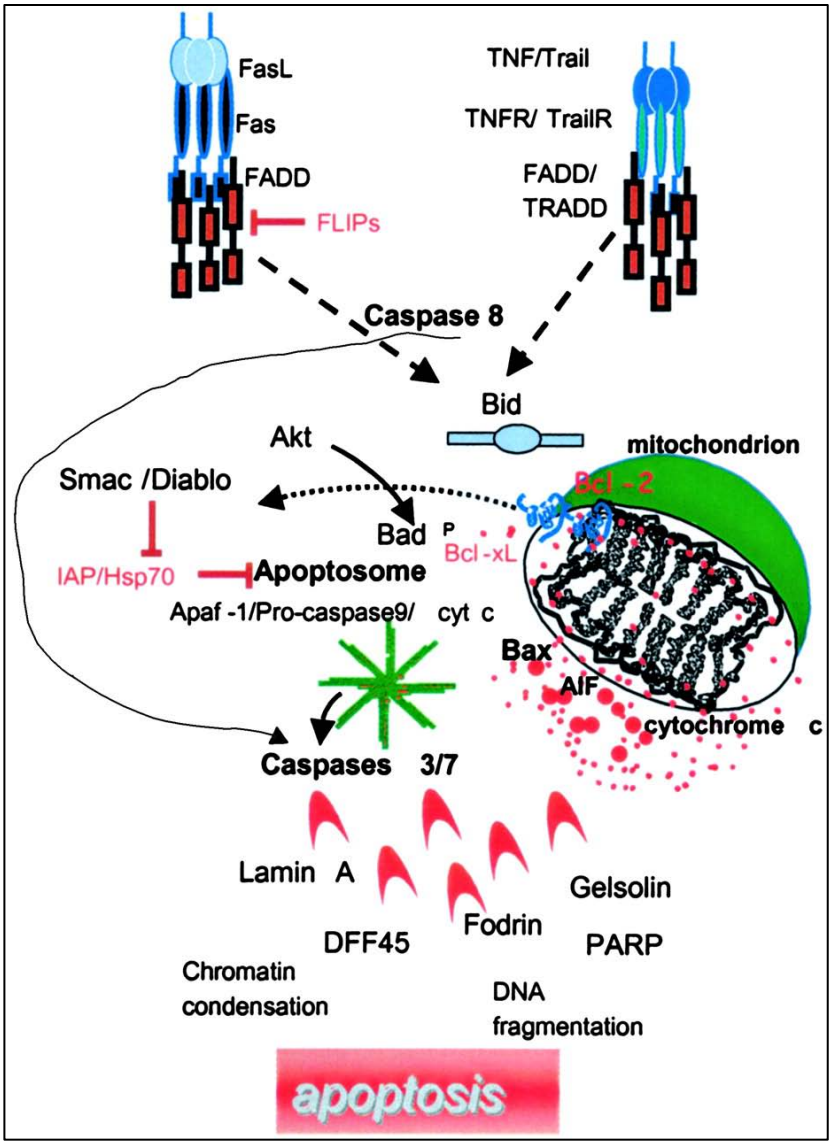

Figure 3.4 Schematic illustrating mechanisms of apoptosis. Intrinsic apoptosis mediates via release of Cyt c from mitochondria and extrinsic apoptosis via death receptors TNF and Fas. Figure from Kashibhatla et al.(Kasibhatla and Tseng, 2003).

3.10 References

Abbing, A., Blaschke, U.K., Grein, S., Kretschmar, M., Stark, C.M., Thies, M.J., Walter, J., Weigand, M., Woith, D.C., Hess, J., Reiser, C.O., 2004. Efficient intracellular delivery of a protein and a low molecular weight substance via recombinant polyomavirus-like particles. J Biol Chem 279, 27410-27421.

Ahern, T.J., Klibanov, A.M., 1985. The mechanisms of irreversible enzyme inactivation at 100C. Science 228, 1280-1284.

Astafieva, I.V., Eberlein, G.A., Wang, Y.J., 1996. Absolute on-line molecular mass analysis of basic fibroblast growth factor and its multimers by reversed-phase liquid chromatography with multi-angle laser light scattering detection. J Chromatogr A 740, 215-229.

Azuaga, A.I., Dobson, C.M., Mateo, P.L., Conejero-Lara, F., 2002. Unfolding and aggregation during the thermal denaturation of streptokinase. Eur J Biochem 269, 4121-4133.
Bareford, L.M., Swaan, P.W., 2007. Endocytic mechanisms for targeted drug delivery. Adv Drug Deliv Rev 59, 748-758.

Bargou, R.C., Wagener, C., Bommert, K., Mapara, M.Y., Daniel, P.T., Arnold, W., Dietel, M., Guski, H., Feller, A., Royer, H.D., Dorken, B., 1996. Overexpression of the death-promoting gene bax-alpha which is downregulated in breast cancer restores sensitivity to different apoptotic stimuli and reduces tumor growth in SCID mice. J Clin Invest 97, 2651-2659.

Becker, G.W., Tackitt, P.M., Bromer, W.W., Lefeber, D.S., Riggin, R.M., 1988. Isolation and characterization of a sulfoxide and a desamido derivative of biosynthetic human growth hormone. Biotechnol Appl Biochem 10, 326-337.

Bernal, F., Wade, M., Godes, M., Davis, T.N., Whitehead, D.G., Kung, A.L., Wahl, G.M., Walensky, L.D., 2010. A stapled p53 helix overcomes HDMX-mediated suppression of p53. Cancer Cell 18, 411-422.

Brange, J., Langkjaer, L., Havelund, S., Volund, A., 1992. Chemical stability of insulin. 1. Hydrolytic degradation during storage of pharmaceutical preparations. Pharm Res 9, 715-726.

Briscoe, P., Caniggia, I., Graves, A., Benson, B., Huang, L., Tanswell, A.K., Freeman, B.A., 1995. Delivery of superoxide dismutase to pulmonary epithelium via pH-sensitive liposomes. Am J Physiol 268, L374-380.

Bushnell, G.W., Louie, G.V., Brayer, G.D., 1990. High-resolution three-dimensional structure of horse heart cytochrome c. J Mol Biol 214, 585-595.

Callagy, G.M., Webber, M.J., Pharoah, P.D., Caldas, C., 2008. Meta-analysis confirms BCL2 is an independent prognostic marker in breast cancer. BMC Cancer 8, 153.

Carpenter, J.F., Pikal, M.J., Chang, B.S., Randolph, T.W., 1997. Rational design of stable lyophilized protein formulations: some practical advice. Pharm Res 14, 969-975.

Charache, S., Fox, J., McCurdy, P., Kazazian, H., Jr., Winslow, R., Hathaway, P., van Beneden, R., Jessop, M., 1977. Postsynthetic deamidation of hemoglobin Providence (beta 82 Lys replaced by Asn, Asp) and its effect on oxygen transport. J Clin Invest 59, 652-658.

Chi, E.Y., Krishnan, S., Kendrick, B.S., Chang, B.S., Carpenter, J.F., Randolph, T.W., 2003a. Roles of conformational stability and colloidal stability in the aggregation of recombinant human granulocyte colony-stimulating factor. Protein Sci 12, 903-913.

Chi, E.Y., Krishnan, S., Randolph, T.W., Carpenter, J.F., 2003b. Physical stability of proteins in aqueous solution: mechanism and driving forces in nonnative protein aggregation. Pharm Res 20, 1325-1336.

Cho, Y.W., Kim, J.D., Park, K., 2003. Polycation gene delivery systems: escape from endosomes to cytosol. J Pharm Pharmacol 55, 721-734.

Cromwell, M.E., Hilario, E., Jacobson, F., 2006. Protein aggregation and bioprocessing. AAPS J 8, E572-579.

Dalkara, D., Chandrashekhar, C., Zuber, G., 2006. Intracellular protein delivery with a dimerizable amphiphile for improved complex stability and prolonged protein release in the cytoplasm of adherent cell lines. J Control Release 116, 353-359.

De Rosa, E., Chiappini, C., Fan, D., Liu, X., Ferrari, M., Tasciotti, E., 2011. Agarose surface coating influences intracellular accumulation and enhances payload stability of a nano-delivery system. Pharm Res 28, 1520-1530.

Derjaguin, B.V., Landau, L.D., 1941. Theory of the stability of strongly charged lyophobic sols and of the adhesion of strongly charged particles in solutions of electrolytes. Acta Physicochim URSS 14, 733-762.

Dickerson, R.E., 1971. The structures of cytochrome c and the rates of molecular evolution. J Mol Evol 1, 26-45.

Didenko, V.V., Ngo, H., Baskin, D.S., 2005. Polyethyleneimine as a transmembrane carrier of fluorescently labeled proteins and antibodies. Anal Biochem 344, 168-173.

Dill, K.A., 1990. Dominant forces in protein folding. Biochemistry 29, 7133-7155.
Evaluatepharma, 2012. http://www.evaluatepharma.com/Press-Release-EvaluatePharma-Surveys-Tomorrows-BioPharma-Landscape-Providing-Close-Up-Look-at-NASDAQ-Biotech-Index.aspx.

Foltopoulou, P.F., Tsiftsoglou, A.S., Bonovolias, I.D., Ingendoh, A.T., Papadopoulou, L.C., 2010. Intracellular delivery of full length recombinant human mitochondrial L-Sco2 protein

into the mitochondria of permanent cell lines and SCO2 deficient patient's primary cells. Biochim Biophys Acta 1802, 497-508.

Friedman, A.R., Ichhpurani, A.K., Brown, D.M., Hillman, R.M., Krabill, L.F., Martin, R.A., Zurcher-Neely, H.A., Guido, D.M., 1991. Degradation of growth hormone releasing factor analogs in neutral aqueous solution is related to deamidation of asparagine residues. Replacement of asparagine residues by serine stabilizes. Int J Pept Protein Res 37, 14-20.

Frokjaer, S., Otzen, D.E., 2005. Protein drug stability: a formulation challenge. Nat Rev Drug Discov 4, 298-306.

Furaya, K., Johnson-Jackson, D., Ruscio, D.T., 2006. Deamidated Interferon-Beta, United States.

Geiger, T., Clarke, S., 1987. Deamidation, isomerization, and racemization at asparaginyl and aspartyl residues in peptides. Succinimide-linked reactions that contribute to protein degradation. J Biol Chem 262, 785-794.

Gibbons, A., Padilla-Carlin, D., Kelly, C., Hickey, A.J., Taggart, C., McElvaney, N.G., Cryan, S.A., 2011. The effect of liposome encapsulation on the pharmacokinetics of recombinant secretory leukocyte protease inhibitor (rSLPI) therapy after local delivery to a guinea pig asthma model. Pharm Res 28, 2233-2245.

Gibbons, A.M., McElvaney, N.G., Taggart, C.C., Cryan, S.A., 2009. Delivery of rSLPI in a liposomal carrier for inhalation provides protection against cathepsin L degradation. J Microencapsul 26, 513-522.

Graziano, G., Catanzano, F., Riccio, A., Barone, G., 1997. A reassessment of the molecular origin of cold denaturation. J Biochem 122, 395-401.

Greber, U.F., Willetts, M., Webster, P., Helenius, A., 1993. Stepwise dismantling of adenovirus 2 during entry into cells. Cell 75, 477-486.

Griebenow, K., Klibanov, A.M., 1996. On Protein Denaturation in Aqueous-Organic Mixtures but Not in Pure Organic Solvents. Journal of American Chemical Society 118, 11695-11700.

Gu, Z., Biswas, A., Zhao, M., Tang, Y., 2011. Tailoring nanocarriers for intracellular protein delivery. Chem Soc Rev 40, 3638-3655.

Hafez, I.M., Maurer, N., Cullis, P.R., 2001. On the mechanism whereby cationic lipids promote intracellular delivery of polynucleic acids. Gene Ther 8, 1188-1196.

Haley, E.E., Corcoran, B.J., Dorer, F.E., Buchanan, D.L., 1966. Beta-aspartyl peptides in enzymatic hydrolysates of protein. Biochemistry 5, 3229-3235.

Hickman, J.A., 1992. Apoptosis induced by anticancer drugs. Cancer Metastasis Rev 11, 121-139.

Hogle, J.M., 2002. Poliovirus cell entry: common structural themes in viral cell entry pathways. Annu Rev Microbiol 56, 677-702.

Hsu, Y.R., Narhi, L.O., Spahr, C., Langley, K.E., Lu, H.S., 1996. In vitro methionine oxidation of Escherichia coli-derived human stem cell factor: effects on the molecular structure, biological activity, and dimerization. Protein Sci 5, 1165-1173.

Iden, D.L., Allen, T.M., 2001. In vitro and in vivo comparison of immunoliposomes made by conventional coupling techniques with those made by a new post-insertion approach. Biochim Biophys Acta 1513, 207-216.

Jiskoot, W., Randolph, T.W., Volkin, D.B., Middaugh, C.R., Schoneich, C., Winter, G., Friess, W., Crommelin, D.J., Carpenter, J.F., 2011. Protein instability and immunogenicity: roadblocks to clinical application of injectable protein delivery systems for sustained release. J Pharm Sci 101, 946-954.

Kasibhatla, S., Tseng, B., 2003. Why target apoptosis in cancer treatment? Mol Cancer Ther 2, 573-580.

Kauzmann, W., 1959. Some factors in the interpretation of protein denaturation. Adv Protein Chem 14, 1-63.

Krajewski, S., Blomqvist, C., Franssila, K., Krajewska, M., Wasenius, V.M., Niskanen, E., Nordling, S., Reed, J.C., 1995. Reduced expression of proapoptotic gene BAX is associated with poor response rates to combination chemotherapy and shorter survival in women with metastatic breast adenocarcinoma. Cancer Res 55, 4471-4478.

Krajewski, S., Krajewska, M., Turner, B.C., Pratt, C., Howard, B., Zapata, J.M., Frenkel, V., Robertson, S., Ionov, Y., Yamamoto, H., Perucho, M., Takayama, S., Reed, J.C., 1999. Prognostic significance of apoptosis regulators in breast cancer. Endocr Relat Cancer 6, 29-40.

Kundu, J., Chung, Y.I., Kim, Y.H., Tae, G., Kundu, S.C., 2009. Silk fibroin nanoparticles for cellular uptake and control release. Int J Pharm 388, 242-250.

Lackey, C.A., Press, O.W., Hoffman, A.S., Stayton, P.S., 2002. A biomimetic pH-responsive polymer directs endosomal release and intracellular delivery of an endocytosed antibody complex. Bioconjug Chem 13, 996-1001.

Langer, R., 1990. New methods of drug delivery. Science 249, 1527-1533.

Lee, Y., Ishii, T., Cabral, H., Kim, H.J., Seo, J.H., Nishiyama, N., Oshima, H., Osada, K., Kataoka, K., 2009. Charge-conversional polyionic complex micelles-efficient nanocarriers for protein delivery into cytoplasm. Angew Chem Int Ed Engl 48, 5309-5312.

Li, F., Srinivasan, A., Wang, Y., Armstrong, R.C., Tomaselli, K.J., Fritz, L.C., 1997. Cell-specific induction of apoptosis by microinjection of cytochrome c. Bcl-xL has activity independent of cytochrome c release. J Biol Chem 272, 30299-30305.

Li, S., Schoneich, C., Borchardt, R.T., 1995. Chemical instability of protein pharmaceuticals: Mechanisms of oxidation and strategies for stabilization. Biotechnol Bioeng 48, 490-500.
Liang, W., Lam, J.K.W., 2012. Molecular Regulation of Endocytosis. Intech.

Lin-Lee, Y.C., Nakamura, S., Gandhi, V., Curley, S.A., Stuber, D., Burkot, T.R., Kuo, M.T., 2002. Prolonged stability and sustained prodrug cell killing activity using receptor-mediated delivery of malarial circumsporozoite-cytosine deaminase fusion protein into liver cancer cells. Mol Cancer Ther 1, 461-467.

Li, Y., Wang, J., Wientjes, M.G., Au, J.L., 2012. Delivery of nanomedicines to extracellular and intracellular compartments of a solid tumor. Adv Drug Deliv Rev 64, 29-39.

Lowe, S.W., Lin, A.W., 2000. Apoptosis in cancer. Carcinogenesis 21, 485-495.
Manning, M.C., Patel, K., Borchardt, R.T., 1989. Stability of protein pharmaceuticals. Pharm Res 6, 903-918.

Matsumura, M., Becktel, W.J., Matthews, B.W., 1988. Hydrophobic stabilization in T4 lysozyme determined directly by multiple substitutions of Ile 3. Nature 334, 406-410.

Mayer, L.D., Bally, M.B., Hope, M.J., Cullis, P.R., 1986. Techniques for encapsulating bioactive agents into liposomes. Chem Phys Lipids 40, 333-345.

Mayer, L.D., Hope, M.J., Cullis, P.R., Janoff, A.S., 1985. Solute distributions and trapping efficiencies observed in freeze-thawed multilamellar vesicles. Biochim Biophys Acta 817, 193-196.

Mellman, I., Fuchs, R., Helenius, A., 1986. Acidification of the endocytic and exocytic pathways. Annu Rev Biochem 55, 663-700.

Mirkin, N., Jaconcic, J., Stojanoff, V., Moreno, A., 2007. High resolution X-ray crystallographic structure of bovine heart cytochrome c and its application to the design of an electron transfer biosensor. Proteins: Structure, Function, and Bioinformatics 17, 83-92.

Moellering, R.E., Cornejo, M., Davis, T.N., Del Bianco, C., Aster, J.C., Blacklow, S.C., Kung, A.L., Gilliland, D.G., Verdine, G.L., Bradner, J.E., 2009. Direct inhibition of the NOTCH transcription factor complex. Nature 462, 182-188.

Morris, M.C., Depollier, J., Mery, J., Heitz, F., Divita, G., 2001. A peptide carrier for the delivery of biologically active proteins into mammalian cells. Nat Biotechnol 19, 1173-1176.

Moss, C.X., Matthews, S.P., Lamont, D.J., Watts, C., 2005. Asparagine deamidation perturbs antigen presentation on class II major histocompatibility complex molecules. J Biol Chem 280, 18498-18503.

Mulkerrin, M.G., Wetzel, R., 1989. pH dependence of the reversible and irreversible thermal denaturation of gamma interferons. Biochemistry 28, 6556-6561.

Mumtaz, S., Bachhawat, B.K., 1994. Enhanced intracellular stability and efficacy of PEG modified dextranase in the treatment of a model storage disorder. Biochim Biophys Acta 1199, 175-182.

Nabuchi, Y., Fujiwara, E., Ueno, K., Kuboniwa, H., Asoh, Y., Ushio, H., 1995. Oxidation of recombinant human parathyroid hormone: effect of oxidized position on the biological activity. Pharm Res 12, 2049-2052.

Nadler, Y., Camp, R.L., Giltnane, J.M., Moeder, C., Rimm, D.L., Kluger, H.M., Kluger, Y., 2008. Expression patterns and prognostic value of Bag-1 and Bcl-2 in breast cancer. Breast Cancer Res 10, R35.

Nilsson, M.R., Driscoll, M., Raleigh, D.P., 2002. Low levels of asparagine deamidation can have a dramatic effect on aggregation of amyloidogenic peptides: implications for the study of amyloid formation. Protein Sci 11, 342-349.

Ow, Y.P., Green, D.R., Hao, Z., Mak, T.W., 2008. Cytochrome c: functions beyond respiration. Nat Rev Mol Cell Biol 9, 532-542.

Pace, C.N., Shirley, B.A., McNutt, M., Gajiwala, K., 1996. Forces contributing to the conformational stability of proteins. FASEB J 10, 75-83.

Pekar, A.H., Frank, B.H., 1972. Conformation of proinsulin. A comparison of insulin and proinsulin self-association at neutral pH. Biochemistry 11, 4013-4016.

Philo, J.S., Arakawa, T., 2009. Mechanisms of protein aggregation. Curr Pharm Biotechnol 10, 348-351.

PHRMA, 2012. http://www.phrma.org/sites/default/files/1776/biotech2011.pdf.

Pick, U., 1981. Liposomes with a large trapping capacity prepared by freezing and thawing of sonicated phospholipid mixtures. Arch Biochem Biophys 212, 186-194.

Powell, M.F., 1994. Peptide Stability in Aqueous Parentral Formulations. American Chemical Society Washington D.C.

Privalov, P.L., 1990. Cold denaturation of proteins. Crit Rev Biochem Mol Biol 25, 281-305.

Privalov, P.L., Gill, S.J., 1988. Stability of protein structure and hydrophobic interaction. Adv Protein Chem 39, 191-234.

Reddy, M.K., Wu, L., Kou, W., Ghorpade, A., Labhasetwar, V., 2008. Superoxide dismutase-loaded PLGA nanoparticles protect cultured human neurons under oxidative stress. Appl Biochem Biotechnol 151, 565-577.

Reed, J.C., 1996. Balancing cell life and death: bax, apoptosis, and breast cancer. J Clin Invest 97, 2403-2404.

Rees, E.D., Singer, S.J., 1956. A preliminary study of the properties of proteins in some nonaqueous solvents. Arch Biochem Biophys 63, 144-159.

Riniker, B., Neher, R., Maier, R., Kahnt, F.W., Byfield, P.G., Gudmundsson, T.V., Galante, L., MacIntyre, I., 1968. [Human calcitonin. I. Isolation and characterization]. Helv Chim Acta 51, 1738-1742.

Sah, H., 1999. Protein behavior at the water/methylene chloride interface. J Pharm Sci 88, 1320-1325.

Schafer, Z.T., Parrish, A.B., Wright, K.M., Margolis, S.S., Marks, J.R., Deshmukh, M., Kornbluth, S., 2006. Enhanced sensitivity to cytochrome c-induced apoptosis mediated by PHAPI in breast cancer cells. Cancer Res 66, 2210-2218.

Schulz, J., 1967. Cleavage at aspartic acid. Methods Enzymol 11, 255-263.

Shu, S., Zhang, X., Wu, Z., Wang, Z., Li, C., 2010. Gradient cross-linked biodegradable polyelectrolyte nanocapsules for intracellular protein drug delivery. Biomaterials 31, 6039-6049.

Soane, L., Fiskum, G., 2005. TAT-mediated endocytotic delivery of the loop deletion Bcl-2 protein protects neurons against cell death. J Neurochem 95, 230-243.

Son, S., Lee, W.R., Joung, Y.K., Kwon, M.H., Kim, Y.S., Park, K.D., 2009. Optimized stability retention of a monoclonal antibody in the PLGA nanoparticles. Int J Pharm 368, 178-185.

Tang, X., Pikal, M.J., 2004. Design of freeze-drying processes for pharmaceuticals: practical advice. Pharm Res 21, 191-200.

Teh, L.C., Murphy, L.J., Huq, N.L., Surus, A.S., Friesen, H.G., Lazarus, L., Chapman, G.E., 1987. Methionine oxidation in human growth hormone and human chorionic somatomammotropin. Effects on receptor binding and biological activities. J Biol Chem 262, 6472-6477.

Teixeira, C., Reed, J.C., Pratt, M.A., 1995. Estrogen promotes chemotherapeutic drug resistance by a mechanism involving Bcl-2 proto-oncogene expression in human breast cancer cells. Cancer Res 55, 3902-3907.

Thomadaki, H., Scorilas, A., 2008. Molecular profile of the BCL2 family of the apoptosis related genes in breast cancer cells after treatment with cytotoxic/cytostatic drugs. Connect Tissue Res 49, 261-264.

Torchilin, V.P., Lukyanov, A.N., 2003. Peptide and protein drug delivery to and into tumors: challenges and solutions. Drug Discov Today 8, 259-266.

Torchilin, V.P., 2006. Multifunctional nanocarriers. Adv Drug Deliv Rev 58, 1532-1555.

Trabulo, S., Cardoso, A.L., Mano, M., Lima, M.C.P.d., 2010. Cell-Penetrating Peptides—Mechanisms of Cellular Uptake and Generation of Delivery Systems. Pharmaceuticals 3, 961-993.

Vale, W., Spiess, J., Rivier, C., Rivier, J., 1981. Characterization of a 41-residue ovine hypothalamic peptide that stimulates secretion of corticotropin and beta-endorphin. Science 213, 1394-1397.

Varkouhi, A.K., Scholte, M., Storm, G., Haisma, H.J., 2011. Endosomal escape pathways for delivery of biologicals. J Control Release 151, 220-228.

Vazquez, E., Corchero, J.L., Burgueno, J.F., Seras-Franzoso, J., Kosoy, A., Bosser, R., Mendoza, R., Martinez-Lainez, J.M., Rinas, U., Fernandez, E., Ruiz-Avila, L., Garcia-Fruitos, E., Villaverde, A., 2012. Functional inclusion bodies produced in bacteria as naturally occurring nanopills for advanced cell therapies. Adv Mater 24, 1742-1747.

Ventura, S., Villaverde, A., 2006. Protein quality in bacterial inclusion bodies. Trends Biotechnol 24, 179-185.

Verdine, G.L., Hilinski, G.J., 2012. Stapled peptides for intracellular drug targets. Methods Enzymol 503, 3-33.

Verwey, E.J.W., Overbeek, J.T., 1948. Theory of the stability of lyophobic Colloids. Elsevier, Amsterdam.

Villaverde, A., Garcia-Fruitos, E., Rinas, U., Seras-Franzoso, J., Kosoy, A., Corchero, J.L., Vazquez, E., 2012. Packaging protein drugs as bacterial inclusion bodies for therapeutic applications. Microb Cell Fact 11, 76.

Wang, W., 1999. Instability, stabilization, and formulation of liquid protein pharmaceuticals. Int J Pharm 185, 129-188.

Wang, W., 2005. Protein aggregation and its inhibition in biopharmaceutics. Int J Pharm 289, 1-30.

www.rcsb.org, http://www.rcsb.org/pdb/explore/explore.do?structureId=1HRC.

Yadav, S., Laue, T.M., Kalonia, D.S., Singh, S.N., Shire, S.J., 2012. The influence of charge distribution on self-association and viscosity behavior of monoclonal antibody solutions. Mol Pharm 9, 791-802.

Yan, M., Du, J., Gu, Z., Liang, M., Hu, Y., Zhang, W., Priceman, S., Wu, L., Zhou, Z.H., Liu, Z., Segura, T., Tang, Y., Lu, Y., 2010. A novel intracellular protein delivery platform based on single-protein nanocapsules. Nat Nanotechnol 5, 48-53.

Zale, S.E., Klibanov, A.M., 1986. Why does ribonuclease irreversibly inactivate at high temperatures? Biochemistry 25, 5432-5444.

Zhang, Y., Cremer, P.S., 2006. Interactions between macromolecules and ions: The Hofmeister series. Curr Opin Chem Biol 10, 658-663.

Zhivotovsky, B., Orrenius, S., Brustugun, O.T., Doskeland, S.O., 1998. Injected cytochrome c induces apoptosis. Nature 391, 449-450.

Chapter IV

Effect of Carbon Coating on the Physico-chemical Properties and Toxicity of Copper and Nickel Nanoparticles

4.1 Summary

The primary aim of these interdisciplinary studies was to investigate the effect of a distinguishing characteristic, *i.e.*, surface carbon coating on the physico-chemical properties and toxicity of matched pairs of carbon-coated and non-coated copper and nickel NPs (Cu, C-Cu, Ni and C-Ni) in A549 alveolar epithelial cells. The effect of carbon coating on particle size, zeta potential, oxidation state, cellular uptake, release of soluble metal and concentration dependent toxicity of Cu and Ni NPs was systematically evaluated. A significant effect of carbon coating was observed on the physico-chemical properties, interaction with cellular membranes, and overall toxicity of the NPs. Compared to Cu NPs, C-Cu NPs showed protection against surface oxidation, ten-fold higher cellular uptake and 4.4-fold lower release of soluble Cu. Similarly, in toxicity assays significant differences were observed between Cu and C-Cu NPs. Specifically, while C-Cu NPs elicited a pronounced effect on mitochondrial function, Cu NPs were associated with a significant damage to plasma membrane integrity. Compared to Cu and C-Cu NPs, Ni and C-Ni NPs were less

---

S. Minocha, and R.J. Mumper, "Effect of Carbon Coating on the Physico-chemical Properties and Toxicity of Copper and Nickel Nanoparticles." *Small,* 2012 Jul 26. doi: 10.1002/smll.201200478. [Epub ahead of print].

toxic as evaluated by their effect on mitochondrial function and lysosomal membrane integrity. These studies demonstrated that correlations can be drawn between physico-chemical properties and resultant toxicity of NPs as a function of unique NP characteristics such as surface carbon coating.

4.2 Introduction

NPs are being produced in high tonnage for their applications in semiconductor, textile, agricultural and pharmaceutical industries. The estimated market for nanotechnology containing products is expected to reach $ 1 trillion by 2015 (Nel et al., 2006; Roco, 2005). Although the unique properties of NPs such as their higher surface area to volume ratio compared to their bulk counterparts offer exciting opportunities for applications as catalysts, conducting materials, semiconductors and targeted nanotherapeutics, the same unique properties also predispose them to interact more closely with cellular and sub-cellular structures which may lead to a variety of toxicological end points (Magrez et al., 2006; Nel et al., 2006; Oberdorster, 2004). Therefore, much emphasis has been placed upon understanding the toxicity profiles of NPs in order to fully realize the potential of nanotechnology. The concern among industrialists, regulatory authorities, academicians and researchers about the potential health impact of nanotechnology is understandable as exposure to airborne ultrafine particulate material and asbestos has been linked to the occurrence of cardiovascular diseases and mesothelioma, respectively (Seaton et al., 2010). The field of nanotoxicology is still in its infancy and several questions regarding relevant dose and exposure are under debate and unanswered (Rivera Gil et al., 2010; Warheit, 2010). Workplace safety has already been questioned after a recent report that showed possible links between the exposure of workers to NPs and toxicity symptoms (Song et al., 2009). Many challenges are associated with determining the underlying cause of NP toxicity since various particle characteristics such as size, shape, surface area, charge, surface dissolution and coatings can contribute towards toxicity and their role in assessing NP toxicity has been much emphasized (Rivera Gil et al., 2010; Warheit, 2010; Zhao et al., 2011). Therefore, it

becomes difficult to assess the contribution of nanoparticulate state towards a specific observed toxic effect. It has also been reported that the nanometer size range is not always the primary factor that best correlates with NP toxicity. Sayes et al. (2006) showed that when toxicity of rutile, anatase and rutile/anatase forms of TiO_2 NPs were compared in cell-based assays, the anatase TiO_2 polymorph showed higher lactate dehydrogenase (LDH) release in HDF and A549 cells as compared to the rutile polymorph (Sayes et al., 2006). Another important consideration in evaluation of NP toxicity studies is the characterization of NPs in relevant biological media since NPs are usually dispersed in biological media before toxicity testing in vitro. Depending on the media composition such as the presence of serum proteins and varied ionic strength, NP size profiles may be different than that observed in water (Maiorano et al., 2010; Murdock et al., 2008; Warheit, 2008).

Reproducibility of results across different labs is another concern in nanotoxicity studies (Lanone et al., 2009). The variation in toxicity data of NPs in general can be attributed to source, method of dispersion, interference with absorbance or fluorescence and most importantly lack of detailed characterization. For instance, both false positive and false negative results have been reported when carbon nanotube toxicity was tested with MTT (3-(4,5-Dimethyl-2-thiazolyl)-2,5-diphenyl-2H-tetrazolium bromide) assay (Ali-Boucetta et al., 2011; Worle-Knirsch et al., 2006). Similar results were observed while testing carbon NP toxicity with neutral red dye (Monteiro-Riviere and Inman, 2006). As carbon NPs have large surface area and adsorptive properties, neutral red adsorbed on the NP surface showed false negative results. Special precautions, proper controls and use of multiple cytotoxicity assays have been suggested to possibly overcome conflicting results (Stone et al., 2009). Considering that multiple factors can affect NP toxicity, it is increasingly important to

systematically evaluate the toxicity of NPs such that the effect of one characteristic can be studied at one time. Metal based NPs have gained widespread application in several industries. Copper and nickel NPs are commercially relevant and currently used in a variety of applications. Copper NPs are used as bacteriostatic and antifungal agents, conducting inks, batteries, fuel cells, as catalysts and antifouling agents (Barrabes N, 2006; Nicola Cioffi, 2005; Tarasov S, 2002; Yoon et al., 2007; Zhang XF, 2007). Nickel NPs are used for their catalytic and magnetic properties (Park J, 2005; Wang H, 2008). Carbon coating on the surface of metal NPs is a means to protect them against oxidation (Luechinger et al., 2008). Thus, it becomes important to evaluate the effect of surface coating on the physicochemical properties and toxicity of metal NPs. A previous study on copper oxide and C-Cu NPs ascribes differences in toxicity of these NPs to differences in intracellular solubility of copper oxide and C-Cu NPs in buffer acidic solutions mimicking lysosomal conditions (Studer et al., 2010). The conditions for this comparison are buffered systems which do not compare with realistic scenarios where more complex factors such as sonication of particles before suspension and presence of serum can affect solubility and bring about differences in extracellular release of metal ions which can also affect uptake and toxicity of NPs. Therefore, we systematically investigated the effect of surface carbon coating on the physico-chemical properties and toxicity of carbon coated and non-coated copper and nickel NPs in vitro by studying particle size, zeta potential, oxidation state, cellular uptake, release of soluble metal and concentration dependent toxicity of Cu and Ni NPs in cell culture relevant conditions. Our group has been involved in the continuous assessment and prediction of physico-chemical properties of NPs in relation to their biological effects using quantitative – nanostructure activity relationships (Fourches et al., 2010). In this investigation, the

hypothesis was that compared to non-coated Cu and Ni NPs, carbon-coated Cu and Ni NPs will have different physico-chemical properties including their interactions with the surrounding media and cells which will influence the resultant toxicity in cell-based assays.

4.3 Materials and Methods

Materials

Copper, C-Cu, Ni and C-Ni NPs were purchased from Nanostructured and Amorphous Materials Inc. (NanoAmor, Houston, TX). According to NanoAmor, Cu, C-Cu, Ni and C-Ni particles were synthesized using Chemical Vapor Deposition (CVD) method. For coating carbon on the metal, metal and carbon source were electrically heated at the same time (Jiao and Seraphin, 1997; Li et al., 2009). MTT reagent and neutral red dye were purchased from Sigma Aldrich (St. Louis, MO). Ethidium homodimer/calcein AM cell viability kit and DMEM were purchased from Invitrogen (Carlsbad, CA). Cu and Ni ICP/MS standards were purchased from Spex CertiPrep (Metuchen, NJ). A549 alveolar epithelial cell line, Penicillin-streptomycin solution and Fetal Bovine Serum (FBS) were purchased from ATCC. Plasmocin was purchased from Invivogen (San Diego, CA). All chemicals were used without any further purification.

Particle Size and Zeta Potential

Particle size was measured in DI water and DMEM (with and without 10% FBS). Stock of NPs (1 mg/mL) was prepared in DI water after dispersing them using bath sonication (Branson 3510) for three minutes. NPs were further diluted in either DI water or DMEM (+/- 10% FBS) (0.6 μg/mL) for particle size analysis using Beckman Coulter N5 Submicron Particle Size Analyzer. Three independent runs were performed for each sample. Particle size in DI water was also confirmed using TEM (JEOL 100CX II, JEOL USA, Inc., Peabody, MA). Briefly, a droplet of NPs (10 μg/mL) was placed onto a 200 mesh copper grid and allowed to air dry. At least five images were captured for each sample. Zeta potential was measured in DI water (10 μg/mL) using a Malvern Zeta Sizer Nano Z. Viscosity,

refractive index and dielectric constant of water at 25 ºC were used for calculating the zeta potential using the Smoluchowski Model. Zen 1002-Zeta Dip Cell was used for all measurements.

Cell Culture and Incubation with NPs

A549 alveolar epithelial cells were maintained in DMEM with 10% FBS, plasmocin (5 μg/mL), penicillin (100 U/mL) and streptomycin (100 μg/mL) (complete culture medium) in 75 cm^2 flasks and were passaged every two days. For all cell culture studies, cells up to 25 passages were used. NP stock solutions (1 mg/mL) were prepared fresh for all studies by dispersing the NPs in DI water using bath sonication for 3 min. For dose dependent studies, a ten-fold dilution in complete cell culture medium was achieved by using a concentrated NP stock prepared in DI water.

Qualitative NP Cell Uptake using TEM

A549 cells (1 x 10^6 cells/well) were seeded in complete culture medium in six well plates and allowed to attach for 24 h. The cells were washed twice with PBS and treated for 8 h in complete culture medium with Cu, C-Cu, Ni and C-Ni NPs (10 μg/mL). The cells were then washed twice with PBS to remove excess NPs and fixed with glutaraldehyde (2%) in sodium cacodylate buffer (0.1 M) for 24 h at 4 ºC. The samples were post fixed in Osmium tetraoxide (2%) in sodium cacodylate buffer (0.1 M) for 1 h at room temperature (RT). Samples were then en bloc stained with uranyl acetate (2%) for 15 min followed by lead citrate (1%) for 5 min. Dehydration of the samples followed in series of ethanol (50%, 75% and 95%) for 5 min each followed by ethanol (100 %) two times for 10 min each, after which the samples were embedded using polybed epoxy resin. Ultrathin sections (90-100 nm) were examined by placing them on 200 mesh carbon coated copper grids using TEM.

Quantitative NP Cell Uptake using ICP-MS

For quantitative analysis of metal NP uptake/association with the cells, ICP-MS was used. A549 cells (1 x 10^6 cells/well) in complete culture medium were allowed to attach for 24 h in six well plates. The cells were then washed twice with PBS and treated for 8 h in complete culture medium with Cu, C-Cu, Ni and C-Ni NPs (10 μg/mL). The cells were then washed twice with PBS to remove excess NPs, trypsinized, counted using a hemacytometer (Bright-Line; Hausser Scientific, Horsham, PA) and centrifuged in glass centrifuge tubes to a pellet which was dried overnight in the oven to remove any moisture. The dried cell pellet was dissolved by adding concentrated nitric acid (0.4 mL) and heating on a water bath at 80 ^oC for 20 min. All samples were diluted to a final concentration of nitric acid (2.6%) with DI water. For assessing the amount of Cu and Ni in untreated A549 cells (4 x 10^6) were seeded in a 100 mm x 20 mm petridish in complete culture medium and allowed to attach for 24 h. The cells were then washed twice with PBS and incubated for 8 h in complete culture medium at 37 ^oC and treated the same way as the samples. Cu and Ni standards were prepared by serial dilution of Cu and Ni ICP-MS standards (1000 μg/mL from Spex CertiPrep) in nitric acid (2.6%). The solutions were then analyzed using Varian 820 ICP-MS (Agilent Technologies, Santa Clara, CA) and In-115 was used as an internal standard for all measurements.

Assessment of Metal Ion Release from NPs using ICP-MS

Metal ion release from Cu and C-Cu NP (50 μg/mL) was performed in complete culture medium and medium without FBS at 37 ^oC. Released fraction was assessed at 0 h, 2 h, 12 h and 24 h. Briefly NP suspension (100 μL) from freshly prepared stocks in DI water (1 mg/mL) was added to media (1.9 mL) (with and without 10% FBS) in a six well plate,

slightly shaken to mix the contents and incubated for the required time period at 37 ^{o}C. For 0 h time point, NPs were allowed to incubate for 1 min with the media. After incubation for the required time period, NPs with the media were collected in a centrifuge tube and centrifuged at 22,000 g for 20 min at 4 ^{o}C using an Eppendorff Centrifuge. After centrifugation, supernatant (1.5 mL) was carefully removed and transferred to an Amicon Ultra Centrifugal Filter Tube with 100,000 molecular weight cutoff (Millipore, Billerica, MA) and centrifuged at 1200 g for 15 min using an IEC CL40R centrifuge (Thermo Electron Corporation, Ashville, NC). The filtration step was added after the centrifugation step to ensure complete separation of NPs from dissolved fraction. The separation was also confirmed after the intensity measurements using the dynamic light scattering measurements with Beckman Coulter N5 submicron particle size analyzer. Dilutions from the filtrate were made with nitric acid (3%) solution and analyzed using Varian 820 ICP-MS (Agilent Technologies, Santa Clara, CA) using In115 as an internal standard. The data are reported as wt % Cu (mg) released from Cu NP (mg) normalized by particle size (nm) in DMEM media in the presence or absence of 10% FBS.

Composition Analysis using XPS and XRD

Surface composition for Cu, C-Cu, Ni, C-Ni NPs were analyzed using Kratos AXIS Ultra DLD Photoelectron Spectrometer (Kratos Analytical, Manchester, UK). Analysis was carried out on gold sputtered silicon wafers on which a droplet of NP suspension (2 mg/mL) was placed and allowed to air dry. Energy source was Al Kα rays (1486.6 eV) and the area analyzed for XPS was 300µ x 700 µm^2. For each sample, full spectrum as well as high resolution spectrum was obtained for the metal of interest, carbon and oxygen. In addition, Cu auger peaks were analyzed as well. A charge neutralizer was used and the energy of the

spectra was corrected to C 1s peak at 284.8 eV. X-ray diffraction analysis was performed using Rigaku Miniflex II instrument. X-ray diffraction spectrum were recorded from $2\theta = 10^{o}$ to 100^{o} with a step size of 0.02^{o} and a scan time of 1 sec per step using CuKα radiation with a wavelength of 1.5406 Å. The data was analyzed by comparing diffractograms of samples with reference spectra using ICDD PDF-2 database.

Mitochondrial Function Assay

In cells with functional mitochondria, MTT (yellow colored) is reduced to a formazan derivative (blue color) which is quantified after solubilization of the formazan derivative in DMSO. MTT was used to evaluate the mitochondrial function of A549 cells (25,000 cells/well in a 96 well plate) after 24 h incubation with Cu, C-Cu, Ni and C-Ni NPs (0.01, 0.1, 1, 10 and 100 µg/mL). All dilutions for different doses were made 10X in DI water and the desired concentration in well was achieved after a ten-fold dilution. After 24 h treatment, cells were washed twice with PBS to remove excess NPs and MTT reagent in media (0.5 mg/mL) was allowed to incubate with the cells for 4 h. After 4 h, the MTT reagent was aspirated and the reduced formazan derivative was solubilized using DMSO (200 µL), after which the plate was centrifuged for 10 min and DMSO (100 µL) was transferred to a new plate and absorbance was measured at 570 nm. NPs with MTT reagent and without cells were used as controls to account for any interference. A549 cells without any treatment were the negative control for this experiment. The results were reported as percent mitochondrial function compared to negative control.

Neutral Red Lysosomal Membrane Integrity Assay

Neutral red is permeable to all cells but is retained only in cells with intact lysosomal membrane as its binds to the anionic sites in the lysosomes (Repetto et al., 2008). Any insult

to cell resulting in lysosomal membrane damage results in decreased uptake of neutral red; which is also the principle of this assay. Briefly, A549 cells (25,000 cells/well in a 96 well plate) were allowed to attach 24 h. For 24 h, cells were treated with Cu, C-Cu, Ni and C-Ni NPs (0.01, 0.1, 1, 10 and 100 μg/mL). All dilutions for different doses were made 10X in DI water and the desired concentration in well was achieved after a ten-fold dilution. After 24 h treatment, cells were washed twice with PBS to remove excess NPs after which neutral red dye (40 μg/mL) in media was added and allowed to incubate with the cells for 4 h. NPs with neutral red dye without cells were used as controls to account for any interference. A549 cells without any treatment were the negative control for this experiment. After washing the cells once with PBS, the incorporated neutral red dye was extracted using a mixture of water, ethanol and glacial acetic acid. The absorbance was measured at 540 nm and results were reported as percent membrane integrity compared to negative control.

Ethidium Homodimer/Calcein AM Plasma Membrane Integrity Assay

In order to determine plasma membrane damage, membrane integrity was assessed using ethidium homodimer/calcein AM dyes. Ethidium homodimer enters cells with damaged plasma membranes and fluorescence enhancement occurs after binding with nucleic acids. Calcein AM is cell permeable and by the action of cellular esterases, it gets converted into anionic calcein which is fluorescent and trapped inside the cells. Thus, one can distinguish between cells with compromised plasma membrane from the cells with intact membranes. Manufacturer's protocol was followed for this assay. Briefly, 100,000 A549 cells were plated/well in Lab-Tek II chambered cover glass slides and allowed to attach for 24 h. Copper, C-Cu, Ni, C-Ni NP and $CuCl_2$ treatments with equivalent dose (5, 10 and 25 μg/mL) were added and allowed to incubate with the cells for 2 h. Untreated A549 cells were

used as negative control and 5 min treatment with Triton® X-100 (0.1%) was used as a positive control. After treatment, cells were washed twice with PBS followed by addition of ethidium homodimer (4 µM) and calcein AM (2 µM) in PBS. After 20 min of incubation at RT, images were taken using Olympus 1X51 Fluorescence Microscope and analyzed using Olympus DP2BSW Software.

Statistical Analysis

Statistical analysis was performed using either one-way analysis of variances (ANOVA) followed by pair-wise comparison using Tukey's multiple comparison test or two way ANOVA followed by bonferroni post tests using GraphPad Prism software. Data were considered statistically significant when p value was less than 0.05.

4.4 Results

Physico-Chemical Characterization of NPs

According to the manufacturer, the particle size of Cu NPs and C-Cu NPs was 25 nm and Ni NPs and C-Ni NPs was 20 nm. Particle size analysis in de-ionized (DI) water and DMEM (Dulbecco's Modified Eagle Medium) (with and without 10% FBS) using dynamic light scattering (**Table 4.1**) and Transmission Electron Microscopy (TEM) (**Figure 4.1**) show that NPs were aggregated upon suspension in various media. The particle size of NPs was highly influenced by the surrounding medium and was orders of magnitude higher than that reported by the manufacturer. The addition of 10% FBS to the medium decreased the aggregation of NPs as the average particle sizes were lower than that observed in DI water.

For surface composition analyses of NPs, XPS **(**X-ray Photoelectron Spectroscopy) measurements were performed. In XPS analysis (**Figure 4.2**), characteristic peaks from copper, oxygen and carbon were observed for both Cu and C-Cu NPs. The presence of carbon in the Cu NP samples was attributed to atmospheric contamination. There was much more carbon present on the C-Cu NPs than the Cu NPs, as evidenced by the C:Cu atomic concentration ratio in these samples (1.87 ± 0.05 and 0.61 ± 0.04 for C-Cu and Cu NPs, respectively). In addition, much more oxygen was observed in the Cu NP samples; O:Cu ratios were 0.6 ± 0.3and 0.99 ± 0.02 for the C-Cu NPs and Cu NPs, respectively. These data, in combination with the Cu $2p_{3/2,}$ Cu auger, O1s, and C 1s peak positions in **Table 4.2**, indicate that the C-Cu NP sample contained a significant amount of Cu metal with some oxidized Cu attributed to Cu_2O, while the Cu NP surface had been largely oxidized and was mostly composed of Cu_2O and some oxidized carbon.

For Ni and C-Ni NPs (graphs not shown), similar trends were observed. The ratio of percent atomic concentration of carbon:nickel in C-Ni NPs and Ni NPs were 6.8 ± 0.5 and 2.0 ± 0.2, whereas the ratio of percent atomic concentration of O:Ni in C-Ni NPs and Ni NPs were 1.5 ± 0.3 and 2.7 ± 0.2, respectively. The peak positions in **Table 4.2** suggest that the C-Ni NP surface is composed mostly of Ni metal although the presence of some surface $NiO/Ni_2O_3/Ni(OH)_2$ cannot be ruled out. The Ni NP sample was significantly more oxidized compared to C-Ni NPs and was composed predominantly of NiO (854.35 ± 0.08), and Ni_2O_3 and/or $Ni(OH)_2$ (856.20 ± 0.07), but some residual Ni^0 (852.81 ± 0.03) was also observed. A diffraction pattern characteristic of Cu was observed in both Cu and C-Cu NPs with the strongest characteristic peak of Cu at d = 2.087, $2\Theta = 43.3158$. A Cu_2O peak was observed in Cu NPs at d = 2.453. A small Cu_2O peak was also observed in C-Cu NPs at d = 2.4601. The ratio of intensities of strongest Cu peak to strongest Cu_2O peak was three-fold higher in C-Cu NP compared to Cu NP.

Differential Effects of Carbon-Coated and Non-Coated NPs on Mitochondrial Function and Lysosomal Membrane Integrity

The effect of NPs on mitochondrial function and lysosomal membrane integrity was assessed using the MTT and neutral red assays, respectively (**Figure 4.3A and 4.3B**). After 24 h incubation with various doses, Cu and C-Cu NPs had similar effects on lysosomal membrane integrity. Major differences were observed between the effects of carbon-coated versus non-coated Cu NPs on mitochondrial function. Upon treatment with low concentrations of C- Cu NPs (0.01, 1 and 1 µg/mL) an effect on mitochondrial membrane was evident whereas with Cu NPs, no mitochondrial effect was observed. A similar effect on mitochondrial membrane was observed at 100 µg/mL for both Cu NP and C-Cu NPs. C-Cu

NP treated cells displayed 30% and 45% decrease in mitochondrial function at doses of 1 and 10 µg/mL compared to control untreated cells, respectively. However, only a 18% decrease in mitochondrial function was observed with Cu NPs at10 µg/mL. Interestingly, Ni and C-Ni NPs had no measurable effect on membrane integrity. C-Ni NPs treatment at 10 µg/mL resulted in a 40% decrease in cell mitochondrial function followed by a plateau in the response with increasing dose. In contrast, Ni NPs did not have any effect on mitochondrial function.

Cellular Uptake and Release of Soluble Metal from NPs

In order to understand the underlying reasons for differences observed in cell-based toxicity assays, it was decided to qualitatively and quantitatively assess the uptake of NPs in A549 cells using TEM and ICP-MS, respectively. Cell uptake by ICP MS measures Cu/Ni content in cells from NPs both associated with cell surface and internalized fractions. TEM images in **Figure 4.4** show that all four types of NPs were taken up by A549 cells. Nanoparticles were mostly centered around the nuclear membranes and in the vicinity of the mitochondria. To better understand the interaction of carbon-coated versus non-coated NPs, the amount of NPs associated with the cells was quantified after 8 h of incubation with A549 cells using ICP-MS (Inductively Coupled Plasma Mass Spectroscopy). Significant ($P < 0.05$) differences exist between the uptake of Cu and C-Cu NPs as C-Cu NPs shows almost a ten-fold higher uptake (4261 ± 553 ng Cu/million cells) than Cu NPs (302 ± 33 ng Cu/million cells) (**Figure 4.5**). However, this trend was not seen in the case of Ni and C-Ni NPs where the uptake of both NPs was similar and the differences were not statistically significant ($P > 0.05$). Since a significant difference was observed in the uptake C-Cu and Cu NPs, it was decided to investigate in more detail the effect of carbon coating on the release of Cu from

Cu and C-Cu NPs in cell culture medium using ICP-MS. A kinetic assessment of the amount of released Cu from NPs is shown in **Figure 4.6**. Consistent with the uptake data, the presence of carbon coating on the surface of Cu NPs had a significant impact on the amount of Cu released from these NPs. After 2 h of incubation four-fold less Cu was released from C-Cu NPs in DMEM ± FBS compared to Cu NPs + 10% FBS. Furthermore, the presence of serum enhanced the release of Cu from Cu NPs as two-fold greater Cu was released from Cu NPs in DMEM with 10% FBS compared to Cu NPs in DMEM (no FBS) after 2 h incubation.

Plasma Membrane Integrity Analysis using Ethidium homodimer and Calcein AM

To gain insight into the mechanisms of toxicity, plasma membrane integrity was evaluated at time points as early as 2 h. Ethidium homodimer only enters cells with compromised membranes and calcein AM is taken up by all viable cells by passive absorption. Using a fluorescence microscope, images were taken for each treatment. Representative images from each treatment are shown in **Figure 4.7A**. The average ethidium homodimer positive cells (cell membrane compromised) from four fields selected randomly are plotted in **Figure 4.7B**. After 2 h incubation, Cu NPs started inducing membrane damage at doses as low as 5 µg/mL and 10 µg/mL. In Cu NP treated cells, ethidium homodimer positive cells (red cells) were present in clusters. After 2 h treatment with 25 µg/mL Cu NPs, 40% cells were positive for ethidium homodimer whereas only 1-3% of cells stained positive for ethidium homodimer when treated with C-Cu NPs and $CuCl_2$ at 25 µg/mL. This experiment was also carried out for Ni and C-Ni NPs but no effect on plasma membrane integrity was observed.

4.5 Discussion

The questions asked in these studies pertained to how the carbon coating affected i) the physicochemical properties of metal NPs, ii) the toxicity end points in cells exposed to these NPs and iii) whether the changes in physicochemical properties could be correlated to toxicity of NPs as a function of carbon coating. However, the focus of these studies was not to prove that carbon coating offers protection against toxic effects of metal based NPs. Specifically, Cu, C-Cu, Ni and C-Ni NPs were tested. The results of these studies suggests that carbon coating influenced i) NP physico-chemical properties, and interaction with surrounding media and ii) toxicity, in cell-based assays compared to the non-coated NPs especially in the case of Cu and C-Cu NPs.

Due to high surface energy, agglomeration of NPs was observed upon suspension in various media. Higher agglomeration of Ni and C-Ni particles was observed in DMEM compared to DI water whereas for Cu NPs agglomeration was lower in DMEM compared to DI water and for C-Cu NPs, degree of agglomeration was similar in DMEM and DI water. To explain these findings, DLVO [Derjaguin and Landau (Derjaguin and Landau, 1941); Verwey and Overbeek (Verwey and Overbeek, 1948)] theory was considered. According to DLVO theory, agglomeration and stability of particles depends upon attractive van der waals forces and repulsive electrostatic forces. Repulsive electrostatic forces depend upon zeta potential and thickness of electrical double layer. Ionization of particle surface, adsorption of counter ions and lattice ion dissolution determine surface zeta potential and ionic strength determines thickness of electrical double layer. Increase in either zeta potential or thickness of electrical double layer increases repulsive electrostatic forces and decreases agglomeration (Jiang et al., 2008; Stumm and Morgan, 1996). High ionic strength usually encountered in

physiological conditions such as DMEM can result in decrease of the thickness of electrical double layer of particles resulting in increased agglomeration which has been reported in literature (Jiang et al., 2008) and was the case with Ni and C- Ni particles in our studies. An investigation into the effect of low and high ionic strengths on zeta potential was carried out by measuring zeta potential in 0.015 mM and 0.15 mM ionic strengths using phosphate buffered saline (PBS, pH 7). Zeta potential of Ni and C-Ni particles could not be determined in 0.015 M and 0.15 M PBS solutions as rapid settling of large agglomerates were observed. For Cu NPs, the average zeta potential was -9 mV in DI water, -28 mV in 0.015 M PBS and -24.8 in 0.15 M PBS. Surface Cu ionization on Cu NPs and interaction with chloride ions in PBS explains higher negative zeta potential and lower agglomerate sizes of Cu NPs in DMEM.

For C-Cu NPs, the average zeta potential was -6 mV in DI water, -31 mV in 0.015 M PBS and -24 mV in 0.15 M PBS but the particle size was similar in DI water and DMEM. This could be due to formation of aggregates (Jiang et al., 2008) (made up of tightly bonded NPs possibly due to presence of carbon coating) which cannot be dispersed by changing ionic strength or surface charge; conditions which can usually disperse loose NP agglomerates which primarily interact by electrostatic forces.

Compared to DI water, when NPs were suspended in DMEM with 10% FBS, considerable decrease in agglomeration of all particles was observed. This observation was consistent with literature reports as protein in serum may coat the particle surface (Murdock et al., 2008; Xia et al., 2008). Impact of changing media composition on particle size was more prominent for non-coated NPs compared to carbon coated NPs. Since major applications of Cu NPs are in conducting inks and catalysts, oxidation of Cu NPs can lead to

an increase in resistivity and a decrease in conductance. Carbon coating is used as a way to protect the NP surface from oxidation without interfering with the functionality of these NPs in various applications (Luechinger et al., 2008). Surface carbon coating can lend a hydrophobic surface which may lead to a differential interaction of these particles with surrounding media, cells and different toxicity profile as compared to their non-coated counterparts. Higher percent atomic concentration of oxygen and lower percent atomic concentration of carbon in Cu and Ni NPs compared to C-Cu and C-Ni confirms the presence of carbon coating and suggests relative protection of carbon coated NP surface from oxidation although some level of surface oxides were also observed in carbon coated NPs as indicated by XPS and XRD analysis. X-ray photoelectron spectroscopy is a very surface sensitive technique compared to XRD which is not very surface sensitive.

The release studies in cell free media (**Figure 4.6**) clearly showed that the carbon coating decreased the release of soluble metal ions from NPs. Compared to Cu NPs in DMEM with 10% FBS, four-fold less Cu was released from C-Cu NPs after 2 h incubation. Furthermore, the presence of serum enhances the release of Cu from Cu NP surface which is in agreement with previous reports (Cronholm et al., 2011). However, presence of serum in cell culture medium did not have any influence on release of Cu from C-Cu NPs suggesting stabilization offered by carbon coating. Another interesting difference was almost an order of magnitude higher cellular uptake of C-Cu NPs was observed compared to the non-coated Cu NPs (**Figure 4.5**). Cell uptake for C-Cu NPs was almost 10-times greater compared to Cu NPs despite their similar size in DMEM+10% FBS because carbon coating provides a hydrophobic surface to NPs and thus is more favorable for uptake by cells. Also, in the presence of carbon coating the release of soluble Cu from C-Cu NPs was less compared to

Cu NPs and thus quantitatively less Cu NPs compared to C-Cu NPs were available for uptake by cells.

In addition to the differential uptake and interaction of carbon-coated and non-coated Cu NPs with cellular environment, differences were also observed in cell-based assays. After 24 h incubation with A549 cells, significant differences ($P < 0.01$) were found between the effects of Cu and C-Cu NPs on mitochondrial function but not on lysosomal membrane damage at 0.1, 1 and 10 µg/mL doses (**Figures 4.3A and 4.3B**). Copper ion induced damage to lysosomal membrane has previously been reported (Grillo et al., 2009). Recently it was reported that Cu NPs with an oxidized copper oxide shell undergoes enhanced dissolution in acidic media whereas in the absence of oxidized layer, the reaction to solubilized Cu metal from the surface of Cu NPs is less energetically favored (Elzey and Grassian, 2010). Interestingly, irrespective of carbon coating, equivalent damage to lysosomal membrane was observed from Cu and C-Cu NPs. One hypothesis to explain this effect can be that despite a higher release of Cu ions from Cu NPs relative to C-Cu NPs, the total amount of released Cu inside acidic compartments such as lysosomes was similar from both NPs due to higher cellular uptake of C-Cu NPs relative to Cu NPs. Almost a log-fold higher cellular uptake of C-Cu NPs compared to Cu NPs and a slower dissolution inside the cells may lead to accumulation of C-Cu NPs in the cells over time. It is possible that with C-Cu NPs, the carbon coating may allow only limited but extended release of Cu ions in the cells which over time would be available for inducing damage to the mitochondria compared to Cu NPs which demonstrate a burst release. This scenario may explain the damage to mitochondria due to C-Cu NPs at doses as low as 1 µg/mL. Although it was not the intent of the present studies to investigate the mechanisms of toxicity, oxidative stress inducing potential of NPs

was evaluated since oxidative stress has been correlated to metal NP toxicity (Nel et al., 2006). In fact after 17 h of incubation of Cu and C-Cu NPs with A549 cells, a two and ten-fold increase in reactive oxygen species (ROS) compared to control at relatively high concentrations of 25 and 50 µg/mL, respectively, was observed only with C-Cu NPs and not with Cu NPs (data not shown), indicating persistence of C-Cu NPs in the cells. Furthermore, when NP effects on plasma membrane integrity was evaluated using ethidium homodimer/calcein AM assay after 2 h incubation with the cells, significant differences ($P < 0.001$ at 25 µg/mL) were observed between the effects of Cu and C-Cu NPs on plasma membrane integrity (**Figure 4.7A & 4.7B**). Copper NPs damaged the plasma membrane at doses of 5 and 10 µg/mL and it was observed that the cells with damaged plasma membrane were present in clusters whereas C-Cu NPs had no effect on the plasma membrane integrity. A time point of 2 h was chosen to allow sufficient time for most of the NP dose to accumulate on the cell surface (Teeguarden et al., 2007). The release, uptake and cell toxicity data suggests that after Cu and C-Cu NPs were added to the wells, Cu NPs continuously dissolved in cell culture medium. As a consequence, the cells were exposed to high localized concentrations of soluble Cu which may have lead to plasma membrane damage of a group of cells possibly by oxidizing the membrane lipids and proteins (Bremner, 1998; Cecconi et al., 2002). Simultaneously, Cu NPs taken up by cells can end up in cell compartments such as lysosomes which are similarly exposed to high concentrations of Cu ions possibly by a trojan horse type effect (Limbach et al., 2007; Park et al., 2010). The release data suggests that at a given time and dose, C-Cu NPs release only a fraction of soluble Cu ions by weight compared to Cu NPs and thus plasma membrane damage is not observed with C-Cu NPs. At doses equivalent to Cu NPs, plasma membrane damage was

also not observed with aqueous salts like $CuCl_2$. One explanation of why $CuCl_2$ did not show any effect on plasma membrane integrity could be the uniform availability of Cu ions in cell culture medium and hence are unlikely to reach the cell surface in doses equivalent to soluble Cu from Cu NPs in 2 h. Cu NPs are more prone to settling and likely to cause a localized response due to their aggregated nature.

These results corroborate with a recent study on Cu and CuO NPs by Midander et al. (2009) where they showed that most of the Cu NPs were dissolved after 4 h in DMEM. They also reported 80% non-viable cells (assessed using trypan blue assay which measures membrane integrity) after 4 h treatment with Cu NPs as opposed to only a small percentage of non-viable cells after treatment with either CuO NPs or Cu and CuO microparticles. Additionally, they showed relatively low toxicity to dissolved fraction of Cu and CuO NPs (20% non-viable cells) compared to Cu and CuO NPs themselves (90-100% non-viable cells) after 18 h incubation with the cells. This further strengthens the proposed hypothesis that Cu NPs are more likely to cause membrane damage early on due to their aggregated nature helping them to settle on NP surface and making the cells more likely to see the dissolved fraction as opposed to a uniform solution of dissolved Cu in form of $CuCl_2$. NPs can change size, shape and composition in media and thus their delivered dose to the cell surface can be different from their solution counterparts. An extensive review on particokinetics by Teeguarden et al. (2007) covered in detail various factors affecting delivered dose of NPs. A recent report by Wittmaack (Wittmaack, 2011) also highlights the importance of gravitational settling while interpreting nanotoxicity results. *In vivo* toxicity of Cu NPs is also attributed to their conversion to cupric ions. Chen et al. (2006) and Meng et al. (2007) reported grave toxicity of copper NPs especially to kidney, liver and spleen after oral gavage administration

in mice. Authors reported LD_{50} of Cu NP and Cu microparticles as 413 mg kg^{-1} and >5000 mg kg^{-1}, respectively. Their studies suggest that higher conversion of Cu NP to ionic form compared to micro NPs was responsible for higher toxicity observed with Cu NPs.

Nickel and C-Ni NPs were relatively not toxic to A549 cells compared to Cu and C-Cu NPs. Ni NPs were inert in MTT and neutral red membrane integrity assay and some decrease in mitochondrial function (40% compared to control) was observed with C-Ni NPs. This is consistent with literature reports, Peters et al. (2004) found no toxicity to Ni NPs using MTS assay in HDMEC cells. Another study (Lanone et al., 2009) compared the toxicity of Ni NPs in THP cells across various labs using MTT assay, either the IC_{50} was not reached after 24 h or was very high (79 µg/mL). Surprisingly, in the studies reported herein, although some toxicity was observed with C-Ni NP versus Ni NP in MTT assay, the Ni uptake of cells was not significantly different ($P > 0.05$) between Ni and C-Ni NPs. In fact, with Ni and C-Ni NPs, almost the entire administered dose (10 µg/mL) was found to be taken up by cells. However, caution should be exercised when interpreting these data since the quantitative measure of Ni content associated with the cells includes both un-internalized (NPs sticking on cell surface) as well as internalized (NPs inside the cells) components. Therefore, it is possible that although no differences were observed between total Ni uptake by cells treated with Ni and C-Ni NPs, in reality there might be a difference in internalized versus surface Ni fractions. Literature reports (Fletcher et al., 1994; Liu et al., 2007) suggest a "nickel ion hypothesis" for explaining toxicity, mutagenicity and carcinogenicity observed with various Ni compounds. According to this hypothesis, the toxicity, mutagenicity and carcinogenicity observed with various Ni compounds is directly related to the Ni (II) ion concentration in the cells and is independent of the form of the parent Ni compound. It has also been shown that

accelerated dissolution of Ni compounds can happen in acidic conditions of vacuoles in cells (Abbracchio et al., 1982). Therefore, it is possible that the interplay between internalized fraction and subsequent dissolution in the cells may be the determining factors that may account for differences in toxicity between Ni and C-Ni NPs. However, this is an area of future research.

Table 4.1 Particle Size and Zeta Potential Analyses of NPs in Various Media. Particle size was measured in DI water and DMEM (± 10% FBS) using dynamic light scattering. Zeta potential was measured in DI water using a Malvern Zeta Sizer Nano Z. Average particle size (intensity analysis) and zeta potential values were calculated from three independent measurements.

NP Type	Manufacturer	Particle Size*(nm)	Surface area* (m^2/g)	Particle Size in DMEM + 10% FBS (nm ± SD	Particle Size in DMEM (nm ± SD)	Particle Size in H_2O (nm ± SD)	Zeta Potential in H_2O (mV ± SD)
Ni	NanoAmor	20	50	560 ± 214	2778 ± 107	1210± 180	3 ± 0.7
C-Ni	NanoAmor	20	50	427 ± 150	954 ± 382	728 ± 281	-16 ± 2
Cu	NanoAmor	25	40	272 ± 93	537 ± 167	1175 ± 369	-9 ± 3
C-Cu	NanoAmor	25	40	253 ± 8	447 ± 121	392± 90	-6 ±0.7

*Provided by manufacturer.

Table 4.2 Comparison of Binding Energies (BE) of Cu and C-Cu NPs with range of BE for Standard Reference Compounds (Wagner., 1978).

NP Type	BE Cu $2p_{3/2}$	BE Cu Auger	BE Ni $2p_{3/2}$	BE O 1s	BE C 1s
Cu NP	932.85 ± 0.04	569.87 ± 0.06	-	529.92 ± 0.06 530.81 ± 0.02* 531.82 ± 0.03	284.8* 285.95 ± 0.09 288.84 ± 0.06
C-Cu NP	932.99 ± 0.07	568.03 ± 0.06	-	530.9 ± 0.1	284.8
Ni NP	-	-	852.81 ± 0.03 854.35 ± 0.08* 856.20 ± 0.07	529.79 ± 0.08 531.46 ± 0.08* 532.8 ± 0.2	284.8* 286.6 ± 0.3 289.08 ± 0.03
C-Ni NP	-	-	852.98 ± 0.02	532.4 ± 0.2	284.8* 286.1 ± 0.2
Reference Data [a]					
Cu	932.6 - 933	567.7-568	-	-	-
Cu_2O	932.2 -932.8	569.7-570	-	530.2-530.7	-
CuO	933.4 -933.9	568.5-568.8	-	529.5-529.8	-
Ni	-	-	852-853	-	-
NiO	-	-	854-854.7	529.5-529.8	-
Ni_2O_3	-	-	855.8-856	531.5-531.7	-
$Ni(OH)_2$	-	-	855.6-856	531.2-531.5	-

*Represents the predominant peak

[a] A range of BE for standard reference compounds was identified from the X-ray Photoelectron Spectroscopy Database, Version 3.5 (National Institute of Standards and Technology, Gaithersburg, 2003); http://srdata.nist.gov/xps

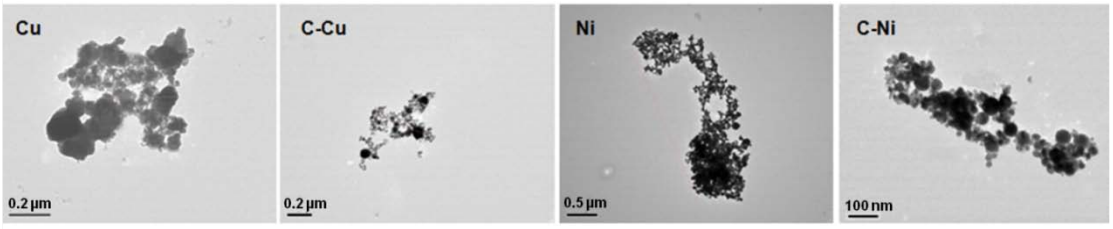

Figure 4.1 Transmission electron microscopy images of NPs. NPs were suspended at concentration of 10 µg/mL in DI water for TEM analysis. The average particle sizes measured by TEM correlated with the dynamic light scattering data.

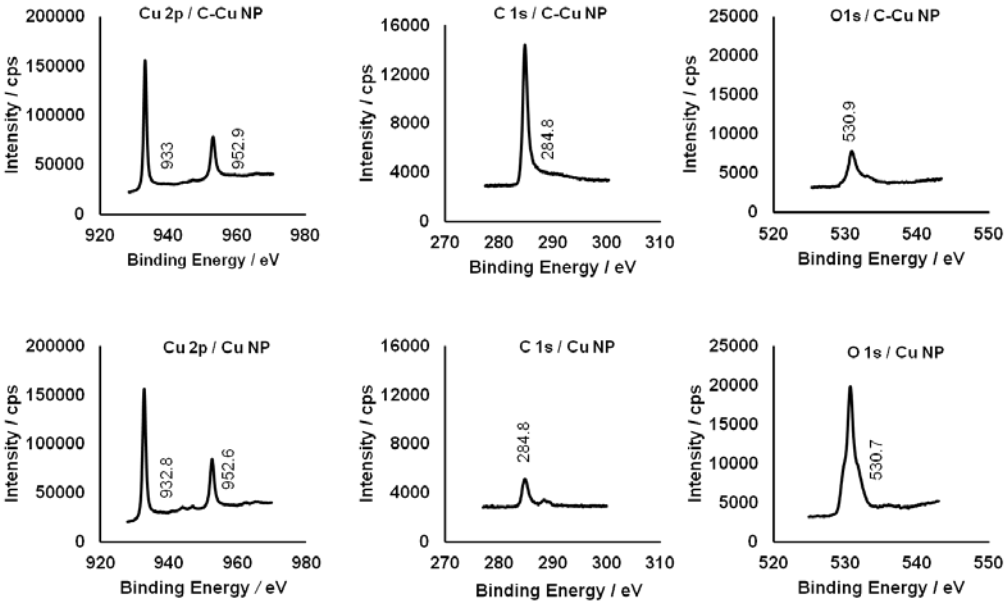

Figure 4.2 Representative XPS analysis for C-Cu NPs (top panel) and Cu NPs (lower panel) shows the differences in carbon and oxygen content of the surface of these NPs. Percent atomic concentration of oxygen and carbon were 13 ± 3% and 54 ± 4% in C-Cu NPs and 38 ± 0.1% and 23 ± 1% in Cu NPs and suggested less surface oxidation of C-Cu NP

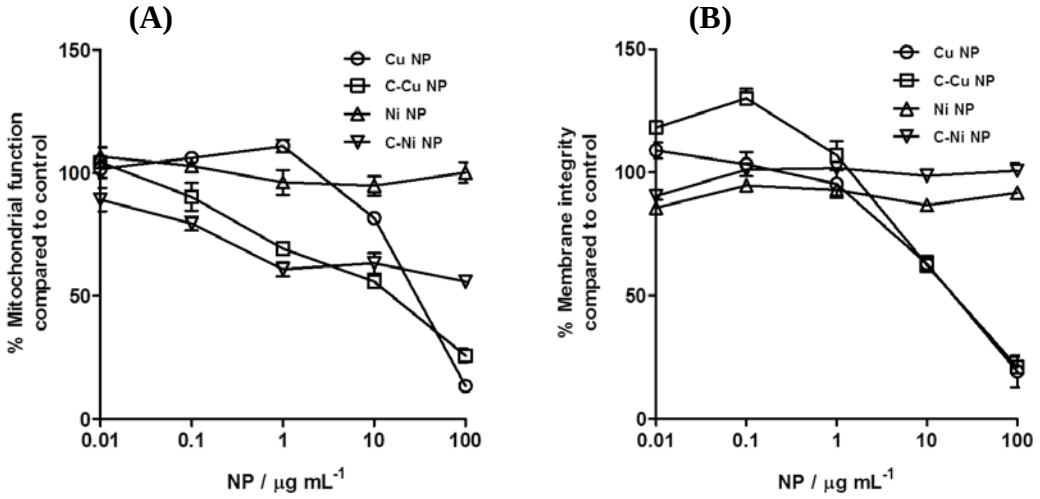

Figure 4.3 Dose dependent effects of NPs on mitochondrial function and lysosomal membrane integrity. (A) MTT assay and (B) lysosomal membrane integrity after 24 h treatment with Cu, C-Cu, Ni and C-Ni NPs. Each value is an average ± SE of n= 8 per treatment per dose.

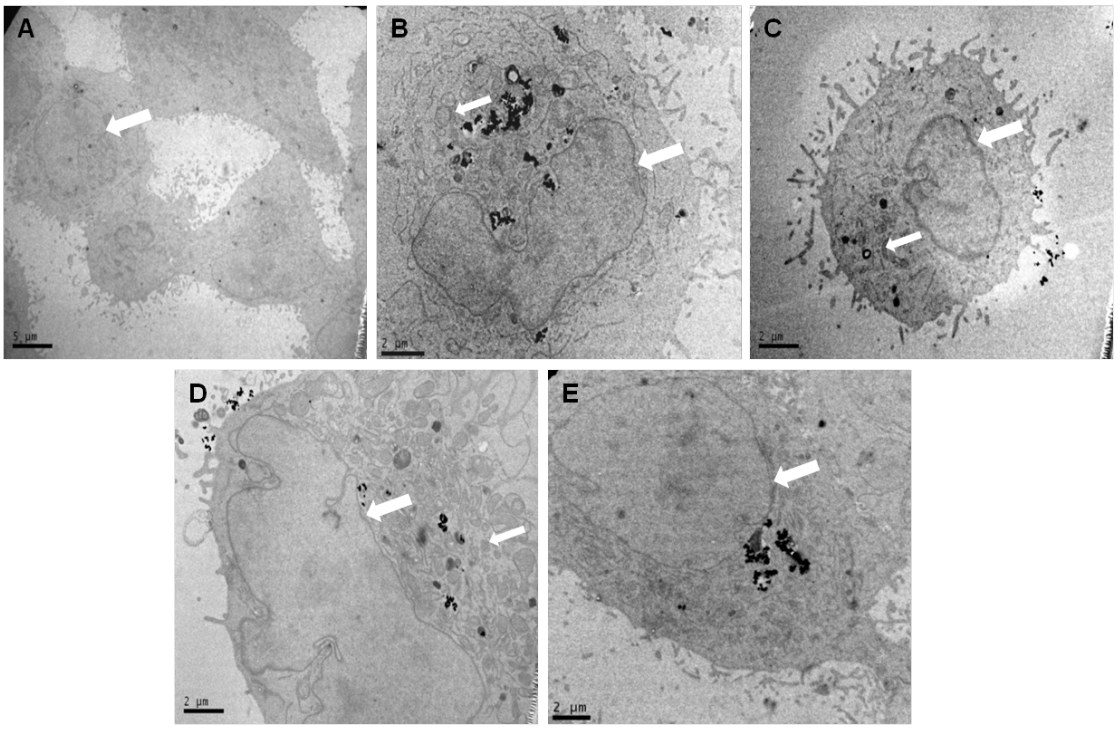

Figure 4.4 Transmission electron microscopy images of NP uptake by A549 cells. A) Control A549 cells, B) Cu treated, C) C-Cu treated, D) Ni treated and E) C-Ni treated A549 cells. Cells were treated with NPs at concentration of 10 µg/mL for 8 h. Arrows indicate nucleus and mitochondria.

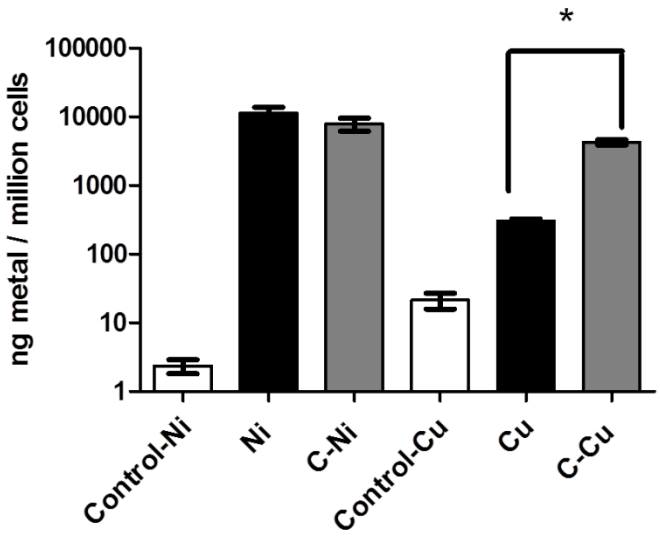

Figure 4.5 Quantitative analyses of Cu and Ni uptake in A549 cells (uptake signifies Cu/Ni content in cells from NPs both associated with cell surface and internalized fractions). Uptake of Cu from C-Cu NPs was a log-fold higher (* $P < 0.05$) than from Cu NPs. No significant difference was found between uptake of Ni from Ni and C-Ni NPs. Control-Ni and control-Cu signifies the amount of Ni and Cu in untreated A549 cells. Quantitative metal uptake analyses were performed using ICP-MS. Each value is an average ± SE of three independent measurements.

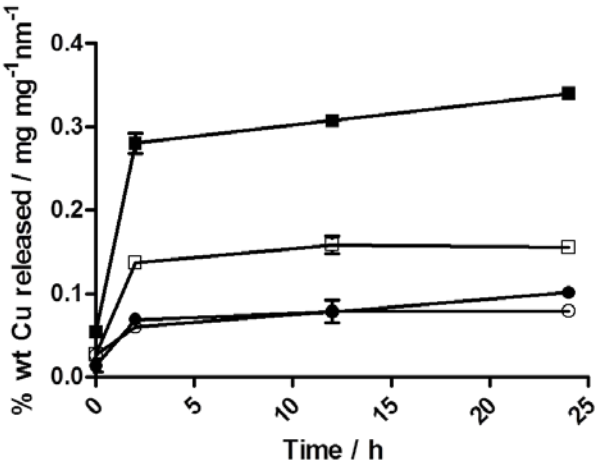

Figure 4.6 Release studies for Cu and C-Cu NPs in DMEM media. Percent wt Cu (mg) released from NPs (mg) in DMEM ± FBS normalized by particle size (nm). Cu NP, DMEM + FBS (■), Cu NP, DMEM (□), C-Cu NP, DMEM + FBS (●), C-Cu NP, DMEM (○). After 2 h incubation, four-fold and two-fold greater Cu was released from Cu NPs in DMEM + 10% FBS compared to C-Cu NPs in DMEM ± FBS and Cu NPs in DMEM (no FBS), respectively. Therefore, the carbon coating retards release of Cu from C-Cu NPs and the presence of FBS enhances release of Cu from Cu NPs but has no effect on C-Cu NPs. Each value is an average ± SE of three independent measurements.

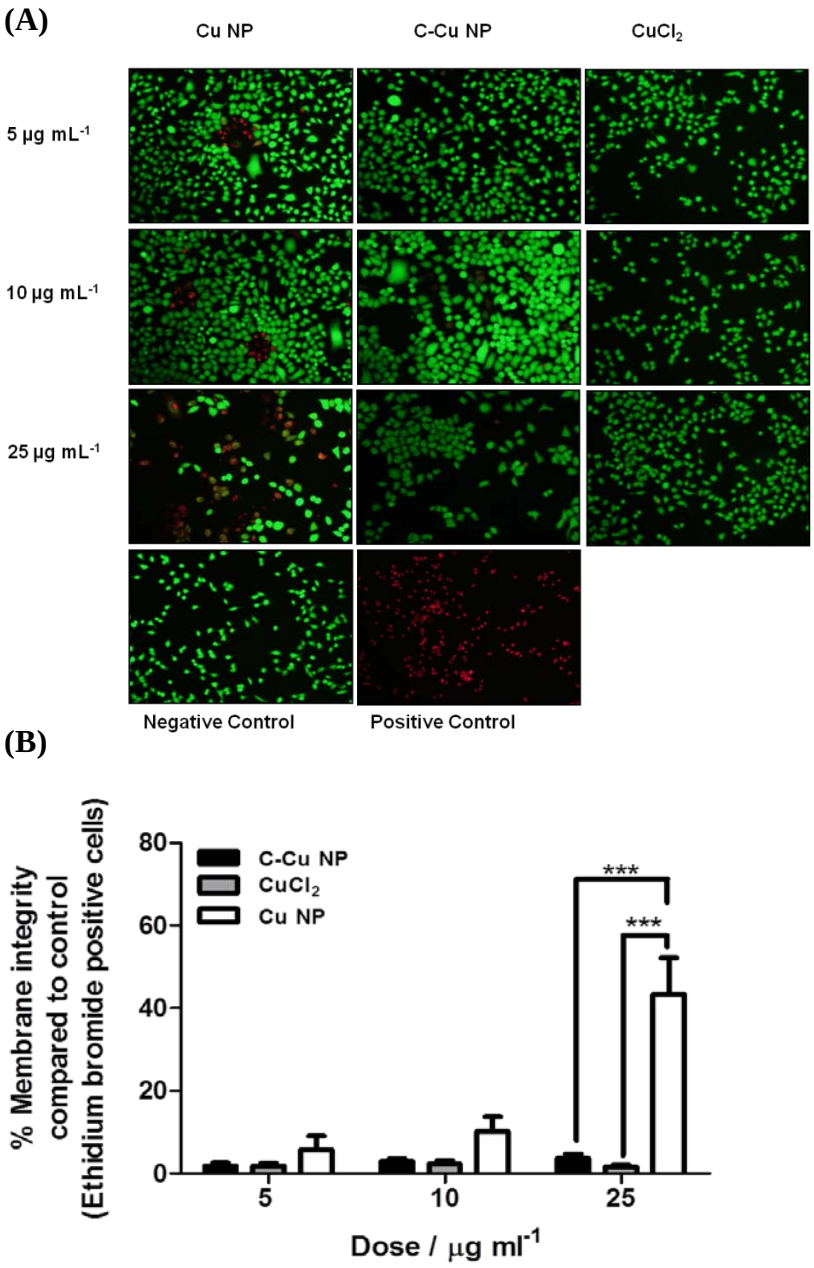

Figure 4.7 Membrane integrity assay using ethidium homodimer/calcein AM (A) Membrane integrity assay using ethidium homodimer/calcein AM revealed that membrane damage can be initiated as early as 2 h by Cu NPs. No damage was observed with either C-Cu NPs or $CuCl_2$ after 2 h treatment. Red cells are ethidium homodimer positive and damaged because ethidium homodimer can enter only plasma membrane damaged cells. Green cells are calcein positive and not damaged as calcein AM enters all cells. Note the clustering of red cells in Cu treated groups at 5 and 10 µg/mL. (B) Percent ethidium homodimer positive cells compared to untreated control (negative control) are plotted. (Average ± SE four fields). Significant difference (*** $P < 0.001$) was found between effects of C-Cu NP, $CuCl_2$ and Cu NP at 25 µg /mL.

4.6 References

Abbracchio, M.P., Heck, J.D., Costa, M., 1982. The phagocytosis and transforming activity of crystalline metal sulfide particles are related to their negative surface charge. Carcinogenesis 3, 175-180.

Ali-Boucetta, H., Al-Jamal, K.T., Muller, K.H., Li, S., Porter, A.E., Eddaoudi, A., Prato, M., Bianco, A., Kostarelos, K., 2011. Cellular uptake and cytotoxic impact of chemically functionalized and polymer-coated carbon nanotubes. Small 7, 3230-3238.

Barrabes N, J.J., Dafinov A, Medina F, Fierro JLG, Sueiras JE, Salagre P, Cesteros Y., 2006. Catalytic reduction of nitrate on Pt-Cu and Pd-Cu on active carbon using continuous reactor: The effect of copper nanoparticles. Appl Catal B-Environ 62, 77-85.

Bremner, I., 1998. Manifestations of copper excess. Am J Clin Nutr 67, 1069S-1073S.

Cecconi, I., Scaloni, A., Rastelli, G., Moroni, M., Vilardo, P.G., Costantino, L., Cappiello, M., Garland, D., Carper, D., Petrash, J.M., Del Corso, A., Mura, U., 2002. Oxidative modification of aldose reductase induced by copper ion. Definition of the metal-protein interaction mechanism. J Biol Chem 277, 42017-42027.

Chen, Z., Meng, H., Xing, G., Chen, C., Zhao, Y., Jia, G., Wang, T., Yuan, H., Ye, C., Zhao, F., Chai, Z., Zhu, C., Fang, X., Ma, B., Wan, L., 2006. Acute toxicological effects of copper nanoparticles in vivo. Toxicol Lett 163, 109-120.

Cronholm, P., Midander, K., Karlsson, H.L., Elihn, K., Wallinder, I.O., Moller, L., 2011. Effect of sonication and serum proteins on copper release from copper nanoparticles and the toxicity towards lung epithelial cells. Nanotoxicology 5, 269-281.

Derjaguin, B.V., Landau, L.D., 1941. Theory of the stability of strongly charged lyophobic sols and of the adhesion of strongly charged particles in solutions of electrolytes. Acta Physicochim URSS 14, 733-762.

Elzey, S., Grassian, V.H., 2010. Nanoparticle dissolution from the particle perspective: insights from particle sizing measurements. Langmuir 26, 12505-12508.

Fletcher, G.G., Rossetto, F.E., Turnbull, J.D., Nieboer, E., 1994. Toxicity, uptake, and mutagenicity of particulate and soluble nickel compounds. Environ Health Perspect 102 Suppl 3, 69-79.

Fourches, D., Pu, D., Tassa, C., Weissleder, R., Shaw, S.Y., Mumper, R.J., Tropsha, A., 2010. Quantitative nanostructure-activity relationship modeling. ACS Nano 4, 5703-5712.
Grillo, C.A., Reigosa, M.A., Lorenzo de Mele, M.F., 2009. Effects of copper ions released from metallic copper on CHO-K1 cells. Mutat Res 672, 45-50.

Jiang, J., Oberdorster, G., Biswas, P., 2008. Characterization of size, surface charge and agglomeration state of nanoparticle dispersions for toxicological studies. J Nanoparticle Research 11, 77-89.

Jiao, J., Seraphin, S., 1997. Carbon encapsulated nanoparticles of Ni, Co, Cu, and Ti. Journal of Applied Physics 83, 2442-2448.

Lanone, S., Rogerieux, F., Geys, J., Dupont, A., Maillot-Marechal, E., Boczkowski, J., Lacroix, G., Hoet, P., 2009. Comparative toxicity of 24 manufactured nanoparticles in human alveolar epithelial and macrophage cell lines. Part Fibre Toxicol 6, 14.

Li, Z., Hu, C., Yu, C., Qiu, J., 2009. Synthesis and characterization of carbon-encapsulated magnetic nanoparticles via arc-plasma assisted CVD. J Nanosci Nanotechnol 9, 7473-7476.

Limbach, L.K., Wick, P., Manser, P., Grass, R.N., Bruinink, A., Stark, W.J., 2007. Exposure of engineered nanoparticles to human lung epithelial cells: influence of chemical composition and catalytic activity on oxidative stress. Environ Sci Technol 41, 4158-4163.

Liu, X., Gurel, D., Morris, D., Murray, D.W., Zhitkovich, A., Kane, A.B., Hurt, R.H., 2007. Advanced Materials 19, 2790.

Luechinger, N.A., Athanassiou, E.K., Stark, W.J., 2008. Graphene-stabilized copper nanoparticles as an air-stable substitute for silver and gold in low-cost ink-jet printable electronics. Nanotechnology 19, 445201.

Magrez, A., Kasas, S., Salicio, V., Pasquier, N., Seo, J.W., Celio, M., Catsicas, S., Schwaller, B., Forro, L., 2006. Cellular toxicity of carbon-based nanomaterials. Nano Lett 6, 1121-1125.

Maiorano, G., Sabella, S., Sorce, B., Brunetti, V., Malvindi, M.A., Cingolani, R., Pompa, P.P., 2010. Effects of cell culture media on the dynamic formation of protein-nanoparticle complexes and influence on the cellular response. ACS Nano 4, 7481-7491.

Meng, H., Chen, Z., Xing, G., Yuan, H., Chen, C., Zhao, F., Zhang, C., Zhao, Y., 2007. Ultrahigh reactivity provokes nanotoxicity: explanation of oral toxicity of nano-copper particles. Toxicol Lett 175, 102-110.

Midander, K., Cronholm, P., Karlsson, H.L., Elihn, K., Moller, L., Leygraf, C., Wallinder, I.O., 2009. Surface characteristics, copper release, and toxicity of nano- and micrometer-sized copper and copper(II) oxide particles: a cross-disciplinary study. Small 5, 389-399.

Monteiro-Riviere, N., Inman, A., 2006. Challenges for assessing carbon nanomaterial toxicity to the skin. Carbon 44, 1070-1078.

Murdock, R.C., Braydich-Stolle, L., Schrand, A.M., Schlager, J.J., Hussain, S.M., 2008. Characterization of nanomaterial dispersion in solution prior to in vitro exposure using dynamic light scattering technique. Toxicol Sci 101, 239-253.

Nel, A., Xia, T., Madler, L., Li, N., 2006. Toxic potential of materials at the nanolevel. Science 311, 622-627.

Nicola Cioffi, L.T., Nicoletta Ditaranto, Giuseppina Tantillo, Lina Ghibelli, Luigia Sabbatini, Teresa Bleve-Zacheo, Maria D'Alessio, P. Giorgio Zambonin, and Enrico Traversa, 2005. Copper Nanoparticle/Polymer Composites with Antifungal and Bacteriostatic Properties. Chemistry of Materials 17, 5255-5262.

Oberdorster, E., 2004. Manufactured nanomaterials (fullerenes, C60) induce oxidative stress in the brain of juvenile largemouth bass. Environ Health Perspect 112, 1058-1062.

Park, E.J., Yi, J., Kim, Y., Choi, K., Park, K., 2010. Silver nanoparticles induce cytotoxicity by a Trojan-horse type mechanism. Toxicol In Vitro 24, 872-878.

Park J, K.E., Son SU, Park MH, Lee KM, Kim J, Kim KW, Noh H-J, Park J-H, Bae CJ, Park J-G, Hyeon T, 2005. Monodisperse nanoparticles of Ni and Nio:synthesis, characterization, self-assembled superlattices and catalytic applications in the suzuki coupling reactions. Adv. Mater 17, 429-434.

Peters, K., Unger, R.E., Kirkpatrick, C.J., Gatti, A.M., Monari, E., 2004. Effects of nano-scaled particles on endothelial cell function in vitro: studies on viability, proliferation and inflammation. J Mater Sci Mater Med 15, 321-325.

Repetto, G., del Peso, A., Zurita, J.L., 2008. Neutral red uptake assay for the estimation of cell viability/cytotoxicity. Nat Protoc 3, 1125-1131.

Rivera Gil, P., Oberdorster, G., Elder, A., Puntes, V., Parak, W.J., 2010. Correlating physico-chemical with toxicological properties of nanoparticles: the present and the future. ACS Nano 4, 5527-5531.

Roco, M.C., 2005. International Perspective on Government Nanotechnology Funding in 2005. Journal of Nanoparticle Research 7.

Sayes, C.M., Wahi, R., Kurian, P.A., Liu, Y., West, J.L., Ausman, K.D., Warheit, D.B., Colvin, V.L., 2006. Correlating nanoscale titania structure with toxicity: a cytotoxicity and inflammatory response study with human dermal fibroblasts and human lung epithelial cells. Toxicol Sci 92, 174-185.

Seaton, A., Tran, L., Aitken, R., Donaldson, K., 2010. Nanoparticles, human health hazard and regulation. J R Soc Interface 7 Suppl 1, S119-129.

Song, Y., Li, X., Du, X., 2009. Exposure to nanoparticles is related to pleural effusion, pulmonary fibrosis and granuloma. Eur Respir J 34, 559-567.

Stone, V., Johnston, H., Schins, R.P., 2009. Development of in vitro systems for nanotoxicology: methodological considerations. Crit Rev Toxicol 39, 613-626.

Studer, A.M., Limbach, L.K., Van Duc, L., Krumeich, F., Athanassiou, E.K., Gerber, L.C., Moch, H., Stark, W.J., 2010. Nanoparticle cytotoxicity depends on intracellular solubility: comparison of stabilized copper metal and degradable copper oxide nanoparticles. Toxicol Lett 197, 169-174.

Stumm, W., Morgan, J.J., 1996. Aquatic Chemistry. Wiley Interscience, New York.
Tarasov S, K.A., Belyaev S, Lerner M, Tepper F, 2002. Study of friction reduction by nanocopper additives to motor oil. Wear 252, 63-69.

Teeguarden, J.G., Hinderliter, P.M., Orr, G., Thrall, B.D., Pounds, J.G., 2007. Particokinetics in vitro: dosimetry considerations for in vitro nanoparticle toxicity assessments. Toxicol Sci 95, 300-312.

Verwey, E.J.W., Overbeek, J.T., 1948. Theory of the stability of lyophobic Colloids. Elsevier, Amsterdam.

Wagner C. D., R.W.M., Davis L.E., Moulder J.F., Muilenberg G.E., 1978. Handbook of X-Ray Photoelectron Spectroscopy. Perkin-Elmer Corporation, Eden Prairie, MN.

Wang H, K.X., Zhang J, Li J, 2008. Large scale synthesis and characterization of Ni nanoparticles by solution reduction method. Bull Mater Sci 31, 97-100.

Warheit, D.B., 2008. How meaningful are the results of nanotoxicity studies in the absence of adequate material characterization? Toxicol Sci 101, 183-185.

Warheit, D.B., 2010. Debunking Some Misconceptions about Nanotoxicology. Nano Lett 10, 4777-4782.

Wittmaack, K., 2011. Excessive delivery of nanostructured matter to submersed cells caused by rapid gravitational settling. ACS Nano 5, 3766-3778.

Worle-Knirsch, J.M., Pulskamp, K., Krug, H.F., 2006. Oops they did it again! Carbon nanotubes hoax scientists in viability assays. Nano Lett 6, 1261-1268.

Xia, T., Kovochich, M., Liong, M., Madler, L., Gilbert, B., Shi, H., Yeh, J.I., Zink, J.I., Nel, A.E., 2008. Comparison of the mechanism of toxicity of zinc oxide and cerium oxide nanoparticles based on dissolution and oxidative stress properties. ACS Nano 2, 2121-2134.

Yoon, K.Y., Hoon Byeon, J., Park, J.H., Hwang, J., 2007. Susceptibility constants of Escherichia coli and Bacillus subtilis to silver and copper nanoparticles. Sci Total Environ 373, 572-575.

Zhang XF, D.X., Huang H, Wang DK, Lv B, Lei JP, 2007. High permittivity from defective carbon coated Cu nanocapsules. Nanotechnology 18.

Zhao, F., Zhao, Y., Liu, Y., Chang, X., Chen, C., 2011. Cellular uptake, intracellular trafficking, and cytotoxicity of nanomaterials. Small 7, 1322-1337.

Chapter V

Investigation of Cytochrome c (Cyt c) Stability and a Liposome Formulation for Its Intracellular Delivery to Induce Apoptosis

5.1 Summary

Cytochrome c is a mitochondrial protein which upon release to cytosol leads to apoptotic cell death. Its mechanism of action reinforces its potential as an anti-cancer therapeutic agent if it could be exogenously delivered to cancer cells. However, Cyt c lacks physicochemical characteristics required for successful cell permeation. Nanocarriers have been widely used to facilitate intracellular delivery of many protein drugs; however, a major limitation of using traditional polymer based nanocarriers for protein drugs is exposure of proteins to organic solvents and high shear/stress conditions during formulation. Another challenge for successful delivery of intra-cellular acting proteins is to induce their endosomal release. The objective of these studies was to investigate stability and intracellular delivery of Cyt c using DOTAP and cholesterol (DOTAP-Chol) liposomes prepared using a film hydration method. The effect of formulation (pH and ionic strength) and process conditions (sonication, freeze thaw cycling and extrusion) on Cyt c stability and entrapment in liposomes was evaluated. Modulation of hydration buffer pH from 7 to 8.5 showed an increase in the entrapment efficiency of Cyt c in DOTAP-Chol liposomes from 2% to 30%. Optimized liposomal Cyt c formulation showed apoptotic activity in MDA-MB-231 cells.

Cytochrome c released from optimized liposomal formulation was physically and chemically stable as no aggregation, secondary and heme crevice structure change and deamidation was observed. Additionally, Cyt c released from optimized liposomal formulation retained apoptotic activity after storage of formulation for twenty eight days at 4 ^{o}C.

5.2 Introduction

Cytochrome c is a 12 KDa, 104 amino acid endogenous heme protein found loosely attached to inner mitochondrial membrane in cells (Dickerson, 1971). Cytochrome c has been historically known to play a vital role in respiration where it acts as an electron carrier between complex III and complex IV in the mitochondria. In recent years, another important function of Cyt c, as a central player in inducing apoptosis after its release from mitochondria into cytosol has been discovered (Ow et al., 2008). Apoptosis is a tightly regulated form of cell death. The intrinsic apoptotic signals such as increased ROS levels in cells triggers release of Cyt c into cytoplasm where Cyt c participates and facilitates apoptotic protease activating factor 1 (APAF1) and caspase 9 recruitment into a complex known as apoptosome. Further downstream signaling involves activation of caspase 9 and other events in apoptosis such as translocation of phosphatidyl serine from inner lipid layer to outer lipid layer in plasma membrane (Kasibhatla and Tseng, 2003). Cytochrome c microinjected in various cancer cells has shown to activate apoptotic cell death (Li et al., 1997; Schafer et al., 2006; Zhivotovsky et al., 1998). Zhivotovsky *et al.*, showed induction of apoptosis after microinjection of 20 uM Cyt c in normal rat kidney cells (NRK cells) (Zhivotovsky et al., 1998). Li *et al.*, also observed apoptosis after microinjection of Cyt c in human embryonic kidney 293 cells (Li et al., 1997). They also tested other heme containing proteins such as myoglobin, hemoglobin in order to check for specificity of Cyt c in inducing apoptotic cell death and only Cyt c was shown to induce apoptosis. Interestingly, breast cancer cells show unique sensitivity to apoptosis to exogenously administered Cyt c. It has been shown that when cytosolic extracts from various cell lines were supplemented with exogenous Cyt c and monitored for caspase activity, higher caspase activity was observed in a series of malignant

mammary epithelial cell lines compared to cancer cells from other origin such as lung, prostate, colon and ovaries (Schafer et al., 2006). Thus, Cyt c is a direct and specific apoptogen and a viable anticancer agent especially for the treatment of breast cancer.

However, due to its hydrophilic, positively charged nature and propensity for degradation by plasma proteases, Cyt c lacks the physicochemical characteristics required for successful permeation and delivery to cancer cells. Various nanocarriers especially polymeric based systems such as poly lactic-co-glycolic acid (PLGA) based systems have been proposed for delivery of proteins, however, their formulation often requires the use of organic solvents and high shear/temperature conditions which may denature proteins (Lassalle and Ferreira, 2007; van de Weert et al., 2000a; van de Weert et al., 2000b; van de Weert et al., 2000c). It has been shown that lysozyme entrapped in PLGA microspheres prepared using w/o/w solvent evaporation process is present as aggregates (van de Weert et al., 2000c). Formulation approaches involving exposure of proteins to organic solvents may lead to entrapment of partly or completely denatured therapeutically inactive proteins which may ultimately require high and even toxic nanocarrier dose for observing activity. Thus, there exists a need to develop processes for formulating proteins in nano-systems which involves minimal exposure to denaturing conditions and to evaluate the effect of process and formulation conditions on not only activity of proteins but also its structural integrity.

Recently, polymeric NPs were proposed for intracellular Cyt c delivery to induce apoptosis. A solvent evaporation method and exposure to water/dimethylformamide (DMF) mixture and acetone was described as steps in prepration (Santra et al., 2010). Exposure to DMF is known to induce protein unfolding as it can form hydrogen bonds with the protein backbone (Mattos and Ringe, 2001). Although, it was reported that activity of encapsulated

Cyt c was equivalent to non-encapsulated Cyt c as measured by peroxidase activity. However, it was not stated if peroxidase activity of Cyt c correlates with its apoptosis inducing activity. Additionally, an increase in peroxidase activity of Cyt c has been linked with partial unfolding of Cyt c (Belikova et al., 2006). Another report describes attachment of a hydrophobic peptide to Cyt c with subsequent attachment to the surface of lipid based NPs for apoptosis induction (Kim et al., 2012). Apoptosis inducing activity (measured by caspase 9 cleavage) of peptide modified Cyt c was two to four fold lower than unmodified Cyt c, indicating some denaturation of Cyt c in the process of conjugation.

Liposomes are bilayered lipid vesicles with an aqueous core suitable for encapsulating hydrophilic proteins (Bangham, 1980). Film hydration method can be used to formulate proteins in liposomes without using organic solvents, high shear or temperature; however, a typical limitation of liposomes is low entrapment efficiencies (EE) (Weiner, 1994). Freeze thaw cycling of protein lipid mixture after film hydration has been shown to increase entrapment of protein drugs, but freeze thaw cycling can also lead to protein denaturation (Mayer et al., 1986; Mayer et al., 1985; Pick, 1981; Weiner, 1994). A recent report on acetylcholine transferase entrapment in liposomes suggested increasing the interaction (specific or non-specific) between protein drugs and lipids as a means of increasing protein entrapment in liposomes (Colletier et al., 2002).

Another challenge in the intracellular delivery of Cyt c is inducing its endosomal release. Failure to escape endosome can result in entrapment of proteins in lysosomes where protein denaturation can occur due to low pH and presence of proteases (Du et al., 2012). It was recently demonstrated that Cyt c adsorbed onto carbon nanotubes permeated cells but could not initiate apoptosis induction until chloroquine (an endosomal disruptor) was co-

incubated (Kam and Dai, 2005). Therefore, for delivering Cyt c in cytosol, it is imperative to include an endosomal releasing agent as a component of delivery system. Dioleoyl-trimethyl-ammonium-propane lipid has been extensively used in the gene delivery and has been shown to induce endosomal release of macromolecular drugs (Fretz et al., 2007).

The hypothesis for these studies was that the entrapment of Cyt c in DOTAP-Chol liposomes prepared using film rehydration method will overcome the challenges for delivery of Cyt c while maintaining conditions for optimal Cyt c stability. We further hypothesized that modulating the pH of hydration buffer will increase the entrapment of Cyt c in liposomes without compromising structural integrity and apoptosis inducing activity of Cyt c.

5.3 Materials and Methods

Materials

Cytochrome c (equine heart) and cholesterol were purchased from Sigma Aldrich (St. Louis, MO). Dioleoyl-trimethyl-ammonium-propane was purchased from Avanti Polar Lipids, Inc. (Alabaster, AL). RPMI media was purchased from Invitrogen (Carlsbad, CA). MDA-MB-231 breast cancer cell line, penicillin-streptomycin solution and fetal bovine serum (FBS) were purchased from ATCC. Plasmocin was purchased from Invivogen (San Diego, CA). Annexin V FITC and propidium iodide (PI) were purchased from BD Pharmingen (San Diego, CA). All chemicals were used without any further purification.

Liposome Preparation

The film hydration method was used to prepare liposomes. A total of 990 µg lipid mixture composed of 1:1 mol ratio of DOTAP and cholesterol in chloroform was added to 7 mL glass vial and dried under nitrogen stream to form a thin film on the sides and bottom of glass vial. This was followed by dessication under vacuum for 4-6 h to ensure complete evaporation of chloroform. A series of Cyt c solutions (2 mg/mL) were prepared, each with a different ionic strength and pH. During the hydration step, the Cyt c solutions were added to separate vials containing the dried lipid film after which the vials were kept at 4 ^{o}C overnight. Cyt c solutions were buffer exchanged with respective buffers using 3KDa Amicon filters before the hydration step. To evaluate the effect of pH and ionic strength on entrapment and stability of Cyt c, three pH levels (5, 7 and 8.5) and two ionic strength conditions (15 mM and 150 mM) were tested. For sizing the multilamellar vesicles formed upon hydration, two methods were used, (1) Sonication + Extrusion (SE) where bath sonication (1 min) and extrusion (ten cycles through 100 nm polycarbonate filters) was used

and (2) Freeze Thaw + Extrusion (FTE) where four cycles of freezing (in liquid nitrogen) and thawing (at 4 ^{o}C) were followed by extrusion (ten cycles through 100 nm polycarbonate filters). Liposome size and zeta potential was measured using Malvern Nano ZS. Unentrapped Cyt c was removed by filtration using 100KDa Amicon filters. Entrapment was calculated by measuring the absorbance of entrapped Cyt C at 410 nm. The absorbance at 410 nm was corrected for any interference from liposome controls (without any Cyt c). Percent entrapment and percent protein loading were calculated as follows:

$$\%\ \text{Entrapment} = \frac{[\text{Protein (mg)in liposomes}]}{[\text{Initial protein added (mg)}]} \times 100$$

$$\%\ \text{Protein Loading} = \frac{[\text{Protein (mg)in liposomes}]}{[\text{Total formulation wt.(mg)}]} \times 100$$

Dynamic Light Scattering (DLS)

DLS was used to study the effect of process (FTE or SE) and formulation (pH and ionic strength) conditions on aggregation potential of Cyt c (processed-Cyt c) and released Cyt c from purified liposomal Cyt c formulation. The effect of pH and ionic strength conditions on aggregation of processed-Cyt c was evaluated after Cyt c (2 mg/mL) was buffer exchanged with respective buffer and ionic strength conditions and incubated overnight at 4 ^{o}C. For assessment of effect of process conditions, Cyt c (2 mg/mL) was buffer exchanged with respective buffer and ionic strength conditions, incubated overnight at 4 ^{o}C and additionally samples were processed through SE and FTE cycles. These conditions mimicked the conditions that were used to evaluate the entrapment of Cyt c in liposomes except that lipids were not included. Samples were centrifuged for 5 min before analysis and 90 uL supernatant was used for analysis. Similar procedure was followed for determining

aggregation of released Cyt c and control Cyt c (Control Cyt c refers to Cyt c that was used as a control for process and storage conditions used for releasing Cyt c from liposomal Cyt c but without any lipids). DynaPro™ Plate Reader (Wyatt Technology) was used to check for presence of any aggregates of Cyt c or change in distribution.

Circular Dichroism (CD)

Circular dichroism was used to study the effect of process (FTE or SE) and formulation (pH and ionic strength) conditions on secondary and heme crevice structure of processed-Cyt c and of released Cyt c from purified liposomal Cyt c formulations. Processed-Cyt c was prepared as described in DLS studies section and diluted before CD analysis so that the concentration was close to 0.1mg/mL. The spectra were recorded using Chirascan™ Plus Spectropolarimeter (Applied Photophysics) under nitrogen flow using 0.1 cm pathlength at 25 ^{o}C. For determining secondary structure, a range of 190 to 260 nm was scanned and for heme crevice structure, a range of 400 to 500 nm was scanned. Spectra were recorded using step size of 0.5 nm. Buffer spectra were subtracted from Cyt c spectra and the resultant spectra were smoothed using the software supplied with the instrument. The spectra were then corrected for concentration of samples using absorbance at 410 nm measured by BioTek Synergy™ Microplate Reader.

Flow Cytometry

Flow cytometry was carried out to quantitate the early apoptotic and late apoptotic cells after treatment of MDA-MB-231 cells with the liposomal formulation and controls. Briefly, MDA-MB-231 cells (300,000) were seeded in a six well plate and allowed to attach for 24 h. The media was changed after 24 h to serum free media and various treatments (Cyt c, control liposomes and purified liposomal Cyt c) were added to cells. Negative control was MDA-

MB-231 cells without any treatment and positive control was staurosporine (STS) treated cells (4 uM overnight treatment). The effect of purified liposomal Cyt c on apoptosis was evaluated after 2, 6, 12 and 24 h after incubation while all controls were incubated for 24 h. After required incubation, the media supernatants (which contained dead cells) were collected; the attached cells were trypsinized, and combined with the supernatants. This was followed by centrifugation of cell suspension and resuspension of cell pellet in 1 mL of Annexin V FITC binding buffer. Cell suspension (300 uL) was transferred to flow tubes and Annexin V FITC (1 uL) and PI (propidium iodide) solution (4uL) was added to each sample tube and allowed to incubate for 15 min in dark. Binding buffer (200 uL) was added and fluorescence was quantitated using BD FACS Caliber using FL1 channel for FITC and FL2 for PI. Analysis was performed using Summit 5.1 software.

Microinjection

Microinjection studies were carried out to (1) estimate the amount of Cyt c required to induce cell death in MDA-MB-231 cells and (2) to check the apoptotic activity of Cyt c upon release from purified liposomal Cyt c after storage for seven and twenty eight days at 4 ^{o}C. Previously published processes in the literature were followed (Kole et al., 2011; Potts et al., 2003). Briefly, microinjections were carried out using Narashigi Micromanipulator mounted on an Inverted Fluorescence Microscope (Leica). MDA-MB-231 cells (150,000) were seeded in 35 mm cell culture petri dishes and allowed to attach overnight. Media was changed next day and cells were microinjected using microinjection needles. Several concentrations of Cyt c (100, 250, 500 and 1000 µg/mL) in microinjection buffer (100 mM potassium chloride and 10 mM potassium phosphate buffer, pH 7.4) were injected. Rhodamine dextran dye (4mg/mL) was included in microinjection buffer to mark the injected

cells. Rhodamine positive viable cells were counted at 0 h and 5 h after microinjection in a particular field. Rounded cells and cells that lifted off the plate were counted as dead cells. Cell death was expressed in percentage. The concentration of Cyt c solution was converted to Cyt c (pg)/cell by assuming a constant microinjection volume of 20 pL per cell. A similar procedure was followed for determining apoptotic activity of released Cyt c and control Cyt c except Cyt c concentration of 1 mg/mL were used.

Iso Electric Focusing (IEF)

The chemical stability of Cyt c released from optimized and purified liposomal Cyt c formulation and of control Cyt c against deamidation was assessed using IEF. Formulations and control Cyt c were stored for seven days at 4 ^{o}C before Cyt c release was induced. A IPGphor Isoelectric Focusing System (Amersham Pharmacia Biotech) was used. Released Cyt c and control Cyt c was concentrated to 1 mg/mL and mixed with rehydration buffer (8 M urea, 2% CHAPS, 0.002% bromophenol blue, 2% DTT and 0.5% carrier ampholyte) so that 125 uL of diluted sample had 50 ug Cyt c. Immobilized pH 6-11, 7 cm strips were hydrated overnight with the rehydration buffer containing Cyt c. The following order of voltage increments was used for focusing: 300 V for 1 min followed by gradient up to 3500 V over 90 min followed by focusing at 3500 V for 5 h. The PI value was assigned based on variation of pH across the length of strip based on data obtained from GE Lifesciences.

UV Aborbance Studies

In order to monitor for pH induced unfolding transitions in Cyt c, Cyt c absorbance was measured at 393 nm (high spin Fe, unfolded state) and 410 nm (low spin Fe, folded state) using BioTek Synergy™ Microplate Reader. Cytochrome c (2mg/mL) solutions of varying pH (from 1 to 8.5) were prepared and kept overnight at 4 ^{o}C. The solutions were

diluted to a concentration of 250 µg/mL using respective pH buffers and absorbance was measured at 393 nm and 410 nm.

Statistical Analysis

Statistical analysis was performed using either one-way analysis of variances (ANOVA) followed by pair-wise comparison using Tukey's multiple comparison test or two way ANOVA followed by bonferroni post tests using GraphPad Prism Software. Data were considered statistically significant when p value was less than 0.05.

5.4 Results

Microinjection studies of Cyt c

Microinjection of Cyt c was carried out to verify the apoptotic inducing activity of Cyt c source used in our studies. Furthermore, dose dependent evaluation of apoptotic activity via microinjection showed potent Cyt c activity (**Figure 5.1A & 5.1B**). Within 5 h of microinjection, 80% cell death was observed with 5 pg Cyt c/cell which indicated highly potent apoptosis inducing activity.

Effect of process and formulation conditions on stability of processed-Cyt c

The effect of change in formulation (pH and ionic strength) and process (sonication and extrusion) conditions on processed-Cyt c to potentially undergo any aggregation and structural integrity change was evaluated using DLS and CD. After overnight incubation of Cyt c at 4 ^{o}C in buffers (pH 5, 7 and 8.5 and ionic strength 15 mM and 150 mM), no increase in aggregation was observed (**Figure 5.2A**). For evaluation of effect of process conditions (SE and FTE) on aggregation and structural change of processed-Cyt c, only pH 7 and pH 8.5 buffer in low ionic strength conditions (15 mM) were used. These conditions were tested because preliminary entrapment results showed aggregation of DOTAP-Chol liposomes in high ionic strength (150 mM) and disintegration in pH 5. The purpose of evaluating the effect of formulation and process condition on stability of Cyt c was to mimic the effect of conditions that would be used for entrapment studies. As seen in **Figure 5.2B**, no increase aggregation of processed-Cyt c was observed in any conditions except in pH 8.5 and FTE conditions, where aggregation (5% by mass) was observed. A characteristic CD spectrum for alpha helical structure was observed for Cyt c with major bands at 208 and 222 nm and was consistent with reported literature (Parthasarthy and Johnson, 1985). No changes in the

secondary structure region were observed for pH 7 and pH 8.5, 15 mM conditions and for the SE and FTE conditions (**Figure 5.3A**). A characteristic heme crevice band at 416 nm was also observed for Cyt c in pH 7, 15 mM condition (**Figure 5.3B**). However, the intensity of this band was lower in pH 8.5, 15mM condition regardless of the process conditions (SE or FTE) tested. In order to investigate whether the change in heme crevice structure due to pH 8.5 was local or affected global stability of Cyt c, the effect of pH on unfolding of Cyt c was determined. Cytochrome c absorbance at 410 nm (characteristic of low spin Fe, folded state) and 393 nm (characteristic of high spin Fe, unfolded state) was monitored (**Figure 5.4**). In pH range from 3 to 8.5, higher absorbance at 410 nm compared to 393 nm was observed, but below pH 3, a sharp increase in absorbance at 393 nm was observed and absorbance of at 410 nm was considerably lower.

Effect of varying ionic strength and pH condition on entrapment of Cyt c

Cytochrome c entrapment in DOTAP-Chol liposomes was studied at three pH's (5, 7 and 8.5) and two ionic strengths (15 mM and 150 mM) using SE and FTE methods. A preliminary assessment of hydration of lipid films (DOTAP-CHOL 1:1 mol to mol) in buffers (pH 5, 7 and 8.5 and ionic strength 150 mM) resulted in non-uniform dispersion of lipid film and presence of lipid aggregates, which were present even upon sonication. Furthermore, when pH 5 buffer was added to DOTAP-Chol liposomes, disintegration into visible lipid fragments was observed. Therefore, for evaluation of the effect of pH on entrapment of Cyt c in DOTAP-Chol liposomes, pH 7 and 8.5 at 15mM ionic strength conditions were studied. Highest entrapment (30-35%) was observed under pH 8.5 & 15 mM ionic strength conditions (**Figure 5.5**). Characteristics of formulations at pH 8.5 are summarized in **Table 5.1.** The average size of liposomal Cyt c formed by SE process at pH

8.5 (Formulation 1 or "Form 1") was 160 ± 10 nm while that formed by FTE process at pH 8.5 (Formulation 2 or "Form 2") was 170 ± 10 nm.

Stability and activity of released Cyt c and liposomal Cyt c

During entrapment studies, it was observed that addition of pH 5 buffer led to disintegration of DOTAP-Chol liposomes. This phenomenon of liposome disintegration was utilized to induce release of Cyt c from purified liposomal Cyt c (Form 1 and Form 2) after storage of formulations at 4 ^{o}C. This procedure of inducing Cyt c release also mimics release of Cyt c from delivery system in cells as endosomes have an acidic pH and cytosol has neutral pH. A schematic describing procedure for induction of Cyt c release from formulations is shown in **Figure 5.6**. Circular dichroism spectra of Cyt c after release from purified Form 1 overlapped with that of the CD spectra of Cyt c, pH 7 and processed-Cyt c, pH 8.5 (**Figure 5.7A**). In contrast, the CD spectra of Cyt c released from purified Form 2 showed lower band intensity at 208 nm. The heme crevice structure was also monitored after release of Cyt c from purified liposomal Cyt c (**Figure 5.7B**). The CD spectra in the 400- 450 nm range of Cyt c released from purified Form 1overlapped with Cyt c at pH 7 indicating that the lower band intensity induced in processed Cyt c due to exposure to alkaline pH (8.5) is reversible upon changing the pH back to pH 7. However, CD spectra of Cyt c released from purified Form 2 showed only partial reversibility and lower band intensity compared with Cyt c released from purified Form 1 and Cyt c, pH 7. Based on these results it was decided to move forward with Form 1 for further stability analysis. Consequently, aggregation potential and chemical stability (against deamidation) of Cyt c released from purified Form 1 and control Cyt c (after seven days storage of Form 1 and control Cyt c at 4 ^{o}C) was assessed using DLS and IEF. As shown in **Figure 5.8A**, no aggregation was

observed in Cyt c released from purified Form 1. Isoelectric focusing analysis (**Figure 5.8B**) showed that mobility of Cyt c released from purified Form 1 and control Cyt c was same as untreated Cyt c. A PI (iso-electric point) value of 9.7 was assigned based on position of Cyt c band relative to the length of immobilized strip. No other band was observed in Cyt c released from purified Form 1 and control Cyt c indicating absence of any deamidated species. The activity of Form 1 was assessed using annexin V FITC which detects the presence of phosphatidyl serine on outer leaflet of plasma membrane (which is a hallmark of early apoptosis) and PI which enters cells with compromised plasma membrane (a sign of late apoptosis). After 24 h incubation with no treatment (negative control), Cyt c only, STS and Form 1; annexin V FITC and PI positive cells were quantified using flow cytometer (**Figure 5.9A**). Each panel in **Figure 5.9A** has four quadrants: Q1 (PI only positive cells or necrotic cells), Q2 (PI and FITC positive or late apoptotic cells), Q3 (FITC only positive or early apoptotic cells) and Q4 (PI and FITC negative or viable cells). For quantifying apoptosis, percent cells in Q2 and Q3 were added together. In untreated and Cyt c only treated cells, 6.3 ± 0.7% and 6.6 ± 1.7% of the cell population were apoptotic whereas Form 1 after 24 h showed 27.0 ± 5 % apoptotic cells. A kinetic analysis of apoptosis induction in MDA-MB-231 cells upon treatment with Form 1 (**Figure 5.9B**) showed basal level of apoptotic cell population after 2 h and 6 h treatment and after 12 h, 18 ± 0.3% apoptotic cell population was present. Released Cyt c from purified Form 1and control Cyt c (after seven and twenty eight days storage of formulation at 4 ^{o}C) was also checked for apoptotic activity using microinjection (**Figure 5.10).** No significant difference ($P > 0.05$) was found between percent cell death after microinjection of fresh Cyt c (0 days), Cyt c released from Form 1 and control Cyt c.

5.5 Discussion

Many barriers exist for successful intracellular delivery of cytosolic proteins such as Cyt c. Nanocarriers can be used to improve cell permeability of hydrophilic and charged proteins, however, one of the major drawbacks of protein delivery using traditional nanocarriers like PLGA based systems is exposure of protein drugs to organic solvents, high temperatures and high shear conditions. In the last five years, many reports have been published on the intracellular delivery of proteins. Most of these reports focus on improving the intracellular delivery of model proteins using various approaches like bacterial inclusions bodies (Villaverde et al., 2012), stapled peptides (Verdine and Hilinski, 2012), cell penetrating peptides (Chugh et al., 2010), silk NPs (Kundu et al., 2009), charge conversional polyionic complexes (Lee et al., 2009), and layer by layer cross linked carriers (Shu et al., 2010). Although it is important to develop approaches for enhanced intracellular delivery of proteins, it is also imperative to evaluate the effect of process and formulation conditions used in these new technologies on structural integrity and specific activity of the protein of interest. Only a few studies (De Rosa et al., 2011; Son et al., 2009) have focused on the protein stability aspect of protein delivery. In this investigation, studies were designed to evaluate the effect of formulation and process conditions on structural integrity, liposomal entrapment and apoptosis inducing activity of Cyt c. Initial studies were focused on characterizing the apoptosis inducing activity of Cyt c using microinjection. After the release of Cyt c from mitochondria to cytosol, specific residues in Cyt c interact with β propeller structures in APAF 1 to induce a conformational change in APAF 1 from closed to open confirmation, which initiates the formation of apoptosome and further downstream signaling for apoptosis (Yuan et al., 2010). Many residues in Cyt c including 7, 62, 65, 25, 39 and 72

have been implicated in mediating binding of Cyt c to APAF 1 and mutation in residue 72 (lysine) is known to abolish Cyt c binding to APAF 1 (Yu et al., 2001). Assessment of apoptotic activity of Cyt c using microinjection technique mimics most closely the cellular environment (in the presence of other required proteins) to determine apoptotic activity of Cyt c (Kole et al., 2011). Microinjection studies showed that Cyt c possesses very potent apoptotic activity, only 5 pg Cyt c/cell led to 80% cell death at 5 h after microinjection. The microinjection studies also provided an estimate (5 pg/cell) of the threshold Cyt c required to induce apoptosis when introduced exogenously in cells. This threshold estimate was very helpful from a protein delivery standpoint. Consequently, the film hydration method was used to entrap Cyt c in DOTAP-Chol liposomes. The film hydration method does not involve exposure of protein to any organic solvents and minimizes the potential of protein denaturation; however, the limitation of this method is low protein entrapment. Freeze –thaw cycling of lipid protein mixtures has been proposed in literature as a method of increasing protein entrapment in liposomes (Mayer et al., 1986; Pick, 1981). However, repeated freeze thaw cycling may also lead to protein denaturation (Weiner, 1994). In these studies, the effect of modulating the pH of Cyt c hydration buffer (and essentially Cyt c net charge) and freeze thaw cycling on Cyt c stability and entrapment in liposomes was studied. Prior to entrapment studies, the effect of various formulation and process related stresses like varying pH conditions, bath sonication, extrusion (increased air water interface) and freeze thaw cycling on aggregation potential and structural integrity of processed-Cyt c was determined. Aggregation was not observed after exposure of processed-Cyt c to changes in pH and ionic strength conditions. Usually, at a pH close to PI of the protein, aggregation is common in high concentration protein solutions (Chi et al., 2003; Shire et al., 2004). However, in our

studies, the utilized protein concentration was 2 mg/mL. This concentration was used because Cyt c entrapment in DOTAP-Chol liposomes was also studied at 2 mg/mL. However after exposure to pH 8.5 and FTE conditions, aggregation (5% by mass) was observed. This could be due to a combination of the pH being closer to PI (9.7-10) of Cyt c where protein has lower net charge and additionally exposure of processed- Cyt c to repeated freeze thaw cycles. Proteins are very sensitive to changes in their environment and in case of repeated freeze thaw cycling, higher stresses due to increased ice/water interface, phase separation and change in pH have been reported to lead to protein aggregation (Wang, 2000). No structural change in the secondary structure of Cyt c (monitored by intensity of CD bands at 222 and 208 nm) was observed after the process and formulation runs. Intensity of CD band at 416 nm (signifying the heme crevice structure) of processed-Cyt c was lower after processed-Cyt c exposure to pH 8.5, pH 8.5 SE and pH 8.5 FTE compared to pH 7 (**Figure 5.3B**). However, when Cyt c was released from purified Form 1, its intensity was similar to processed-Cyt c at pH 7 and suggested that the change in heme crevice structure of Cyt c was reversible in Form 1(**Figure 5.7B**). After Cyt c was released from purified Form 2, its intensity at 416 nm was lower than processed-Cyt c at pH 7 and suggested that the change in heme crevice structure of Cyt c released from Form 2 was not reversible. The CD band at 416 nm signifies the heme crevice structure of Cyt c, specifically the coordination bond between Fe in heme and Met80 but does not signify global unfolding. Absorbances at 393 nm and 410 nm were measured to determine any unfolding. No unfolding was observed at pH 8.5 as no change was observed between absorbance (410 nm and 393 nm) at pH 7 compared to pH 8.5. Furthermore, it has been reported that a transient change between Met 80 and Fe in Cyt c can occur around pH 8.8 but does not signify breakage of Met80 and Fe coordination or lysine misligation since

that requires higher pH of around 9.2 (Weinkam et al., 2008). Additionally, it has been reported that Cyt c loses its tertiary structure only under extreme alkaline conditions (pH 12).

The entrapment results clearly showed a significant difference ($p < 0.05$) between the entrapment of Cyt c in DOTAP-Chol liposomes at different pH's. The entrapment was 30% at pH 8.5 compared to 2% at pH 7. One possible explanation of higher entrapment of Cyt c in DOTAP-Chol liposomes can be lower net positive charge of Cyt c at pH 8.5 compared to pH 7 (Cyt c PI is 9.7-10). Lower net positive charge at pH 8.5 could result in lower electrostatic repulsion between positively charged Cyt c and positively charged DOTAP-Chol film during hydration step and this could lead to lower separation distances between lipid and Cyt c molecules. As per the DLVO [Derjaguin and Landau (Derjaguin and Landau, 1941); Verwey and Overbeek (Verwey and Overbeek, 1948)] theory, at smaller interparticle separation distance the attractive forces start dominating the repulsive forces. Moreover, Cyt c has patches of negatively charged (aspartic acid and glutamic acid) and positively charged (lysine) residues on its surface (Dickerson, 1971). Therefore, it is possible that due to low net charge and decreased electrostatic repulsion between DOTAP and Cyt c, the negatively charged face of Cyt c interacts with DOTAP and leads to higher entrapment. It was also noted that addition of pH 5 buffer to liposomal Cyt c lead to disintegration of blank liposomes and liposomal Cyt c. This phenomenon was then used to induce Cyt c release from liposomal Cyt c and to study aggregation, structural integrity and apoptotic activity of released Cyt c after buffer exchanging the released Cyt c to pH 7. These conditions of inducing Cyt c release from liposomes at pH 5 and changing pH to 7 also mimics the change in pH occurring in cells as the protein/delivery system traverses through endosomes (acidic pH) to cytosol (neutral pH). Released Cyt c from purified Form 2 showed changes in

secondary and heme crevice structure whereas released Cyt c from purified Form 1 showed CD spectra (for secondary structure and heme crevice structure) similar to processed-Cyt c at pH 7. Therefore, Cyt c released from Form1 was studied further for aggregation, deamidation and apoptotic activity. As seen in **Figure 5.8A & 5.8B**, Cyt c released from purified Form 1 showed no aggregation or deamidation. Moreover the apoptotic activity of Cyt c after its release from Form 1 (after Form 1was stored at 4 ^{o}C for seven and twenty eight days) was similar ($P > 0.05$) to fresh Cyt c apoptotic activity at day 0. The apoptotic activity of Form 1 after incubation with MDA-MB-231 cells was checked with Annexin V FITC assay and 27% cells were found apoptotic after 24 h which was significantly higher than negative controls and liposome only blanks. Thus, by systematically evaluating the effect of various process and formulation conditions on structural integrity, aggregation potential and apoptosis inducing activity of Cyt c, a liposomal Cyt c system was developed with sufficient entrapment and without exposing the protein to organic solvent or high shear conditions. DOTAP was included in the formulation to induce endosomal release; however, the positively charged DOTAP-Chol liposomes are known to aggregate in presence of serum. Therefore, pegylation of DOTAP-Chol liposomes is necessary to confer serum stability. Thus, future research studies will be focused on characterizing DOTAP-Chol liposomes interaction with Cyt c in the presence of PEG lipids and the evaluation of pegylated system for Cyt c delivery both *in vitro* and *in vivo*.

Table 5.1 Characteristics of Formulation 1 and Formulation 2

Formulations	Description	Size (nm)
Formulation 1 (Form 1)	Liposomal Cyt c; pH 8.5 SE	160 ± 10
Formulation 2 (Form 2)	Liposomal Cyt c; pH 8.5 FTE	170 ± 10

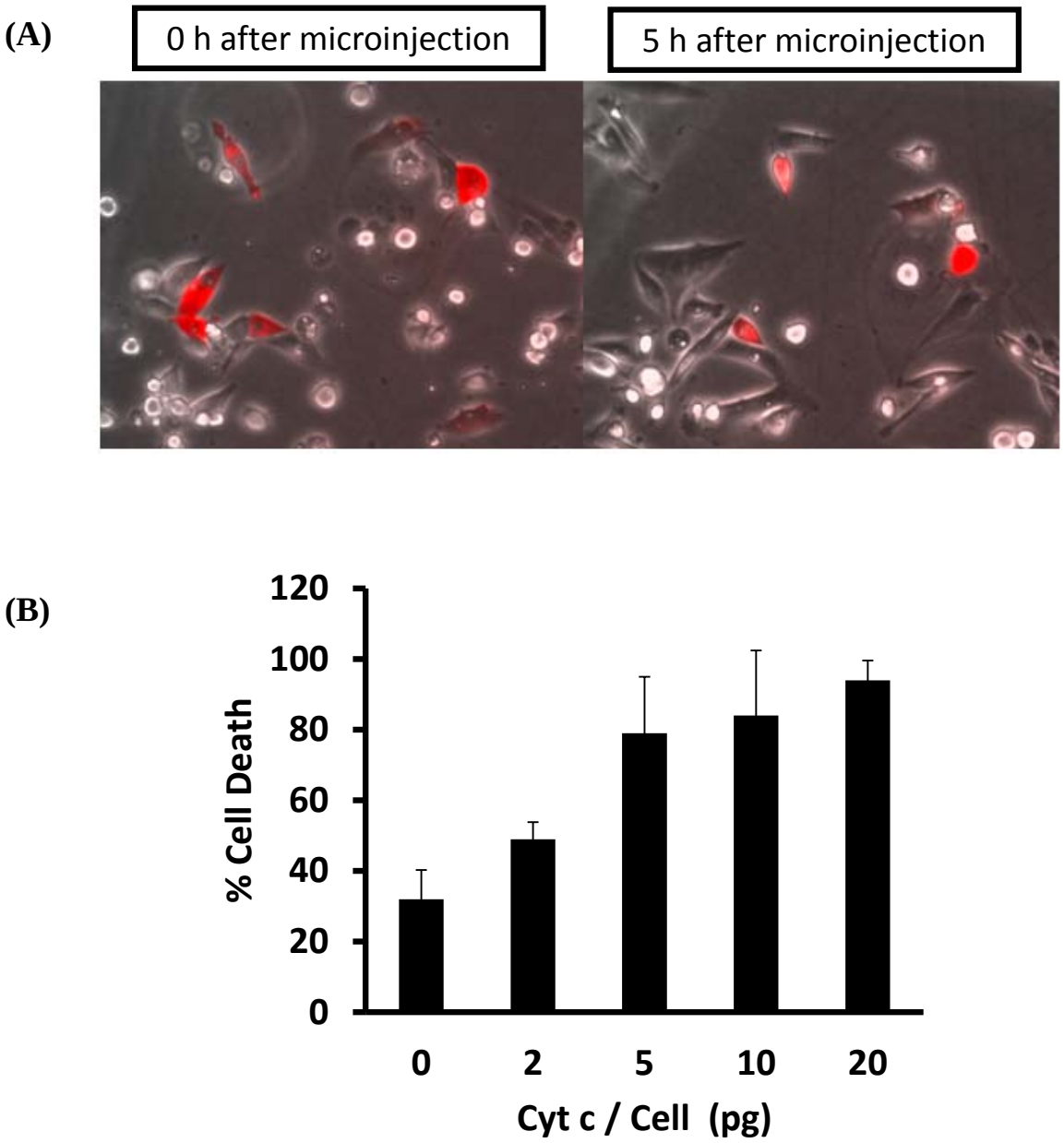

Figure 5.1 Microinjection studies of Cyt c. (A) Image showing MDA-MB-231 cells microinjected with Cyt c (20 pg) and rhodamine dextran (red) mixture. 20 pL volume was injected per injection. Flat and attached cells were counted as viable cells whereas rounded and floating cells were counted as dead cells. 5 h after microinjection, cells round up and number of flat cells could not be found at 20 pg/cell dose (B) Dose dependent cell death induced by Cyt c microinjecton in MDA-MB-231 cells, percent cell death was calculated 5 h after microinjection. For each dose at least 100 -150 cells were counted in total in three separate injections.

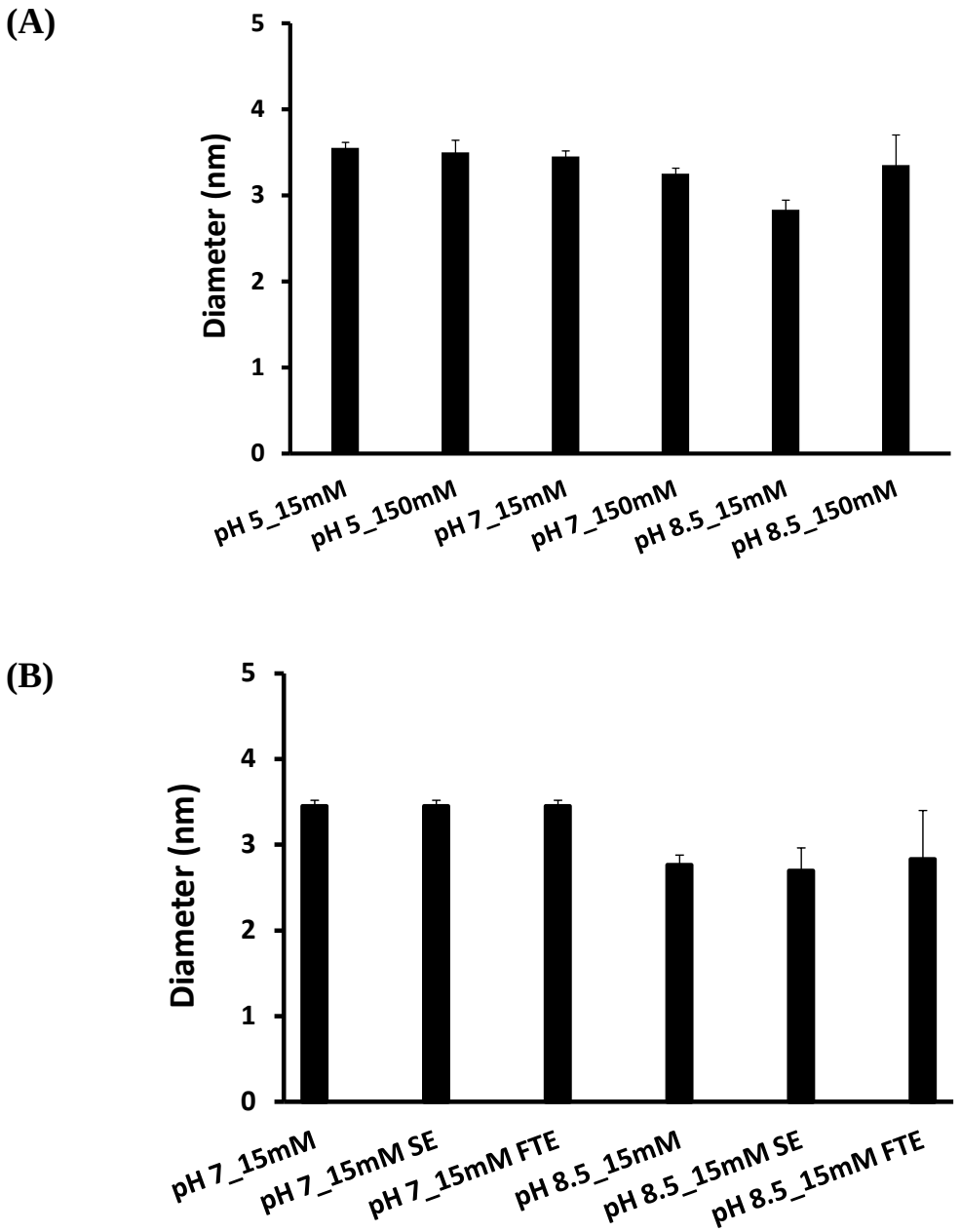

Figure 5.2 Effect of formulation and process conditions on aggregation of processed-Cyt c. Aggregation was measured using dynamic light scattering. (A) Processed-Cyt c did not show any aggregation under the tested conditions. The effect of three pH's (5, 7 and 8.5) and two ionic strengths (15 mM and 150 mM) conditions were tested. (B) Processed-Cyt c showed aggregation (5% by mass) when it was subjected to pH 8.5 and 15 mM conditions and processed using freeze thaw extrusion (FTE) entrapment procedure.

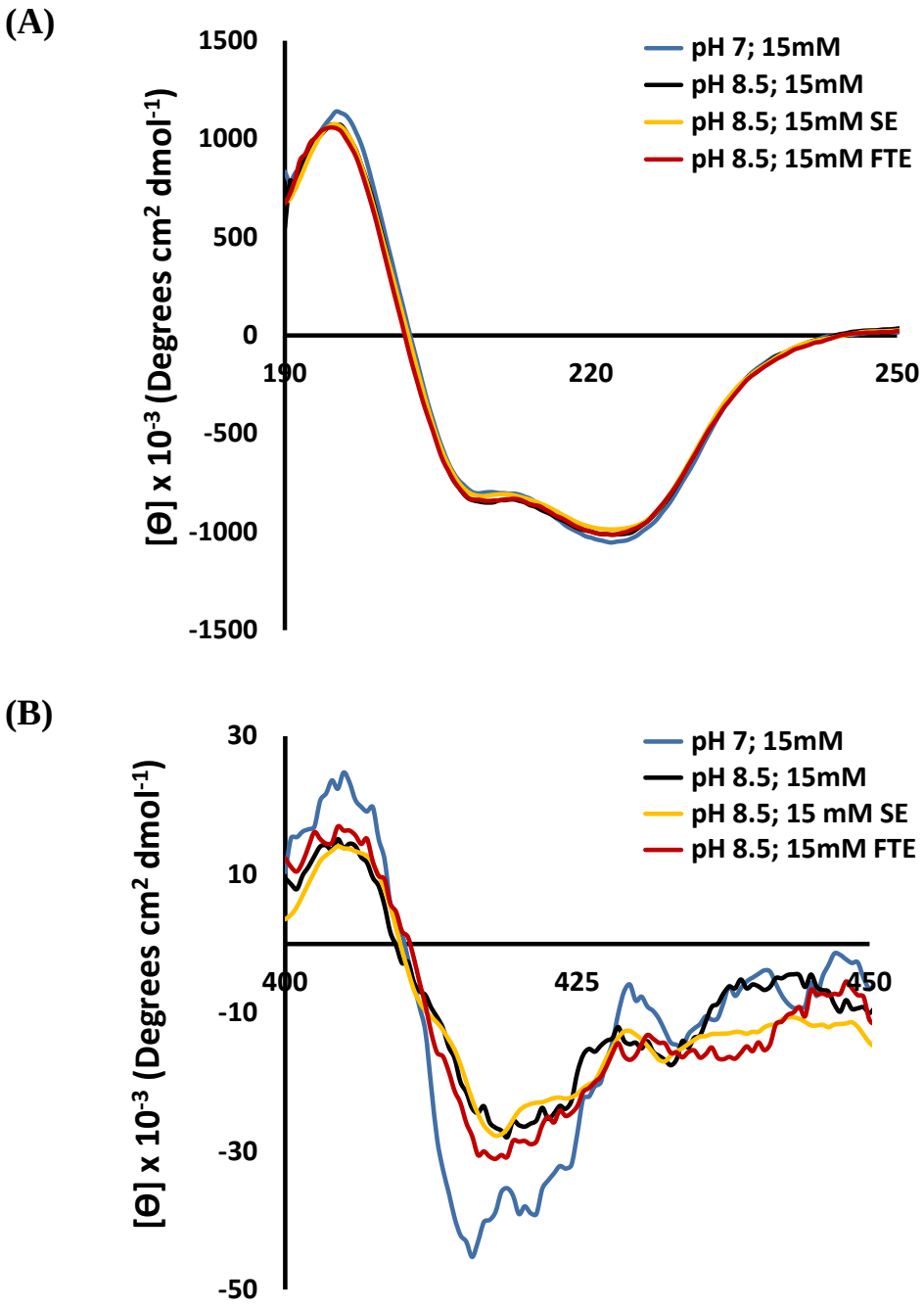

Figure 5.3 Effect of formulation and process conditions on structural integrity of processed-Cyt c. The x-axis is wavelength in nm. (A) α-helical secondary structure (222 nm and 208 nm) of processed-Cyt c was intact after it was subjected to pH 7 and pH 8.5 and processed using sonication extrusion (SE) and freeze thaw extrusion (FTE) entrapment procedure (B) The heme crevice structure of Cyt c showed changes (lower intensity at 416 nm) when subjected to pH 8.5, pH 8.5 SE and pH 8.5 FTE conditions compared to pH 7.

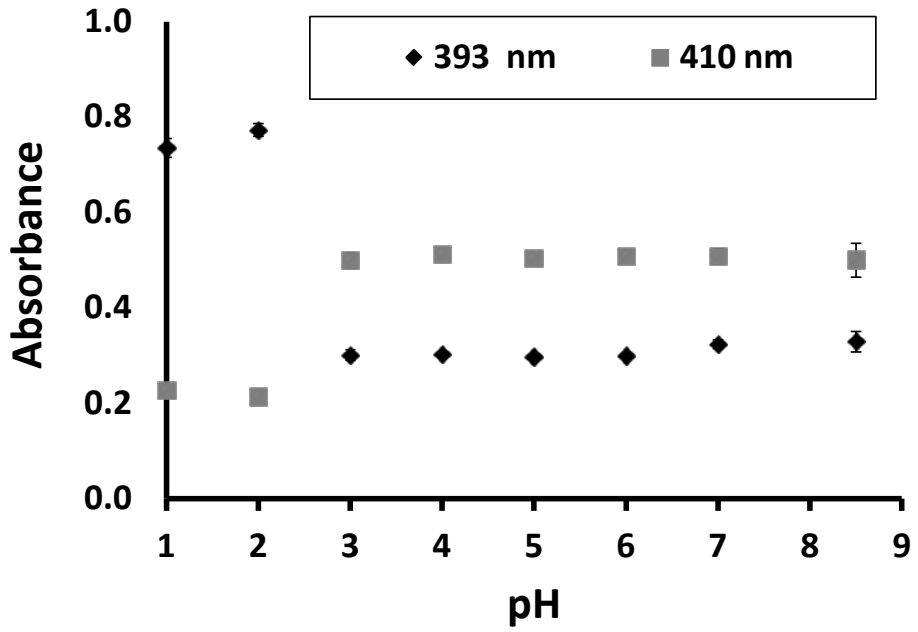

Figure 5.4 Effect of pH on unfolding of Cyt c. Changes in UV absorbance of Fe occurs when Cyt c is unfolded (higher absorbance at 393 vs. 410 nm). Cytochrome c is present in folded confirmation between pH 3 and pH 8.5 and unfolding occurs below pH 3.

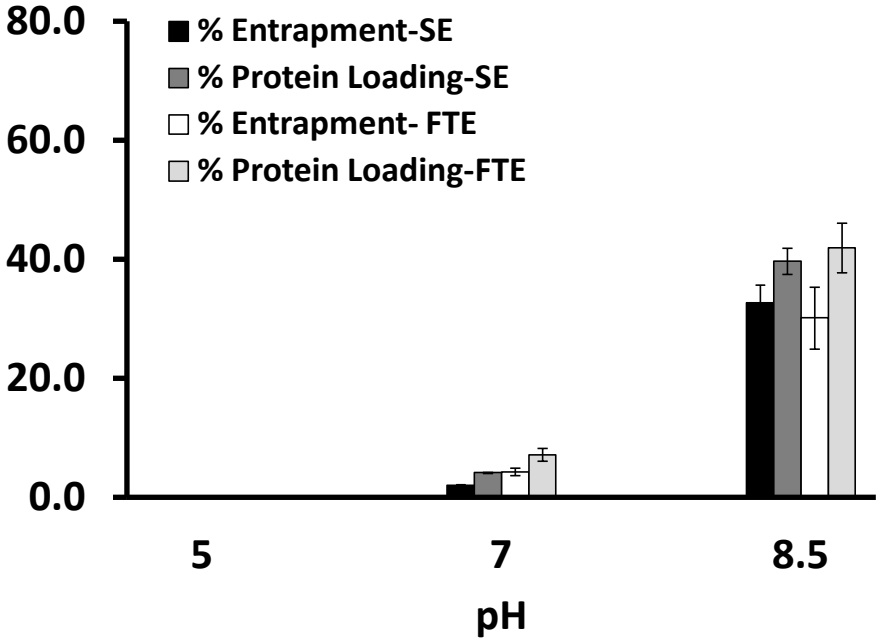

Figure 5.5 Effect of pH modulation of hydration buffer on entrapment of Cyt c in DOTAP-Chol liposomes. A significant ($p < 0.05$) difference in entrapment of Cyt c in DOTAP-Chol liposomes was observed with a change in pH from 7 to pH 8.5 (15 mM). At pH 7 only 2% entrapment was observed, whereas at pH 8.5, the entrapment was 30%. At pH 5, entrapment studies could not be conducted due to disintegration of DOTAP-Chol liposomes. The average and SD of at least three separate experiments are plotted.

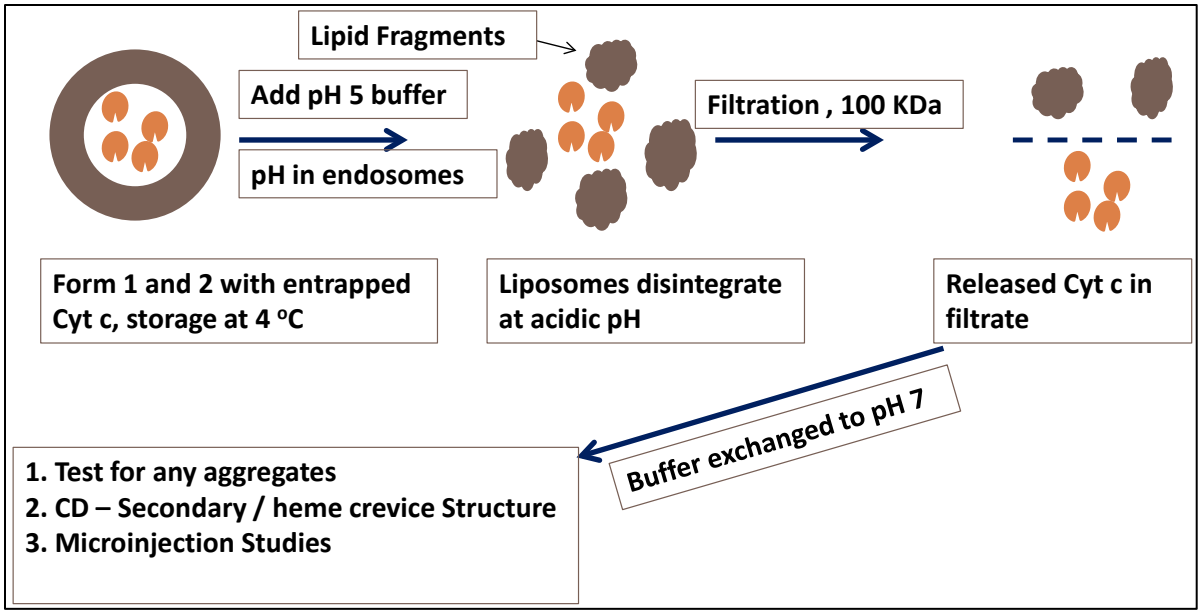

Figure 5.6 Schematic showing the process of inducing Cyt c release from purified liposomal Cyt c. The addition of pH 5 buffer lead to disintegration of liposomes into lipid fragments. Cyt c released in this way was collected in filtrate after passing through 100 KDa centrifugation filters. Released Cyt c pH was changed to pH 7 by buffer exchanging using 3KDa centrifugation filters. Released and buffer exchanged Cyt c was tested for the presence of any aggregates, structural changes and apoptotic activity.

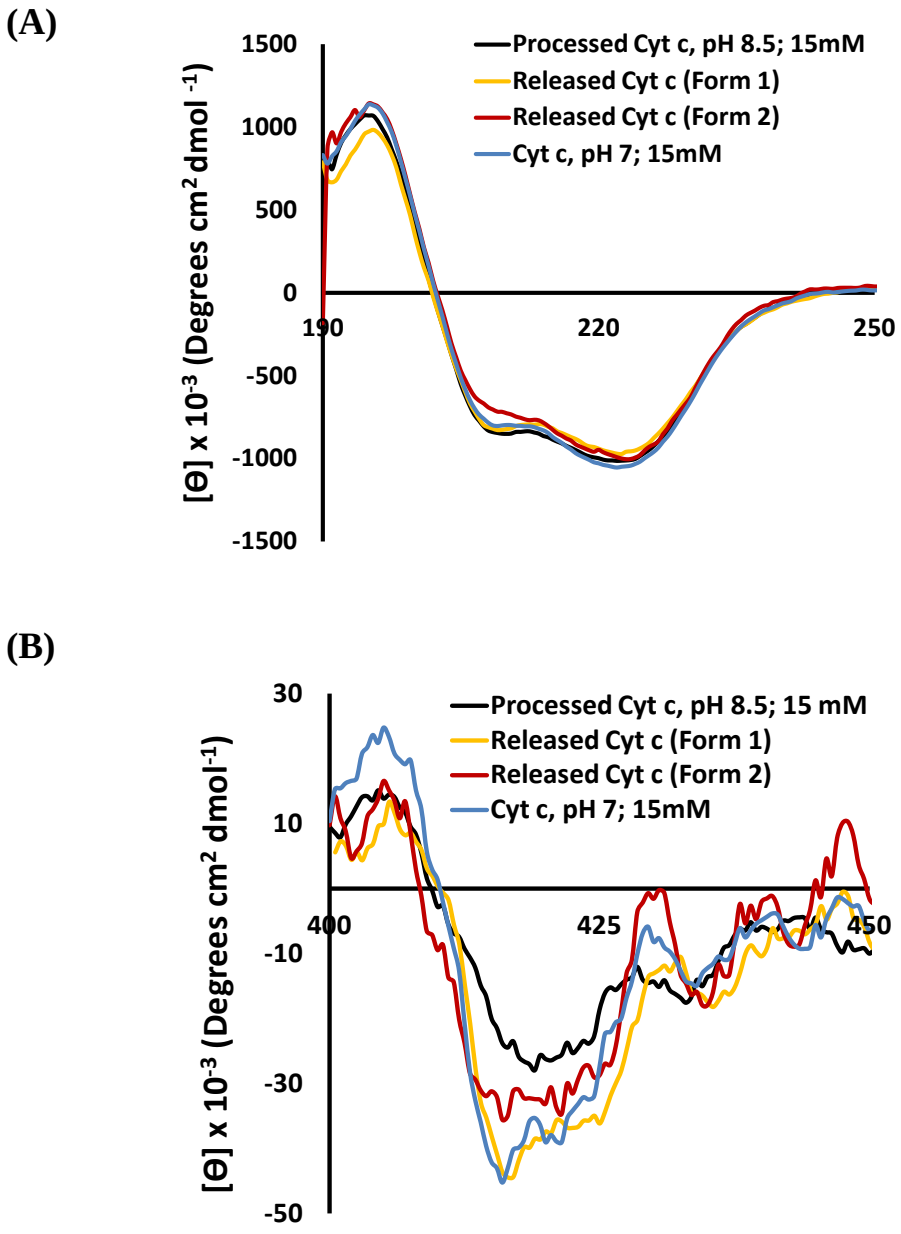

Figure 5.7 Secondary and heme crevice structure of released Cyt c (from purified Form 1and Form 2 were stored at 4 ^{o}C before release studies were conducted). (A) Released Cyt c from Form 1 showed secondary structure similar to Cyt c; pH 7, whereas released Cyt c from Form 2 showed lower intensity at 208 nm. (B) Released Cyt c from Form 1 showed heme crevice structure similar to Cyt c; pH 7 indicating that the change in heme crevice structure that occurred due to exposure to alkaline pH (8.5) was transient and reversible. However, in released Cyt c from Form 2, lower intensity at 416 nm was still observed indicating that the change in heme crevice structure induced due to exposure to pH 8.5 was not completely reversed.

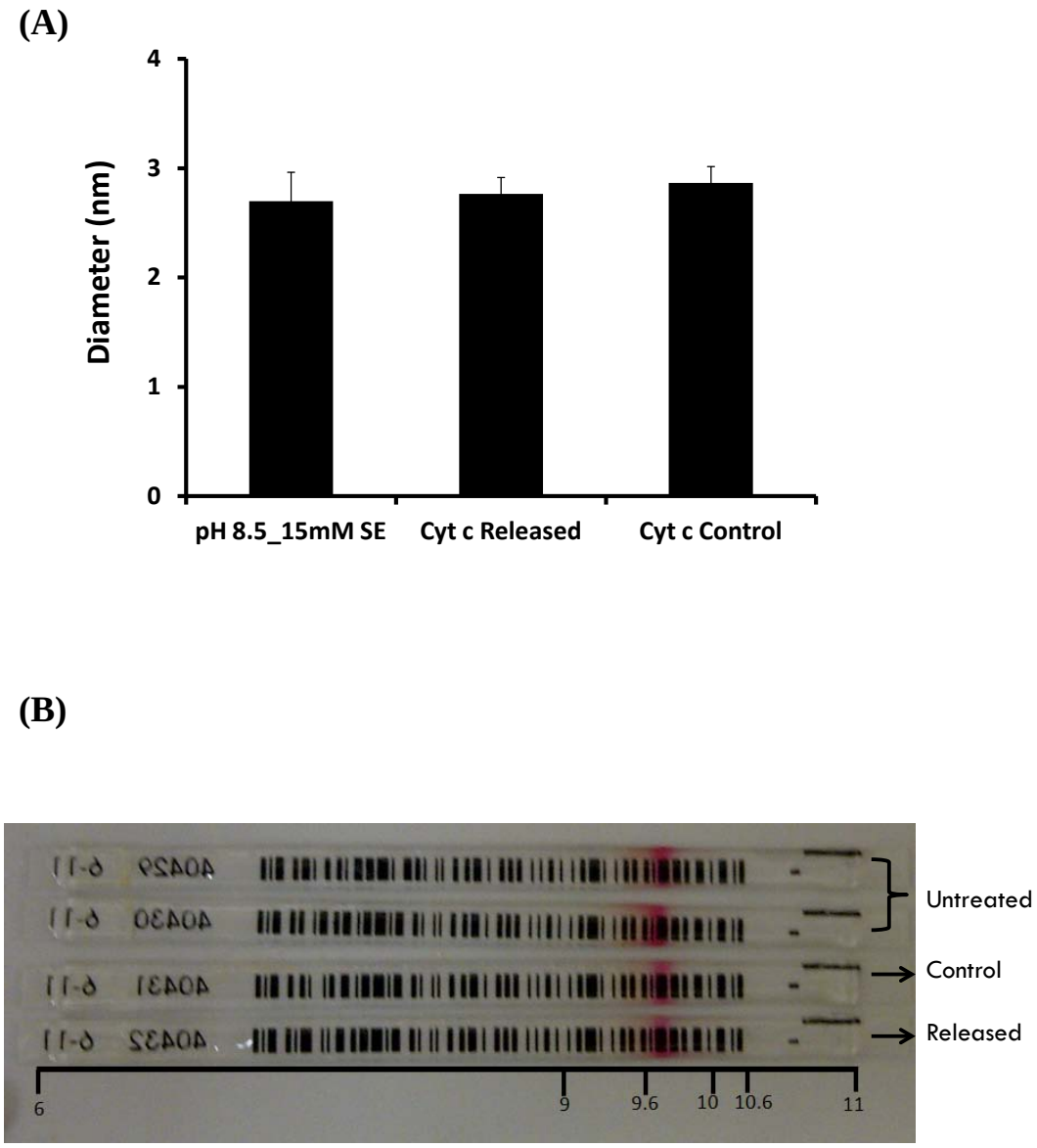

Figure 5.8 Assessment of aggregation potential (A) and deamidation (B) of released Cyt c and control Cyt c. Purified Form 1 and control Cyt c were stored at 4 ^{o}C for seven days before these studies were conducted. (A) No aggregation of released Cyt c was observed. However, aggregates greater than one micron (0.1 % by mass) were observed for control Cyt c. (B) No change in mobility was observed for either released Cyt c or control Cyt c as measured by IEF. PI value of Cyt c was estimated to be 9.7.

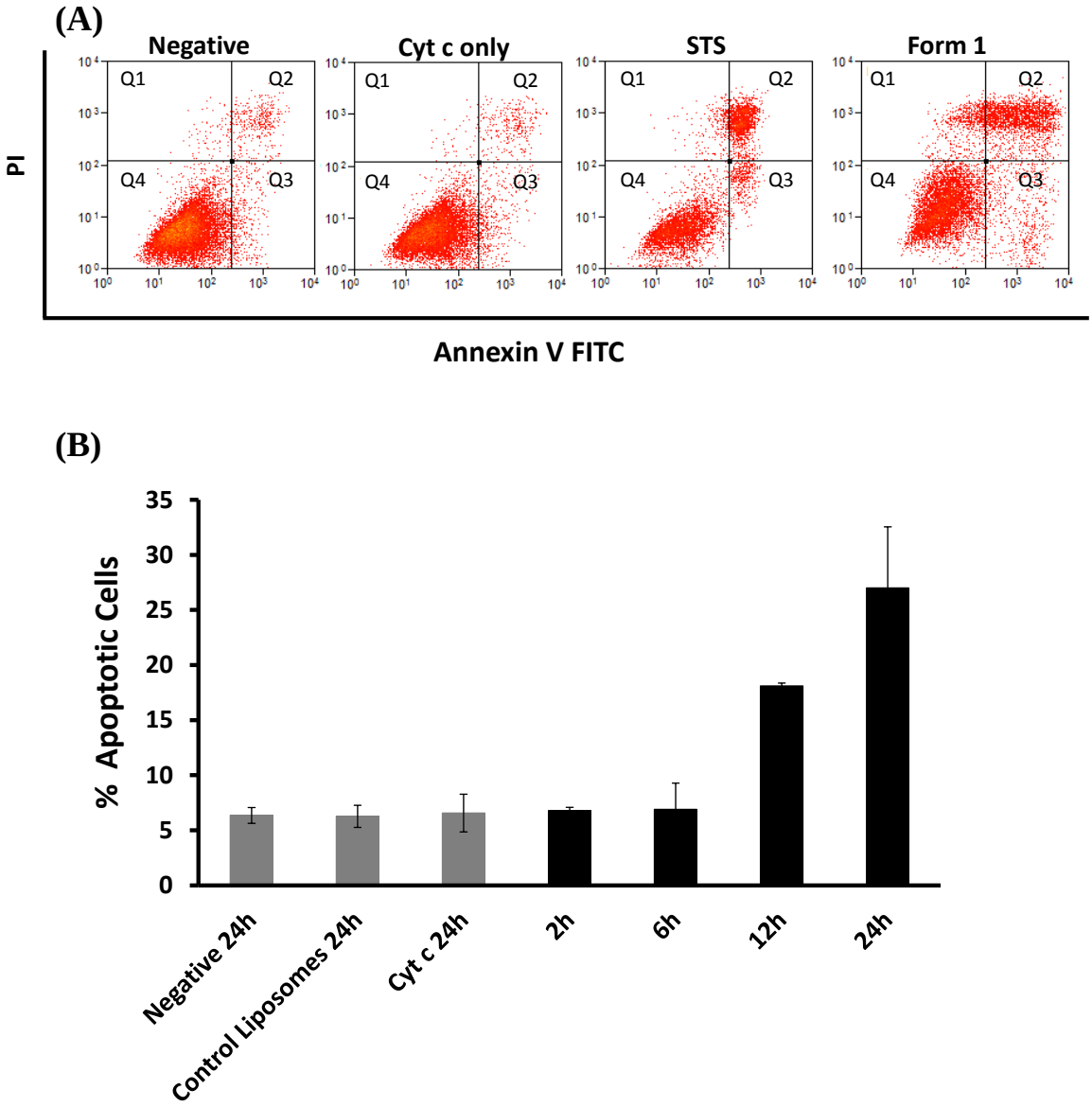

Figure 5.9 Apoptosis induction by Formulation 1 in MDA-MB-231 cells**.** (A) Dual labeling (Annexin V FITC and PI) was used to determine apoptosis induction in MDA-MB-231 cells compared to controls. Percent cells in Q1 (PI only positive cells or necrotic cells), Q2 (PI and FITC positive or late apoptotic cells), Q3 (FITC only positive or early apoptotic cells) and Q4 (PI and FITC negative or viable cells) were quantified using flow cytometer. Significant increase in percent apoptotic cells was present after 24 h treatment with Form 1 and STS. (B) Kinetic study evaluating time dependent apoptosis induction. Percent apoptotic cells were calculated by adding the percentages together in Q2 and Q3. All controls were incubated for 24 h and Form 1 was incubated for different time intervals. Control liposomes denote blank DOTAP-Chol liposomes.

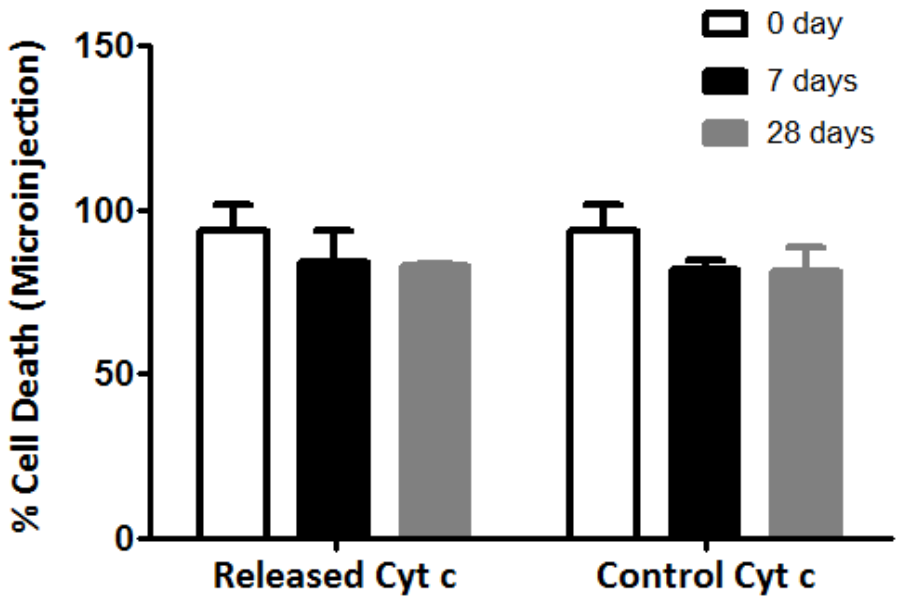

Figure 5.10 Microinjection studies of released Cyt c. Retention of apoptotic activity of released Cyt c and control Cyt c was assessed using microinjection into MDA MB 231 cells. Activity was assessed after Cyt c was released after purified Form1 and control Cyt c were stored for seven and twenty eight days at 4 ^{o}C. No significant difference ($p > 0.05$) was found between activity of released Cyt c, control Cyt c and fresh Cyt c (0 day) indicating that formulation and process conditions did not induce any changes that may interfere with Cyt c's apoptotic activity.

5.6 References

Bangham, A.D., 1980. Liposomes in Biological Systems. John Wiley and Sons.

Belikova, N.A., Vladimirov, Y.A., Osipov, A.N., Kapralov, A.A., Tyurin, V.A., Potapovich, M.V., Basova, L.V., Peterson, J., Kurnikov, I.V., Kagan, V.E., 2006. Peroxidase activity and structural transitions of cytochrome c bound to cardiolipin-containing membranes. Biochemistry 45, 4998-5009.

Chi, E.Y., Krishnan, S., Randolph, T.W., Carpenter, J.F., 2003. Physical stability of proteins in aqueous solution: mechanism and driving forces in nonnative protein aggregation. Pharm Res 20, 1325-1336.

Chugh, A., Eudes, F., Shim, Y.S., 2010. Cell-penetrating peptides: Nanocarrier for macromolecule delivery in living cells. IUBMB Life 62, 183-193.

Colletier, J.P., Chaize, B., Winterhalter, M., Fournier, D., 2002. Protein encapsulation in liposomes: efficiency depends on interactions between protein and phospholipid bilayer. BMC Biotechnol 2, 9.

De Rosa, E., Chiappini, C., Fan, D., Liu, X., Ferrari, M., Tasciotti, E., 2011. Agarose surface coating influences intracellular accumulation and enhances payload stability of a nano-delivery system. Pharm Res 28, 1520-1530.

Derjaguin, B.V., Landau, L.D., 1941. Theory of the stability of strongly charged lyophobic sols and of the adhesion of strongly charged particles in solutions of electrolytes. Acta Physicochim URSS 14, 733-762.

Dickerson, R.E., 1971. The structures of cytochrome c and the rates of molecular evolution. J Mol Evol 1, 26-45.

Du, J., Jin, J., Yan, M., Lu, Y., 2012. Synthetic nanocarriers for intracellular protein delivery. Curr Drug Metab 13, 82-92.

Fretz, M.M., Hogset, A., Koning, G.A., Jiskoot, W., Storm, G., 2007. Cytosolic delivery of liposomally targeted proteins induced by photochemical internalization. Pharm Res 24, 2040-2047.

Kam, N.W., Dai, H., 2005. Carbon nanotubes as intracellular protein transporters: generality and biological functionality. J Am Chem Soc 127, 6021-6026.

Kasibhatla, S., Tseng, B., 2003. Why target apoptosis in cancer treatment? Mol Cancer Ther 2, 573-580.

Kim, S.K., Foote, M.B., Huang, L., 2012. The targeted intracellular delivery of cytochrome C protein to tumors using lipid-apolipoprotein nanoparticles. Biomaterials 33, 3959-3966.

Kole, A.J., Knight, E.R., Deshmukh, M., 2011. Activation of apoptosis by cytoplasmic microinjection of cytochrome c. J Vis Exp.

Kundu, J., Chung, Y.I., Kim, Y.H., Tae, G., Kundu, S.C., 2009. Silk fibroin nanoparticles for cellular uptake and control release. Int J Pharm 388, 242-250.

Lassalle, V., Ferreira, M.L., 2007. PLA nano- and microparticles for drug delivery: an overview of the methods of preparation. Macromol Biosci 7, 767-783.

Lee, Y., Ishii, T., Cabral, H., Kim, H.J., Seo, J.H., Nishiyama, N., Oshima, H., Osada, K., Kataoka, K., 2009. Charge-conversional polyionic complex micelles-efficient nanocarriers for protein delivery into cytoplasm. Angew Chem Int Ed Engl 48, 5309-5312.

Li, F., Srinivasan, A., Wang, Y., Armstrong, R.C., Tomaselli, K.J., Fritz, L.C., 1997. Cell-specific induction of apoptosis by microinjection of cytochrome c. Bcl-xL has activity independent of cytochrome c release. J Biol Chem 272, 30299-30305.

Mattos, C., Ringe, D., 2001. Proteins in organic solvents. Curr Opin Struct Biol 11, 761-764.
Mayer, L.D., Bally, M.B., Hope, M.J., Cullis, P.R., 1986. Techniques for encapsulating bioactive agents into liposomes. Chem Phys Lipids 40, 333-345.

Mayer, L.D., Hope, M.J., Cullis, P.R., Janoff, A.S., 1985. Solute distributions and trapping efficiencies observed in freeze-thawed multilamellar vesicles. Biochim Biophys Acta 817, 193-196.

Ow, Y.P., Green, D.R., Hao, Z., Mak, T.W., 2008. Cytochrome c: functions beyond respiration. Nat Rev Mol Cell Biol 9, 532-542.

Parthasarthy, M., Johnson, W.C.J., 1985. Protein Secondary structure from Circular Dichroism Spectra. Proc. Int. Symp. Biomol. Struct. Interactions, Suppl. J. Biosci. 8, 141-149.

Pick, U., 1981. Liposomes with a large trapping capacity prepared by freezing and thawing of sonicated phospholipid mixtures. Arch Biochem Biophys 212, 186-194.

Potts, P.R., Singh, S., Knezek, M., Thompson, C.B., Deshmukh, M., 2003. Critical function of endogenous XIAP in regulating caspase activation during sympathetic neuronal apoptosis. J Cell Biol 163, 789-799.

Santra, S., Kaittanis, C., Perez, J.M., 2010. Cytochrome C encapsulating theranostic nanoparticles: a novel bifunctional system for targeted delivery of therapeutic membrane-impermeable proteins to tumors and imaging of cancer therapy. Mol Pharm 7, 1209-1222.

Schafer, Z.T., Parrish, A.B., Wright, K.M., Margolis, S.S., Marks, J.R., Deshmukh, M., Kornbluth, S., 2006. Enhanced sensitivity to cytochrome c-induced apoptosis mediated by PHAPI in breast cancer cells. Cancer Res 66, 2210-2218.

Shire, S.J., Shahrokh, Z., Liu, J., 2004. Challenges in the development of high protein concentration formulations. J Pharm Sci 93, 1390-1402.

Shu, S., Zhang, X., Wu, Z., Wang, Z., Li, C., 2010. Gradient cross-linked biodegradable polyelectrolyte nanocapsules for intracellular protein drug delivery. Biomaterials 31, 6039-6049.

Son, S., Lee, W.R., Joung, Y.K., Kwon, M.H., Kim, Y.S., Park, K.D., 2009. Optimized stability retention of a monoclonal antibody in the PLGA nanoparticles. Int J Pharm 368, 178-185.

van de Weert, M., Hennink, W.E., Jiskoot, W., 2000a. Protein instability in poly(lactic-co-glycolic acid) microparticles. Pharm Res 17, 1159-1167.

van de Weert, M., Hoechstetter, J., Hennink, W.E., Crommelin, D.J., 2000b. The effect of a water/organic solvent interface on the structural stability of lysozyme. J Control Release 68, 351-359.

van de Weert, M., van 't Hof, R., van der Weerd, J., Heeren, R.M., Posthuma, G., Hennink, W.E., Crommelin, D.J., 2000c. Lysozyme distribution and conformation in a biodegradable polymer matrix as determined by FTIR techniques. J Control Release 68, 31-40.

Verdine, G.L., Hilinski, G.J., 2012. Stapled peptides for intracellular drug targets. Methods Enzymol 503, 3-33.

Verwey, E.J.W., Overbeek, J.T., 1948. Theory of the stability of lyophobic Colloids. Elsevier, Amsterdam.

Villaverde, A., Garcia-Fruitos, E., Rinas, U., Seras-Franzoso, J., Kosoy, A., Corchero, J.L., Vazquez, E., 2012. Packaging protein drugs as bacterial inclusion bodies for therapeutic applications. Microb Cell Fact 11, 76.

Wang, W., 2000. Lyophilization and development of solid protein pharmaceuticals. Int J Pharm 203, 1-60.

Weiner, A.L., 1994. Liposomes for protein delivery: selecting manufacture and development processes. Immunomethods 4, 201-209.

Weinkam, P., Zimmermann, J., Sagle, L.B., Matsuda, S., Dawson, P.E., Wolynes, P.G., Romesberg, F.E., 2008. Characterization of alkaline transitions in ferricytochrome c using carbon-deuterium infrared probes. Biochemistry 47, 13470-13480.

Yu, T., Wang, X., Purring-Koch, C., Wei, Y., McLendon, G.L., 2001. A mutational epitope for cytochrome C binding to the apoptosis protease activation factor-1. J Biol Chem 276, 13034-13038.

Yuan, S., Yu, X., Topf, M., Ludtke, S.J., Wang, X., Akey, C.W., 2010. Structure of an apoptosome-procaspase-9 CARD complex. Structure 18, 571.

Zhivotovsky, B., Orrenius, S., Brustugun, O.T., Doskeland, S.O., 1998. Injected cytochrome c induces apoptosis. Nature 391, 449-450.

Chapter VI

Summary and Future Studies

6.1 Part 1: Toxicity Evaluation of Cu, C-Cu, Ni and C-Ni NPs

The hypothesis in these studies was that compared to non-coated Cu and Ni NPs, carbon coated Cu and Ni NPs will have different physico-chemical properties including their interactions with the surrounding media and cells which will influence the resultant toxicity in cell-based assays. By utilizing a battery of inter-disciplinary techniques for evaluation of the physico-chemical characteristics and cell based toxicity, it was shown that a correlation between physico-chemical characteristics and toxicity of NPs could be established especially for C-Cu and Cu NPs. Due to the presence of carbon coating, C-Cu NPs had less surface oxide and released lower Cu in cell culture media compared to Cu NPs. Furthermore, the cellular association of C-Cu NP in A549 cells was almost ten-fold higher compared to Cu NPs. These changes in interaction with cell culture media and cellular association for C-Cu NPs compared to Cu NPs also translated to results observed in cell based toxicity assays. C-Cu NPs showed higher mitochondrial damage (45% damage by C-Cu NP versus 18% damage by Cu NP at 24 h) and lower plasma membrane damage (1-3% damage by C-Cu NPs versus 40% by Cu NPs at 25 µg/mL at 2 h) compared to Cu NPs. The higher mitochondrial damage by C-Cu NPs compared to Cu NPs was attributed to higher cellular association and presumably extended release of Cu ions after association with cells. Higher plasma

membrane damage by Cu NPs compared to C-Cu NPs was attributed to greater release of Cu ions by Cu NPs than C-Cu NPs in cell culture media. Thus, it was concluded that by studying the effect of a unique characteristic such as surface carbon coating, correlations could be drawn between toxicity and physico-chemical properties of NPs. In case of Ni and C-Ni NPs, no toxicity was observed in lysosomal membrane integrity test. C-Ni NPs showed only slight toxicity (mitochondrial damage) after 24 h incubation with A549 cells whereas no mitochondrial damage was observed with Ni NPs. These observations contrasted with almost equal cellular association of Ni and C-Ni NPs. Cellular association of metals after treatment of cells with metal NPs was determined using ICP-MS. After the cells were treated with NPs, they were washed twice to remove any surface bound NPs. However, even after washing, it is highly likely that some cell surface bound NP fraction will be present (especially if NPs are very hydrophobic) and that both cell associated as well as internalized fractions were analyzed. Thus, future studies should include quantitative assessment of internalized versus cell surface associated NPs. This will help correlate cellular toxicity results of Ni and C-Ni NPs with cellular uptake rather than cell association. Nickel toxicity has been reported to be dependent upon intracellular Ni ion concentration regardless of the initial dose. Therefore, it will be important to determine cellular uptake of Ni and C-Ni NPs (internalized) and correlate the cell uptake results with the toxicity results. In the studies reported herein, the major goal was to correlate physico-chemical properties with cytotoxicity. Therefore, the MTT assay (to assess mitochondrial damage) and neutral red assay (to assess lysosomal membrane damage) were used. Another important measure of toxicity that should be evaluated for all four NPs is the potential to induce inflammatory responses as this is an important factor for predicting safety *in-vivo*. For this purpose macrophage cell lines could be

used and inflammation may be assessed by measuring interleukin secretion. Moreover, an important goal of nanotoxicology studies *in-vitro* is to predict toxicity *in-vivo*. Therefore, the exposure conditions and cell culture systems that most closely mimic *in-vivo* conditions should be employed in future. Inhalation is the most common exposure route under occupational settings and therefore lung cell culture system with intact mucosal and ciliated barrier should be used in future studies to assess the toxicity of Cu, C-Cu, Ni and C-Ni NPs *in-vitro*. Additionally, it will be important to correlate the results of *in-vitro* toxicity and physico-chemical characterization to *in-vivo* inhalational toxicology studies so that critical parameters that define the correlation between physico-chemical properties and important *in-vivo* end points could be determined. The knowledge derived from correlating physico-chemical properties with toxicological findings will help guide prediction of NP toxicity and will contribute to achieve the ultimate goal of manufacturing safe and useful NPs.

6.2 Part II: Intracellular Delivery of Cyt c to Induce Apoptosis in Breast Cancer Cells

The hypothesis for these studies was that the entrapment of Cyt c in DOTAP-Chol liposomes prepared using film rehydration method will overcome the challenges for delivery of Cyt c while maintaining conditions for optimal Cyt c stability. Further, it was hypothesized that modulating the pH of hydration buffer will increase the entrapment of Cyt c in liposomes without compromising structural integrity and apoptosis inducing activity of Cyt c.

Various formulation and process related stresses are encountered during protein entrapment using traditional nano-carrier approach of using PLGA particles. Therefore, to avoid any exposure to organic solvents and high shear/stress conditions, liposomal approach using film hydration method was used. Dioleoyl-trimethyl-ammonium-propane was used as

one the lipids to induce endosomal release of Cyt c/delivery system from endosomes to cytosol as entrapment in endosome can reduce efficacy. Liposomal formulation of proteins using film hydration method results in only limited protein entrapment. It was showed that by modulating the pH of hydration buffer during entrapment of Cyt c in DOTAP-Chol liposomes, entrapment was increased from 2% at pH 7 to 30% at pH 8.5. Cytochrome c has a PI value close to 10. The overall net charge on Cyt c is positive during conditions employed for entrapment (at pH 7 and 8.5). However, the net charge on a protein decreases at pH values approach closer to protein's PI. Therefore decreased repulsion between the positively charged DOTAP-Chol film and Cyt c, and increased interaction between negatively charged patch on Cyt c (due to aspartic acid and glutamic acid) and positively charged DOTAP-Chol film at pH 8.5 could possibly explain higher entrapment at pH 8.5 compared to pH 7. Furthermore, since Cyt c entrapment in liposomes required pH adjustment closer to protein PI, extrusion and sonication, the effect of these conditions on Cyt c stability (aggregation, structural and chemical integrity) and apoptosis inducing activity was studied. It was shown that Cyt c structural integrity and activity was intact after it was released from optimized formulation stored at 4 ºC for seven and 28 days. Additionally, the apoptotic activity of optimized formulation was shown in MDA-MB -231cells *in-vitro*. The major focus in these studies was on formulation and developing a process to preserve Cyt c activity, which was accomplished as described above. However, inclusion of DOTAP in the formulation resulted in a highly positively-charged liposomal formulation which can result in aggregation of liposomes in the presence of serum proteins. Thus, future studies should examine ways to overcome this limitation. One way this could be accomplished is by inclusion of PEG lipids in liposomes. Interactions between Cyt c and DOTAP can change in presence of PEG.

Therefore, entrapment studies should be carried out in the presence of PEG. Usually, higher temperatures are required for PEG incorporation, therefore optimizing the right temperature for inclusion of PEG, so that Cyt c stability is not affected will also be important. The optimized pegylated formulation containing Cyt c should be tested for *in-vivo* efficacy in animal models and also long term stability of formulations should be investigated. *In-vivo* study design is very elaborate and contains various variables so only some of the important considerations for *in-vivo* studies are presented below.

Various tumor models can be developed to test the anticancer efficacy of formulations. Xenograft, orthotopic and genetically engineered mouse models have been reported in the literature. Each model has its limitations and advantages. Therefore, selection of tumor model will depend on the goal of the study and available resources. *In-vivo* studies requires higher doses than *in-vitro* studies and thus a more concentrated formulation due to limitation in injection volumes via IV (intra-venous) and SC (subcutaneous) routes are required. Therefore, scale up experiments should be performed to test the feasibility of developing concentrated formulations without compromising formulation characteristics and Cyt c stability. Proper control groups along with the formulation group should be included in *in-vivo* studies in order to identify efficacy of formulated drug (Cyt c) over Cyt c alone and pegylated carrier. Another aspect of *in-vivo* studies should examine safety of formulations. Since some aggregated proteins are known to elicit immunogenic reactions, it will be important to test for any immunogenic reactions in addition to standard toxicity indices such as blood chemistry and body weight, etc. If the formulation shows promising anticancer activity in preliminary *in-vivo* studies, it will be important to examine the dosing regimen and pharmacokinetics of optimized formulation. Since repeated dosing is often required to sustain

the anticancer activity, long-term stability of Cyt c in formulation should also be investigated. A formulation should be stable for sufficient period of time at an appropriate storage condition so that repeated dosing could be performed. Thus, detailed characterization of preservation of Cyt c structural and chemical integrity, and retention of apoptosis inducing activity after long term storage should be assessed.

The studies mentioned above will ultimately contribute to the overall goal of developing a viable formulation for intracellular delivery of Cyt c for the treatment of breast cancer.

Appendix A

Characterization and Toxicity Analysis of CeO_2 Nanoparticles

A.1 Summary

The work on evaluation and characterization of CeO_2 NPs described here was part of the report contributed to the round robin effort of studying CeO_2 NPs across different universities funded by SRC (Semiconductor Research Corporation) SEMATECH Engineering Research Center for Environmentally Benign Semiconductor Manufacturing. Following studies were conducted

- Cerium oxide nanoparticle characterization: particle size, zeta potential and surface composition analysis using X-ray Photoelectron Spectroscopy (XPS).
- Cerium oxide nanoparticle *in-vitro* toxicity studies: assessment of mitochondrial function and membrane integrity.

A.2 Materials and Methods

Materials

Cerium oxide NPs (10% wt/wt suspension, pH 4.5 in water) were provided by Dr. Yongsheng Chen from Georgia Institute of Technology. A549 lung cancer cells were purchased from ATCC and maintained in DMEM (Dulbecco's Modified Eagle's Medium) with 10% FBS (Fetal Bovine Serum), 5 µg/mL plasmocin (Invivogen), 100 U/mL penicillin and 100 µg/mL streptomycin (ATCC). MTT and Neutral Red reagents were purchased from Sigma Aldrich. Dispex A40 was provided as a gift by BASF. Beckman Coulter N5 submicron particle size analyzer was used for particle size analysis. This instrument relies upon dynamic light scattering to measure particle size between 3 nm to 3000 nm. A 90º scattering angle was used for all measurements. For zeta potential analysis, Malvern Zeta Sizer NanoZ was used. Viscosity and refractive index and dielectric constant of water at 25º C were used for calculating the potential using Smoluchowski model. Zen 1002-zeta dip cell was used for all measurements. For XPS analysis, Kratos AXIS ultra DLD photoelectron spectrometer. Energy Source was Al Kα rays. Area analyzed for XPS was 300u x 700 μm^2.

Surface Composition Analysis using XPS

The CeO_2 nanoparticle stock (10% wt/wt) was slightly vortexed and sonicated for three minutes using a bath sonicator and diluted to 2 mg/mL concentration in DI water. X-ray photoelectron spectroscopic analysis was carried out on gold sputtered silicon wafers on which a droplet of nanoparticle suspension was placed and allowed to air dry. Full spectrum for CeO_2 NPs as well as high resolution spectrum was obtained for cerium, carbon and oxygen.

Particle Size Analysis

The stock of CeO_2 NPs (10% wt/wt) was slightly vortexed and sonicated for three minutes using a bath sonicator. A diluted suspension of 10mg/mL concentration in DI (De-Ionized) water (pH 6) was prepared from the sonicated stock. A further dilution to 20 µg/mL was made in DI water (pH 6), DI water with 0.5% v/v Dispex A40 , DI water (pH 7), DI water (pH 4.5), DMEM media and DMEM media supplemented with 10% FBS. The diluted samples were further sonicated for three minutes using a bath sonicator. One ml of above mentioned samples were analyzed at 0 h (immediately after preparation) and at 24 h (storage at room temperature) using Beckman Coulter N5 submicron particle size analyzer. Three independent runs were performed for each sample.

Zeta Potential Analysis

The stock of CeO_2 NPs (10% wt/wt) was slightly vortexed and sonicated for three minutes using a bath sonicator. A diluted suspension of 10 mg/mL concentration in DI (De-Ionized) water (pH 6) was prepared from the sonicated stock. A further dilution to 200 µg/mL was made in DI water (pH 6), DI water (pH 7) and DI water (pH 4.5). The diluted samples were further sonicated for three minutes using a bath sonicator. 700 µl of above mentioned samples were analyzed using the Zen 1002-zeta dip cell in the Malvern Zeta Sizer NanoZ. Each measurement cycle comprised of fifteen runs with three sub-runs.

Membrane Integrity Assay

For assessment of membrane integrity, neutral red dye was used. Neutral red is permeable to all cells but is retained only in cells with intact lysosomal membrane as its binds to the anionic sites in the lysosomes. Any insult to cell resulting in lysosomal

membrane damage results in decreased uptake of neutral red; which is also the principle of this assay. A549 cells (15,000 cells/well in a 96 well plate) were allowed to attach overnight. For 24 h, cells were treated with 25, 50, 100, 250, 500 and 1000 µg/mL doses of CeO_2 NPs. All dilutions for different doses were made 10X in DI water and the desired concentration in well was achieved after a tenfold dilution of 20 µL of nanoparticle stocks when added to 180 µL of DMEM media with FBS. After 24 h treatment, cells were washed twice with PBS (Phosphate Buffered Saline) to remove excess NPs and neutral red dye in media was allowed to incubate with the cells for 4 h. Appropriate controls such as NPs alone with neutral red dye and cells with NPs without neutral red dye were incubated to account for any interference. A549 cells without any treatment were the negative control for this experiment. After washing the cells once with PBS, the incorporated neutral red dye was extracted using a mixture of water, ethanol and glacial acetic acid. The absorbance was measured at 540 nm and results were reported as percent membrane integrity compared to negative control. A similar study was also carried out to evaluate the effect of 25, 50, 100, 250, 500 and 1000 µg/mL doses of CeO_2 NPs in the presence of 0.05% v/v Dispex A40. An extra control in this set of experiment was to incubate the cells with 0.05% v/v Dispex A40.

Mitochondrial Function Assay

In cells with functional mitochondria, MTT (yellow colored) is reduced to a formazan derivative (blue color) which is quantified after solubilization of the formazan derivative in DMSO. Dimethyl-thiazolyl-diphenyl-tetrazolium bromide (MTT) was used to evaluate the mitochondrial function of A549 cells (15,000 cells/well in a 96 well plate) after 24 h treatment with 25, 50, 100, 250, 500 and 1000 µg/mL doses of CeO_2 NPs. Similar to the neutral red study, all dilutions for different doses were made 10X in DI water and the desired

concentration in well was achieved after a tenfold dilution of 20 µL of NPs stock when added to 180 µL of DMEM media with FBS. After 24 hr treatment, cells were washed twice with PBS (Phosphate Buffered Saline) to remove excess NPs and MTT reagent in media was allowed to incubate with the cells for 4 h. Appropriate controls such as NPs alone with MTT reagent and cells with NPs without MTT dye were incubated to account for any interference. A549 cells without any treatment were the negative control for this experiment. After washing the cells once with PBS, the reduced formazan derivative was solubilized using DMSO. The absorbance was measured at 570 nm and results were reported as percent mitochondrial function compared to negative control.

A.3 Results and Discussion

XPS Analysis

In the full spectrum of CeO_2 NPs (**Figure A.1**), characteristic peaks from Ce, O and C were observed. The characteristic peaks from Ce were at 122 eV and 124 eV (Ce 4d); 221 eV and 222 eV (Ce 4p); 883 eV, 899 eV and 917 eV (Ce 3d). Cerium auger peaks were observed at 730 eV and 833 eV. The O1s characteristic peak was observed at 530eV. A small C1s peak was also observed at 285 eV and 289 eV. The presence of carbon in the CeO_2 nanoparticle samples is due to atmospheric contamination and some degree of surface carbon contamination is observed on all samples in XPS analysis. A Na peak was also observed at 513 eV. The relative percent atomic concentrations of various elements was 26.8% (Ce), 52.6% (O), 18.3% (C) and 2.2% (Na).

Particle Size Analysis

A summary of particle size average and SD calculated from three independent runs from each sample at 0 h and 24 h respectively is shown in **Table A.1** and **Table A.2**. Clearly a pH, time and media dependent effect on CeO_2 nanoparticle size was observed. At 0 h, average particle size at pH 7 was a log fold higher than that at pH 4.5 or pH 6. The addition of 0.5% v/v Dispex A40 helped maintain the NPs in dispersion and the particle size was comparable to suspensions at pH 4.5 or pH 6. Particle size in the presence of 10% FBS in DMEM media was close to three-fold lower as compared to particle size in DMEM without 10% FBS. This may be a result of stabilization of particles due to coating of proteins present in the serum.

After 24 h storage at room temperature, for NPs in H_2O at pH 4.5, pH 6, 0.5% v/v Dispex A40 and in DMEM media with 10% FBS, no significant change in the average

particle size was observed. Whereas for NPs in H_2O at pH 7 and in DMEM without FBS, most of the particles measured were at the upper limit of the instrument e.g, near 3000 nm. The representative particle size distributions of CeO2 NPs are also shown in **Figure** A.**2**.

Zeta Potential

The zeta potential was measured using 200 µg/mL concentrations of CeO_2 NPs. The average zeta potential (mV) is reported in **Table A.3**. It is important to note that like particle size, zeta potential results obtained from the instrument are an average value for each measurement but there also exists a considerable range for that reported average. This is reported as "SD within one measurement" in **Table A.3**. Considering SD within one measurement, similar value of zeta potentials were obtained at pH 4.5 and pH 6. However, at pH 7, it was difficult to achieve reproducible measurements since the SD within one measurement exceeded the average value.

Mitochondrial Function Assay

No significant alteration in mitochondrial function after treatment with CeO_2 NPs was observed up to 1000 µg/mL (**Figure A.3**). Both controls, NPs alone with MTT dye and cells with NPs without MTT dye did not show any interference with the assay.

Membrane Integrity Assay

No significant alteration in membrane integrity as assessed by uptake of neutral red dye was observed after treatment with CeO_2 NPs up to 1000 µg/ml (**Figure A.4**). Even in the presence of 0.05% v/v Dispex A40, toxicity was not observed with any dose level (**Figure A.5**). Cells with NPs without neutral red dye did not show any interference with the assay, although the data was corrected for interference from NPs with neutral red dye.

A.4 Conclusions

X-ray photoelectron spectroscopy analysis confirmed presence of CeO_2 as the major species on the top 5 nm of the NPs. Except Na, no other contaminating metal was found. Particle Size of CeO_2 NPs was found to be dependent on pH and presence of FBS. Lower pH and presence of proteins seems to stabilize NPs. No significant toxicity of CeO_2 NPs was observed after 24 h treatment of A549 cells *in-vitro* in either mitochondrial function or membrane integrity assay. Addition of Dispex A40 (0.05% v/v) does not alter the toxicity profile of CeO_2 NPs when tested using the membrane integrity assay.

Table A.1 Average particle size and SD of CeO_2 NPs in various medium at 0 h

Sample (CeO_2, 20µg/ml)	pH	Average (nm)	SD
H_2O	4.5	124	16
	6	122	15
	7	1151	450
H_2O with 0.5% v/v Dispex A40	8	140	14
DMEM, No FBS	7.4	1547	155
DMEM + 10% FBS	7.4	455	22

Table A.2 Average particle size and SD of CeO_2 NPs in various medium at 24 h

Sample (CeO_2, 20 µg/ml)	**pH**	**Average (nm)**	**SD**
H_2O	4.5	144	12
	6	114	3
	7	3000	0
H_2O with 0.5% v/v Dispex A40	8	150	26
DMEM, No FBS	7.4	2964	6
DMEM + 10% FBS	7.4	475	66

Table A.3 Average zeta potential and SD

Sample (CeO_2, 200 µg/mL)	**pH**	**Average of three Measurements (mV)**	**SD within one measurement**	**SD between three measurements**
H_2O	4.5	30	11	0
	6	43	17	3
	7	Could not obtain reproducible measurements		

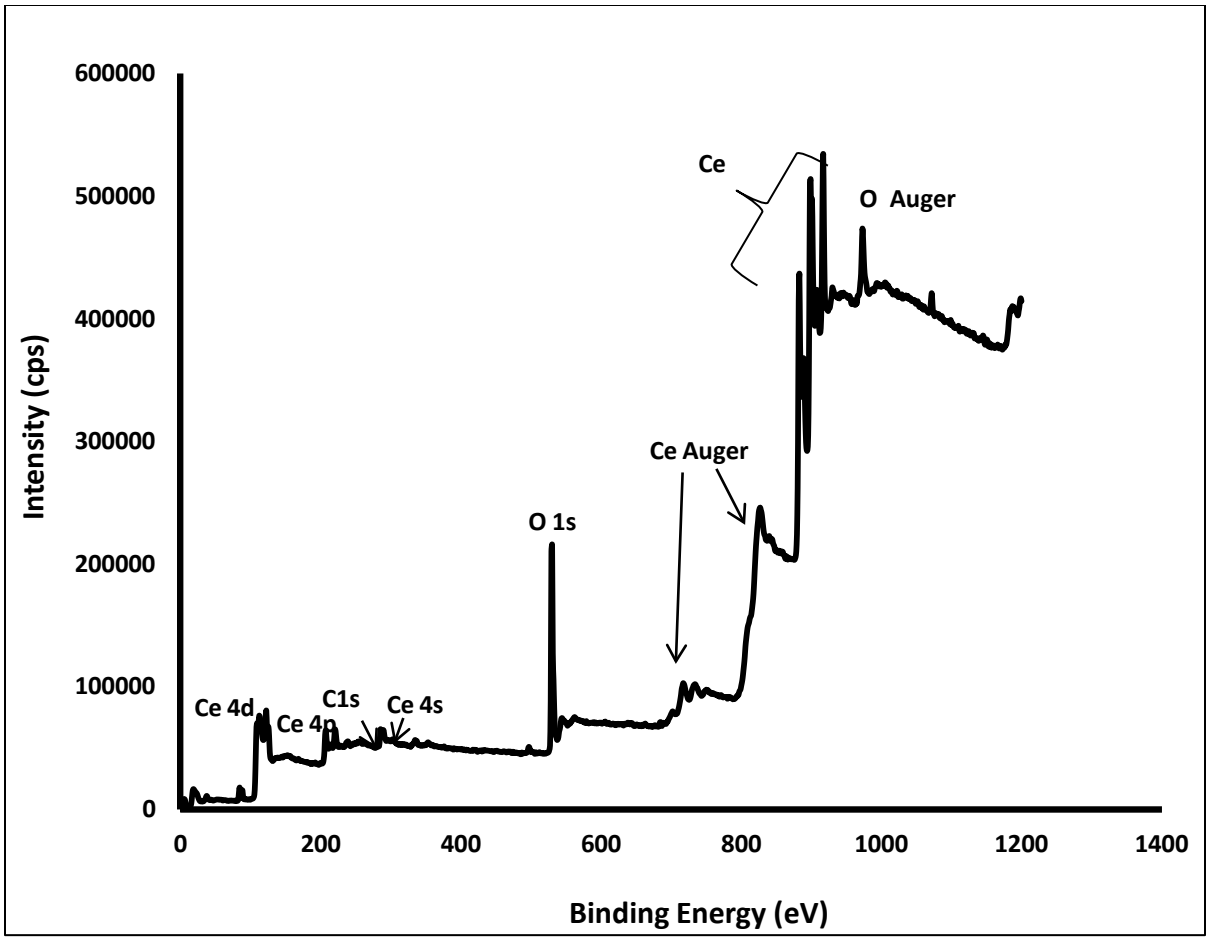

Figure A.1 Full XPS Spectrum of CeO_2 NPs

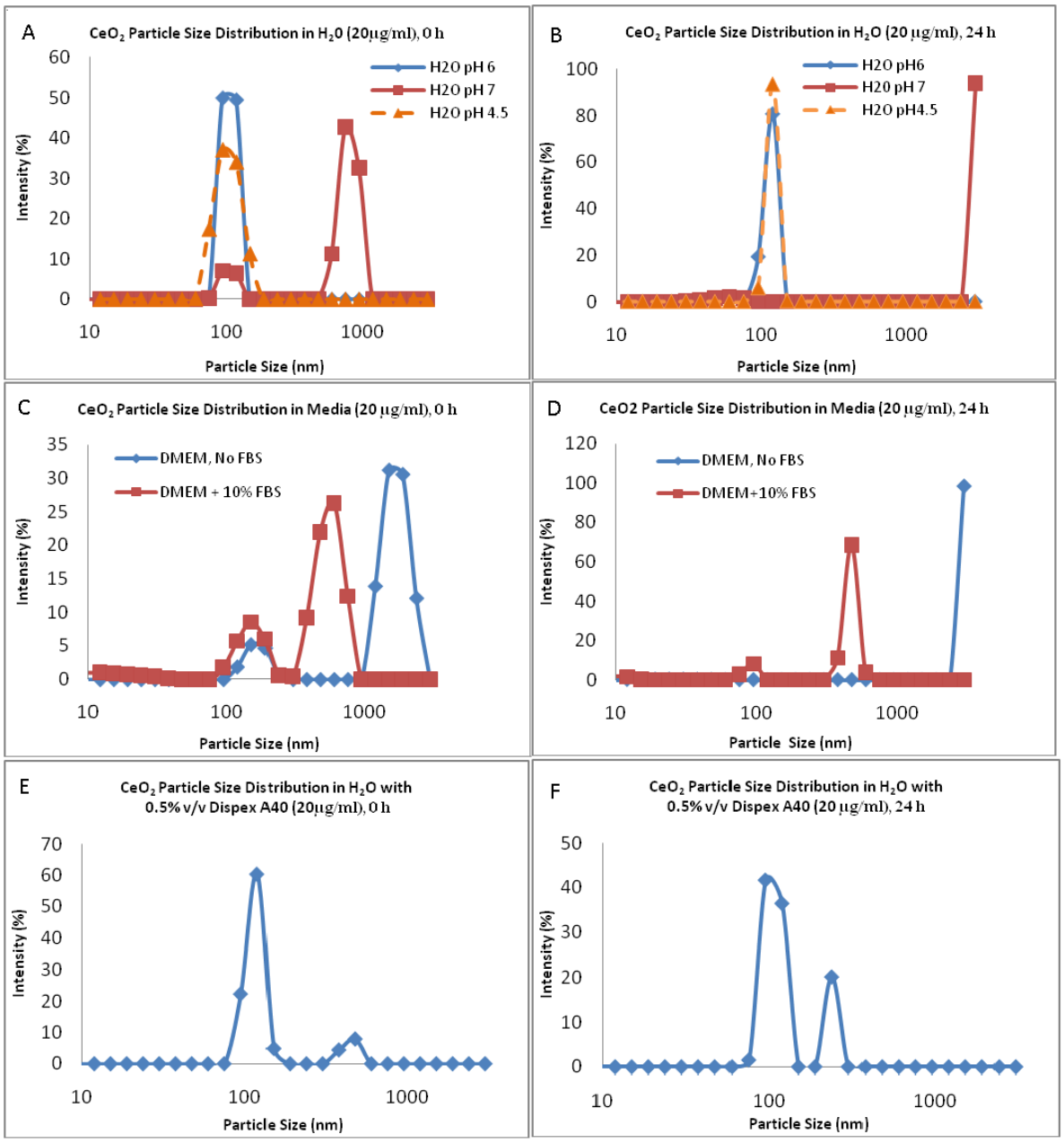

Figure A.2 Particle size distributions of CeO_2 NPs in (A) H_2O, 0 h (B) H_2O, 24 h (C) Media, 0 h (D) Media, 24 h (E) H_2O with Dispex A40, 0 h (F) H_2O with Dispex A40, 24 h

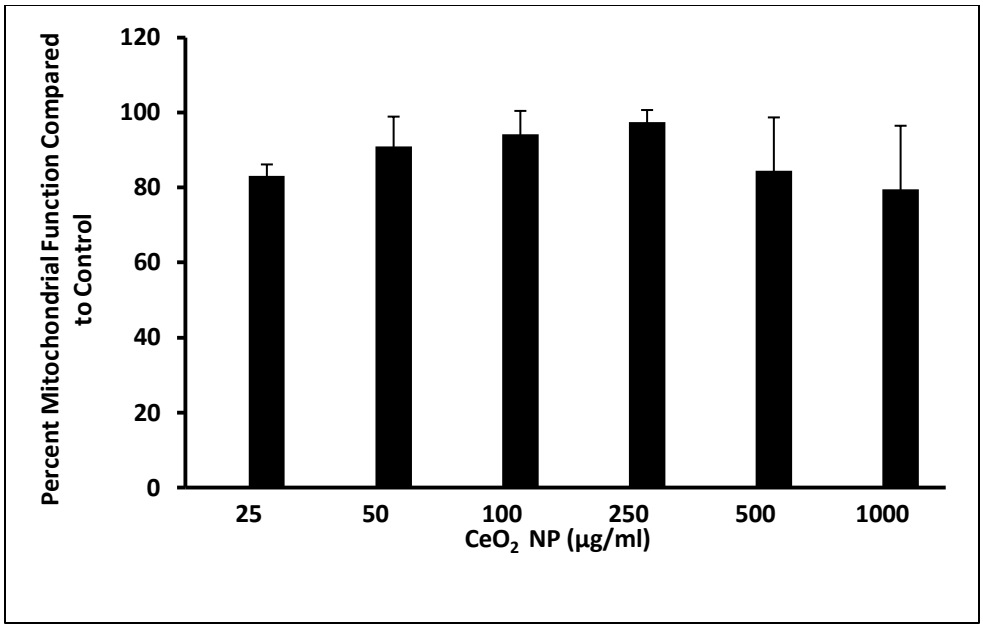

Figure A.3 Mitochondrial function assay. A549 cells were treated with CeO_2 NPs for 24 h (n=3).

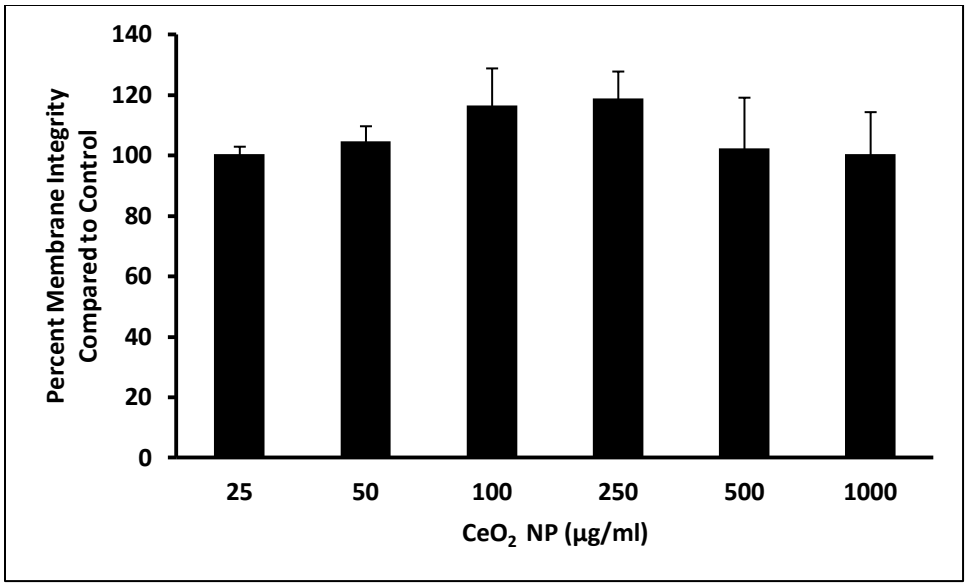

Figure A.4 Neutral red membrane integrity assay. A549 cells were treated with CeO_2 NPs for 24 h (n=3).

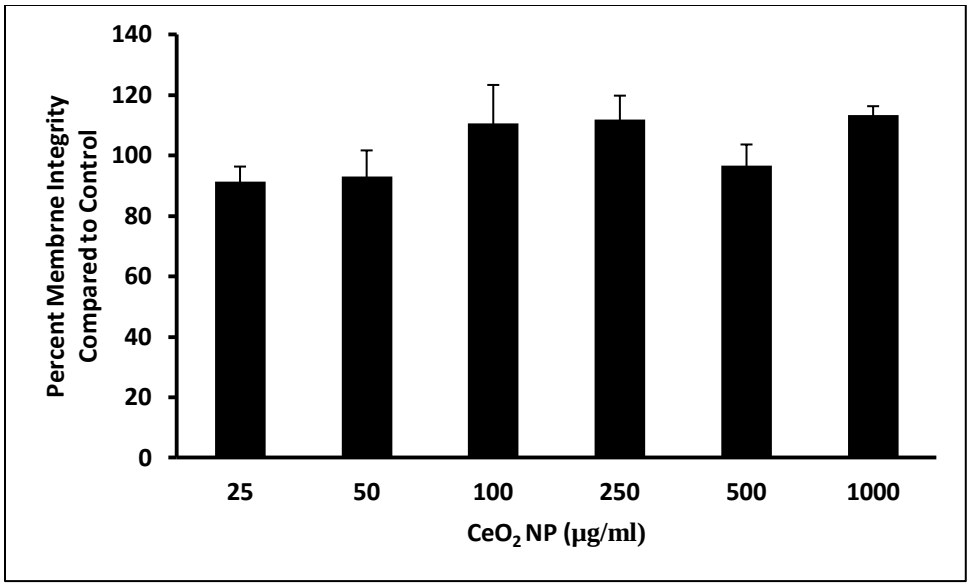

Figure A.5 Neutral red membrane integrity assay with Dispex. A549 cells were treated with CeO_2 NPs with 0.05% v/v Dispex A40 for 24 h (n=3).

Appendix B

Cardiolipin Cytochrome c Complexes for Intracellular Delivery of Cyt c

B.1 Introduction

Cardiolipin (CL) is a diphosphatidyl glycerol lipid with four alkyl chains bound to the glycerol backbone. Cardiolipin is majorly found in inner mitochondrial membranes (Rytomaa et al., 1992). In humans, heart Linoleic acid (C18:2) is the most common component, whereas in lymphoblast cells, oleic acid is the major fatty acid component (C18:1). In mitochondria, Cyt c is present both in free and membrane bound fractions. The bound form of Cyt c is present in association with CL. Cytochrome c (15%) is bound tightly (through both electrostatic and hydrophobic interactions) with CL whereas rest of it is bound loosely (electrostatic interaction) (Kagan et al., 2004). Extensive research has been focused on delineating the mechanism of Cyt c–CL interactions. The current understanding is that Cyt c in a loosely bound form serves as a mobile electron carrier between complex III and IV in the respiratory pathway and in tightly bound form it acts as a peroxidase (Kagan et al., 2005). It has been postulated that Cyt c can bind to CL simultaneously by (a) electrostatic interaction, through interaction between deprotonated phosphate group in CL and Lys 72 and 73 in Cyt c (which is also known as the “A site”) and (b) via the hydrogen binding at the “C site” i.e. Asn 52 in Cyt c and protonated phosphate group in CL. Based on different

conditions such as pH and H_2O_2 concentration, the binding between Cyt c and CL is sensitive to change (Kagan et al., 2004; Rytomaa and Kinnunen, 1995; Rytomaa et al.1992). The loosely bound form of Cyt c–CL can be reversed by increasing ionic strength and does not involve pronounced conformational change and all six coordination sites of heme iron are occupied, whereas at the C site, partial unfolding of protein occurs with the disruption of S-Fe coordination bond between Met-80 and heme iron is possible (Belikova et al., 2006). Binding through C site can also affect secondary structure of Cyt c and a decrease in α-helical content has been reported. It was hypothesized that the electrostatic interaction between Cyt c and CL could be utilized to formulate a negatively charged complex which could then be coated with DOTAP-Chol liposomes so that the resulting positively charged complex could be used for intracellular delivery of Cyt c in MDA-MB-231 breast cancer cells to induce apoptosis.

B.2 Materials and Methods

Materials

Cytochrome c (equine heart) and cholesterol were purchased from Sigma Aldrich (St. Louis, MO). DOTAP and CL (bovine heart) were purchased from Avanti Polar Lipids, Inc. (Alabaster, AL). RPMI media was purchased from Invitrogen (Carlsbad, CA). MDA-MB-231 breast cancer cell line, penicillin-streptomycin solution and fetal bovine serum (FBS) were purchased from ATCC. Plasmocin was purchased from Invivogen (San Diego, CA). Caspase Glo® reagent was purchased from Promega. All chemicals were used without any further purification.

Formulation of CL-Cyt c complexes

For formulation of CL-Cyt c complexes, CL liposomes were first prepared by film hydration method. A series of CL liposomes containing increasing concentration of CL (83, 166, 332, 664, 1328 and 2656 nano mol lipid) were prepared. To a series of glass vials, different volumes of 10 mg/mL CL solution in chloroform were added and chloroform was evaporated under a stream of nitrogen. The glass vials were then kept in vacuum for 3-4 h to allow complete evaporation of chloroform after which, 1 mL DI water was added to each of the glass vials containing dried CL lipid film and the vials were kept at RT for 3-4 h to allow hydration of lipid films. After hydration, the lipid suspension in DI water was vortexed for 1 min and extruded 20 times through polycarbonate filters (50 nm size). To the series of glass vials containing 900 µL of CL liposomes (each with different concentration of CL), 100 µL Cyt c solution (10 mg/mL) was added drop wise while vortexing the vial for 1 min. The resulting complex particle size and zeta potential were measured using Beckman Coulter N5 Submicron Particle Size Analyzer and Malvern Zeta Sizer Nano Z.

Formulation of DOTAP-Chol (DOTAP-Chol) coated CL-Cyt c complex

To prepare DOTAP-Chol coated CL-Cyt c complex, a concentrated suspension containing DOTAP-Chol (1:1 mol to mol) liposomes were prepared using film hydration method. Briefly, lipids (8µmol DOTAP and 8 µmol Chol) dissolved in chloroform were added to a 7 mL glass vial and chloroform was evaporated under a stream of nitrogen. The glass vial was then kept in vacuum for 3-4 h to allow complete evaporation of chloroform after which, 1 mL DI water was added to the vial containing dried lipid film. The lipid suspension in the vial was vortexed for 1 min. This was followed by bath sonication for 1 min, after which the vial was kept at 4 ºC for overnight hydration. The following day the hydrated lipid suspension was serially extruded through 400 nm (12 extrusion cycles), 200 nm (12 extrusion cycles), 100 nm (15 extrusion cycles) and 50 nm (15 extrusion cycles) polycarbonate filters. To coat CL-Cyt c complex, the complex with 8:1 CL: Cyt c (mol to mol) composition was selected. Several dilutions from the concentrated DOTAP-Chol liposomes were prepared by dilution with DI water in eppendorf tubes. To each eppendorf containing 160 µL diluted DOTAP-Chol liposomes, 40 uL of CL-Cyt ccomplex (8:1 mol:mol) was added and the mixture was pipetted up and down twenty times to allow charge interaction between negatively charged CL-Cyt c complex and positively charged DOTAP-Chol liposomes. The dilutions for DOTAP-Chol liposomes was carried out so that after mixing CL-Cyt c complex, different mol to mol ratio of DOTAP:CL could be achieved (1.5:1, 3:1, 6:1, 12:1,18:1, 24:1, 36:1 and 42:1). The particle size and zeta potential of all complexes were measured using Beckman Coulter N5 Submicron Particle Size Analyzer and Malvern Zeta Sizer Nano Z.

TEM analysis of liposomes and complexes

Transmission electron microscopy images of CL liposomes, CL-Cyt c complexes and DOTAP-Chol coated CL-Cyt c complexes were acquired using FEI-Philips Tecnai 12 transmission electron microscope. The samples (liposomes/complexes) were allowed to deposit on carbon coated copper TEM grids for 1 min after which the excess sample was removed using a blotting paper. Negative staining was accomplished by using 1% uranyl acetate solution which was allowed to deposit on the sample for 30 sec to 1 min after which excess was removed using a blotting paper. The sample was air dried for a few minutes and then imaged.

Caspase Assay to study induction of apoptosis in MDA-MB-231 Cells

Caspase 3 and 7 are known as effector caspases which are responsible for breaking down the cell cytoskeleton during apoptosis. To test the apoptosis inducing activity of DOTAP-Chol coated CL-Cyt c complex to induce apoptosis *in-vitro* in MDA-MB-231 cells, caspase assay was used. MDA-MB-231 cells (6,000) were seeded in 96 well plate and allowed to attach for 24 h at 37 ºC. The following day, media was changed to serum free RPMI media and various treatments were added and allowed to incubate for 4 h. Various treatments included Cyt c alone, CL-Cyt c complex, CL liposomes, DOTAP-Chol liposomes, DOTAP-CL complex and DOTAP-CL-Cyt c complex. Negative control was MDA-MB-231 cells without any treatment and positive control was Sturosporine (STS) treated cells (4 µM overnight treatment). Caspase Glo kit® from Promega was used to quantify caspase activity and manufacturer's instructions were followed. Luminescence was quantified using Biotek Synergy Plate Reader.

B.3 Results and Discussion

Formulation of CL-Cyt c complexes

Naturally occurring electrostatic interaction between Cyt c and CL was utilized to form a CL-Cyt c complex which could then be utilized as a core for the DOTAP-Chol coating. The goal was to identify the mol ratio at which a negatively charged CL-Cyt c core could be formed within in a nano size range and then be coated with positively charged DOTAP-Chol liposomes. Complexes with various mol ratios of CL and Cyt c were formulated and monitored for particle size and zeta potential. The particle size of the complexes decreased and zeta potential increased (negative) as the CL amount in the complex was increased (**Table B.1**). Starting with 4:1mol ratio, CL:Cyt c nanosize complex were formed. The large SD values of particle size can be attributed to two sized populations formed upon complexation of Cyt c with CL. Rod shaped structures were formed in addition to spherical complexes (**Figure B.3**). Inverted hexagonal phases (rod shaped structures) are lipid polymorphs where the hydrophobic lipid chains extend out into aqueous medium and the hydrophilic head is towards the core. Lipids with a bulky lipid tail have an increased tendency to form inverted hexagonal phases. Formation of inverted hexagonal phases by CL after association with Cyt c has previously been reported (De Kruijff et al., 1982). It was decided to use CL-Cyt c complex with 8:1 mol ratio for further coating by DOTAP-Chol liposomes because of sub 100 nm size and lower SD values.

Formulation of DOTAP-Chol (DOTAP-Chol) coated CL-Cyt c complex

Dioleoyl-trimethyl-ammonium-propane and cholestrol liposomes were positively charged (50 mV, **Figure B.4**) and about 100 nm in size. For coating the CL-Cyt c complex with DOTAP-Chol liposomes, the mol ratio of DOTAP to CL was varied from 1.5:1 to 42:1.

Between mol ratio of 1:5 and 1:12, very high SD values were observed although the zeta potential values remained in 30-40 mV range. This could be due to insufficient DOTAP coating on the CL-Cyt c core. At 18:1 DOTAP:CL ratio, particle size of 160 nm and zeta potential of 40 mV was observed. The particle size and zeta potential did not change even at higher DOTAP:CL mol ratios, therefore DOTAP:CL 18:1 mol ratio was selected for further cell based assays.

Caspase Assay to study induction of apoptosis in MDA-MB-231 Cells

The caspase assay results (**Figure B.4**) showed that CL-Cyt c complex or DOTAP-Chol coated CL complex did not induce caspase activation above baseline levels as response was similar to the negative control. However, CL liposomes and DOTAP-Chol–CL complex treatment induced caspase activation. Interestingly, the DOTAP-Chol-CL induced activation of caspase was higher than CL liposomes alone and indicated that DOTAP-Chol liposomes facilitated CL induced caspase activation. Baseline level of caspase activation was observed with DOTAP-Chol liposomes alone indicating that the higher caspase response observed after treatment with DOTAP-Chol-CLcomplex may be attributed to higher cell uptake of this complex (due to DOTAP) compared with CL liposomes alone. Although not shown in the figure, it was confirmed that the increased response (caspase activation) observed with CL liposomes and DOTAP-Chol–CL complex was specifically a caspase signal, because after incubating a caspase inhibitor (a selective binding agent for activated caspase that prevents it from cleaving the substrate in the reagent kit and inducing a luminescence response), the baseline luminescence response was observed. Although the incubation time was only 4 h and it can be argued that at longer incubation times, may be some level of caspase activity would have been observed with DOTAP-Chol coated CL-Cyt c complex, but because higher

caspase activation was observed with CL and DOTAP-Chol-CL complexes, it was decided not to move forward with this strategy for encapsulating Cyt c.

B.4 Conclusion

It was shown that a negatively CL-Cyt c complex was formulated with a particle size of about 100 nm. It was also showed that this negatively charged complex was coated with DOTAP-Chol liposomes so that a positively charged complex was formed with a particle size of 160 nm. When the DOTAP-Chol-CL-Cyt c complex was tested for caspase induction activity *in-vitro,* it did not induce caspase induction above baseline levels. However, higher caspase induction was observed after treatment with CL liposomes and DOTAP-Chol-CL complex controls which indicated that CL was toxic and therefore this strategy of using CL to deliver Cyt c was not pursued further.

Table B.1 Particle Size and Zeta Potential Analysis of CL-Cyt c Complex

Mol Ratio (CL_Cyt c)	PS (nm)	SD	ZP (mV)	SD
1_1	2466	668	0.8	5
2_1	544	414	-2	4
4_1	119	67	-27	10
8_1	99	49	-32	10
16_1	120	52	-38	12
32_1	121	48	-37	12

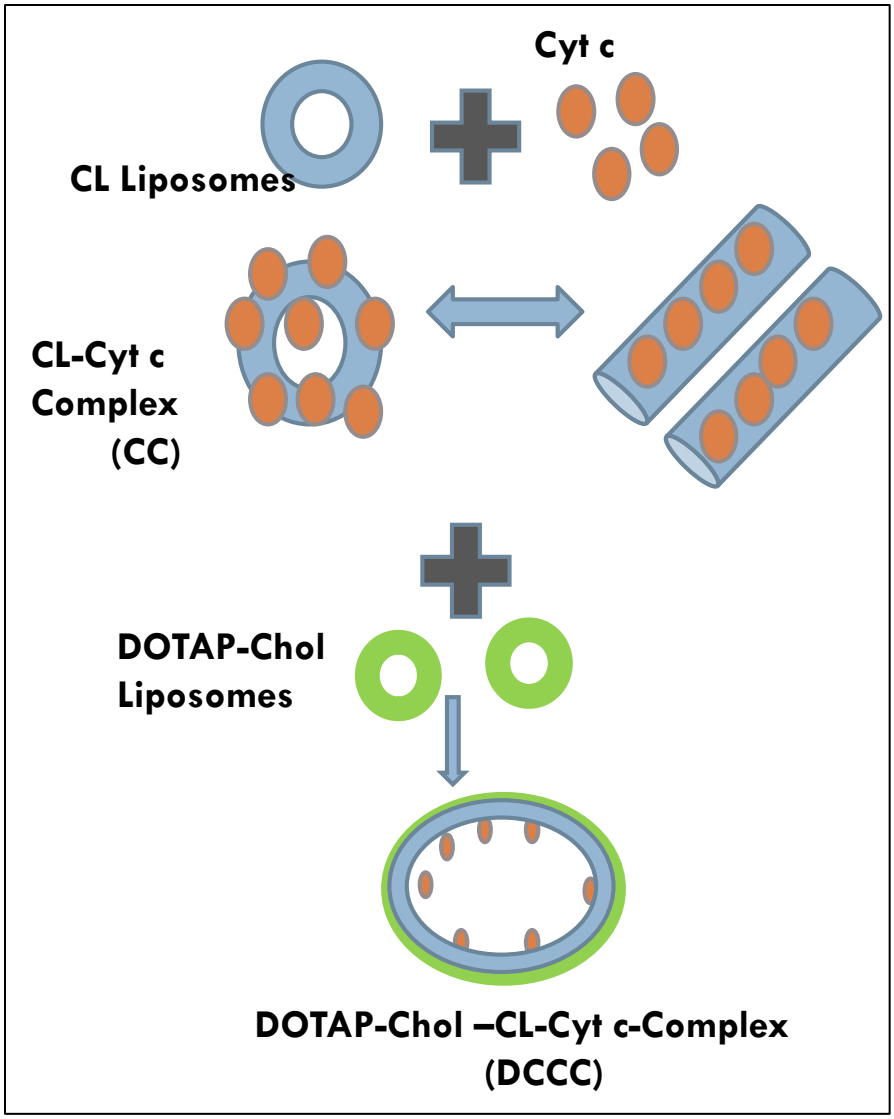

Figure B.1 Schematic illustrating formulation of complexes

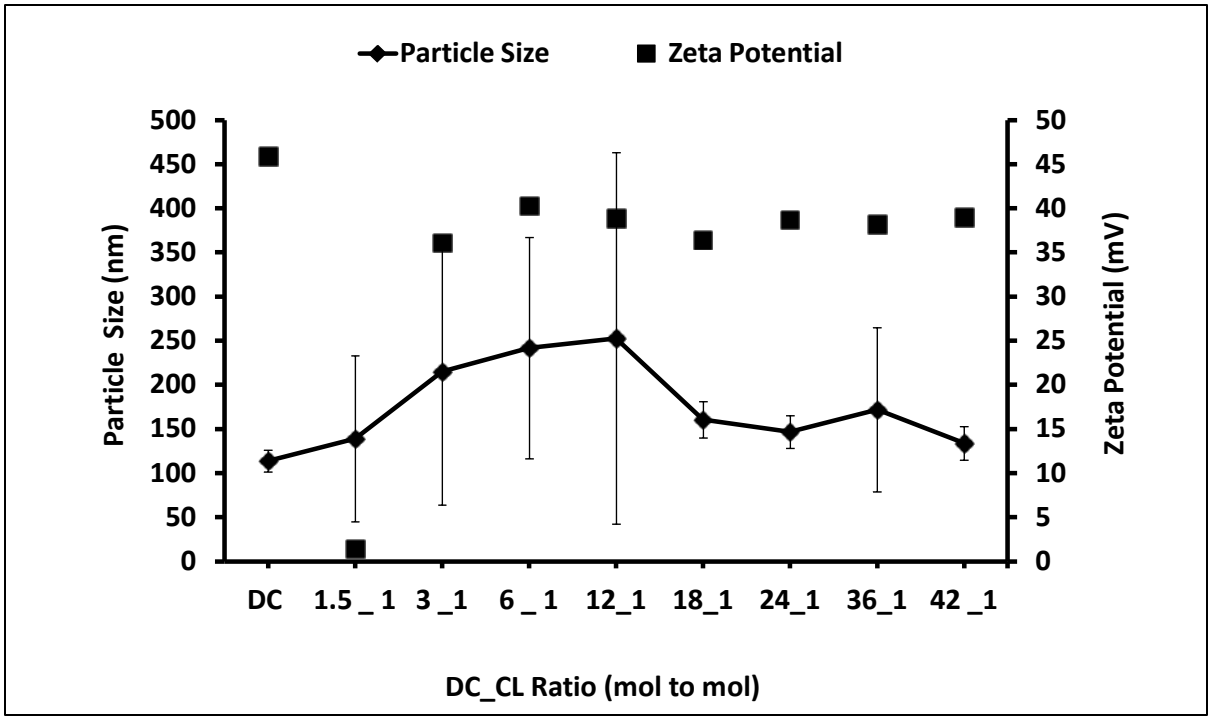

Figure B.2 Particle size and zeta potential analysis of DOTAP-Chol-CL-Cyt complex.

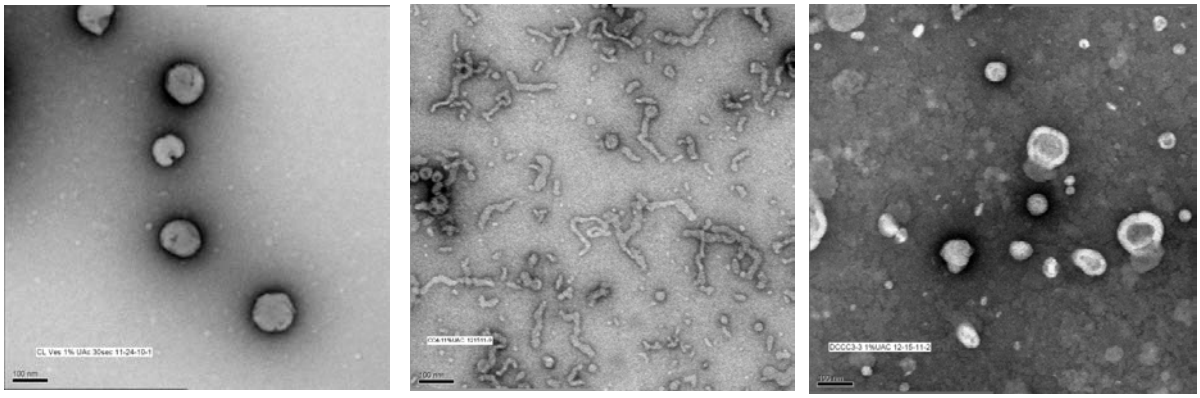

CL Liposomes | CL-Cyt c complex | DCCC complex (DC_CL: 18_1)

Figure B.3 TEM images of liposomes and complexes. DCCC means DOTAPChol-CL-Cyt c.

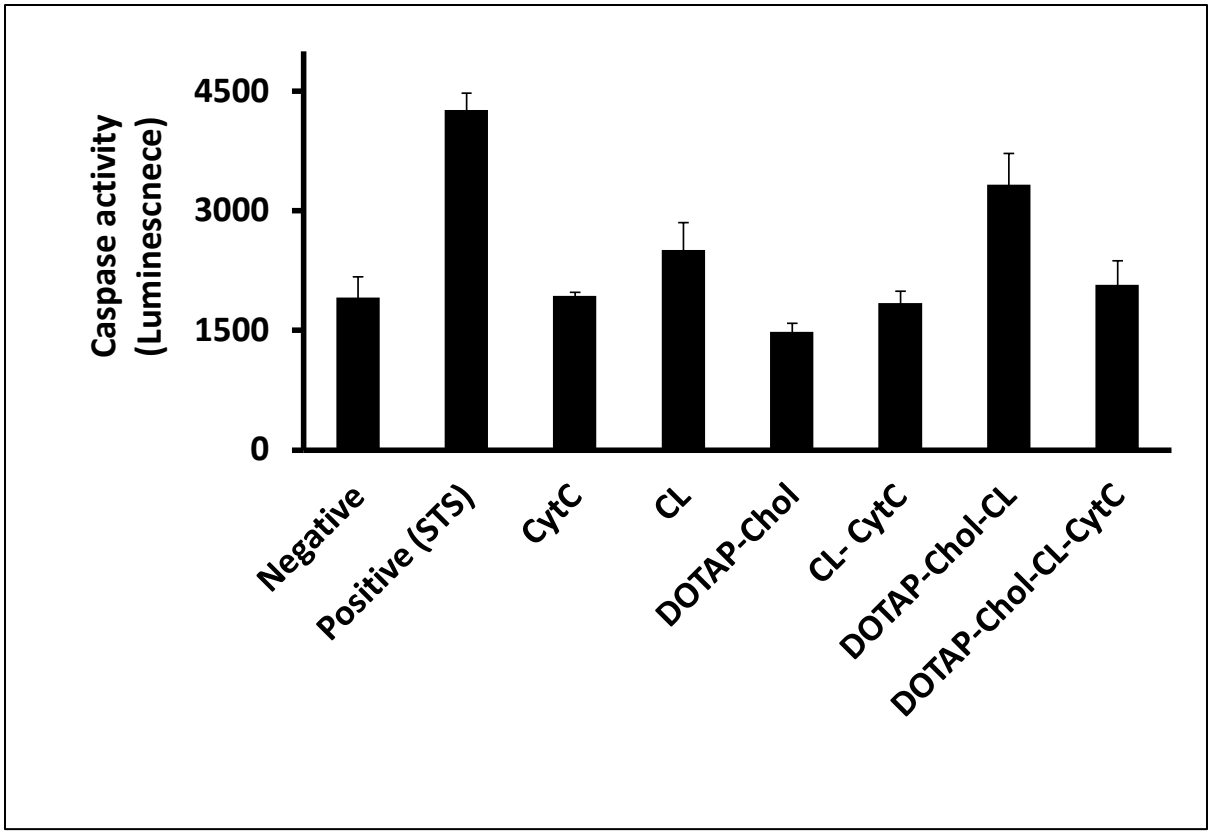

Figure B.4 Evaluation of Caspase activity of various complexes

B.5 References

Belikova, N.A., Vladimirov, Y.A., Osipov, A.N., Kapralov, A.A., Tyurin, V.A., Potapovich, M.V., Basova, L.V., Peterson, J., Kurnikov, I.V., Kagan, V.E., 2006. Peroxidase activity and structural transitions of cytochrome c bound to cardiolipin-containing membranes. Biochemistry 45, 4998-5009.

De Kruijff, B., Verkleij, A.J., Leunissen-Bijvelt, J., Van Echteld, C.J., Hille, J., Rijnbout, H., 1982. Further aspects of the Ca2+-dependent polymorphism of bovine heart cardiolipin. Biochim Biophys Acta 693, 1-12.

Kagan, V.E., Borisenko, G.G., Tyurina, Y.Y., Tyurin, V.A., Jiang, J., Potapovich, A.I., Kini, V., Amoscato, A.A., Fujii, Y., 2004. Oxidative lipidomics of apoptosis: redox catalytic interactions of cytochrome c with cardiolipin and phosphatidylserine. Free Radic Biol Med 37, 1963-1985.

Kagan, V.E., Tyurin, V.A., Jiang, J., Tyurina, Y.Y., Ritov, V.B., Amoscato, A.A., Osipov, A.N., Belikova, N.A., Kapralov, A.A., Kini, V., Vlasova, II, Zhao, Q., Zou, M., Di, P., Svistunenko, D.A., Kurnikov, I.V., Borisenko, G.G., 2005. Cytochrome c acts as a cardiolipin oxygenase required for release of proapoptotic factors. Nat Chem Biol 1, 223-232.

Rytomaa, M., Kinnunen, P.K., 1995. Reversibility of the binding of cytochrome c to liposomes. Implications for lipid-protein interactions. J Biol Chem 270, 3197-3202.

Rytomaa, M., Mustonen, P., Kinnunen, P.K., 1992. Reversible, nonionic, and pH-dependent association of cytochrome c with cardiolipin-phosphatidylcholine liposomes. J Biol Chem 267, 22243-22248.